

SYNTHESIS AND CHARACTERIZATION OF COLLOIDAL INDIUM NITRIDE
NANOCRYSTALS AND STUDY OF THEIR ELECTRONIC STRUCTURE AND
SIZE AND SHAPE DEPENDENT OPTICAL PROPERTIES

By

Basudeb Chakraborty

A THESIS

Submitted to
Michigan State University
in partial fulfillment of the requirements
for the degree of

Chemistry-Master of Science

2014

ABSTRACT

SYNTHESIS AND CHARACTERIZATION OF COLLOIDAL INDIUM NITRIDE NANOCRYSTALS AND STUDY OF THEIR ELECTRONIC STRUCTURE AND SIZE AND SHAPE DEPENDENT OPTICAL PROPERTIES

By

Basudeb Chakraborty

In this work the synthesize colloidal Indium Nitride (InN) nanoparticles and characterization techniques to explain their morphology and different properties have been presented. The efficiency of previously reported synthetic methods have been tested and modifications have been attempted to enhance the quality of the nanocrystals. A novel approach has been successfully developed to synthesize 4-12 nm diameter, wurtzite phase InN nanoparticles with high crystallinity and quantitative photoluminescence quantum yield. This new synthetic method is based on the *in-situ* chemical reduction of indium(III) bidentate amine complexes in high-boiling point solvents. We demonstrate that the electronic structure of these material is strongly dependant on the size and shape of the nanoparticles. Due to quantum confinement playing a significant role the optical band gap of InN can be tuned to be up to 0.4 eV higher than the bulk material. The size of the nanoparticles can be controlled by the varying the precursor ratio, rate of addition of reactant whereas the shape can be modified by adjusting the nature and stoichiometry of the surfactants used during the synthesis.

*Dedicated to....
Ma, Baba and Gutul*

ACKNOWLEDGEMENTS

Firstly, I would like to thank my supervisor Dr. Rémi Beaulac for his guidance, patience, motivation, enthusiasm, and valuable insights. I am truly grateful to Dr. Richard J. Staples, Dr. Kathryn G. Severin and Dr. Askeland Per for their help with the X-ray diffraction, optical and X-ray photoelectron spectroscopy measurements. I would also like to thank my committee members Dr. Viktor Poltavets, Prof. Aaron L. Odom and Prof. James E. Jackson for their support, guidance and suggestions which motivated me to work harder to achieve my research goals.

This thesis would not have been possible without the help and support of the Beaulac Group members and Department of chemistry, Michigan State University.

Last but certainly not the least, I would like to thank my family and friends for always being there for me, and supporting me in whatever pursuit I have chosen.

TABLE OF CONTENTS

LIST OF TABLES.....	vii
LIST OF FIGURES.....	viii
KEY TO ABBREVIATIONS.....	xii
CHAPTER 1 : INTRODUCTION	1
GROUP III-V SEMICONDUCTOR NANOMATERIAL	1
GROUP III-NITRIDE SEMICONDUCTORS	3
SIGNIFICANCE AND APPLICATION OF III-V MATERIALS AND INDIUM NITRIDE (InN)	4
DIRECT AND INDIRECT BAND GAP	6
PREVIOUSLY REPORTED SYNTHETIC METHODS FOR INDIUM NITRIDE (InN)	7
MOTIVATION FOR MOVING TO THE NANO REGIME	9
COMPARISON TO THE BULK MATERIAL	11
THE BAND GAP CONTROVERSY OF INDIUM NITRIDE	14
SCOPE OF THE THESIS	18
CHAPTER 2 : EXPERIMENTAL SECTION	20
MATERIALS	20
INSTRUMENTS	21
SYNTHESIS USING INDIUM NITRIDE NANOPARTICLES USING SODIUM AMIDE	23
CRYSTAL SIZE ANALYSIS	30
SYNTHESIS OF INDIUM NITRIDE BY THERMOLYSIS METHOD	32
NEW APPROACH : SYNTHESIS OF INDIUM NITRIDE USING TMED AS NITROGEN SOURCE	34
MODIFICATIONS TOWARDS IMPROVED QUALITY COLLOIDAL NANOCRYSTALS	39
REVELATION OF SHAPE OF PARTICLES	46
CHAPTER 3: CONTROLLING THE SHAPE OF NANOPARTICLES	49
CHAPTER 4: INSIGHT INTO REACTION MECHANISM	61
SYNTHESIS OF INDIUM NITRIDE USING INDIUM METAL AS THE STARTING MATERIAL	61
XPS (X-RAY PHOTOELECTRON SPECTROSCOPY) STUDIES TO INVESTIGATE THE REACTION PATHWAY	62
SYNTHESIS OF INDIUM NITRIDE WITH EXCESS TMED	65
CHAPTER 5: STUDY OF OPTICAL PROPERTIES	69
PHOTOLUMINESCENCE (PL) FROM INDIUM NITRIDE NANOCRYSTALS	69
QUANTUM YIELD (QY)	74

MANIFESTATION OF SIZE DEPENDANT OPTICAL PROPERTIES	76
CHAPTER 6	79
ELEMENTAL ANALYSIS	79
INDUCTIVELY COUPLED PLASMA ATOMIC EMISSION SPECTROSCOPY	79
CHN ANALYSIS	80
CONCLUSION.....	83
FUTURE WORK.....	84
BIBLIOGRAPHY.....	85

LIST OF TABLES

Table 1: Calculated QY (relative) for the InN samples using OLA:OA ratio 3:1.....	75
Table 2: Calculated QY (relative) for the InN samples using OLA:OA ratio 10:1.....	76
Table 3: Empirical data of bulk wurtzite InN.....	77
Table 4: Results from the CHN analysis.....	81

LIST OF FIGURES

Figure 1: Plot of the solar spectrum. The range between the dotted lines indicate the portion of the spectrum that can be achieved by InGaN.....	4
Figure 2: Schematic image of a InN-based field-effect transistor. InN was epitaxially grown on YSZ (Yttria-stabilized zirconia) substrates. This was performed using conventional photolithography and dry etching. The cubic InN channel layers were covered with Au (source and drain electrodes) and amorphous HfO ₂ (gate insulator).	5
Figure 3: Demonstration of direct (left) and indirect band gap (right).....	7
Figure 4: Increase in band gap with decrease in size of the semiconductor nanomaterial or quantum dot due to the quantum confinement effect	12
Figure 5: Origin of the Burstein-Moss Shift	17
Figure 6: Molecular structure of some chemicals used for different synthesis	21
Figure 7: PXRD pattern of InN nanoparticles; Crystallite Size ~20 nm Structure: Wurtzite; System: Hexagonal; PDF: 01-074-0244; Space Group: P6 ₃ mc.	26
Figure 8: TEM image of InN nanoparticles in hexane (A), (B). The Selected Area Electron Diffraction pattern corresponding to the wurtzite phase of nanocrystals (C)	27
Figure 9: The PXRD pattern of the InN sample using tributylamine, agrees to wurtzite phase of InN	28
Figure 10: The EDS pattern of the sample prepared with TBA which shows presence of Indium.....	29
Figure 11: TEM images of InN nanoparticles synthesized using TBA	29
Figure 12: Scherrer analysis to find crystallite size. Plugging in the values above the size of the nanocrystal is calculated to be 10.9 nm.(However this kind of analysis can give us 20%-30% accuracy at best.....	31
Figure 13: PXRD pattern of InN sample prepared by thermolysis method	33
Figure 14: Absorption spectra of InN samples in TCE (Solvent).....	33
Figure 15: TEM images of InN sample prepared by thermolysis method	33

Figure 16: The absorption spectra of aliquots drawn at 10, 20 and 30 min (Left). Aliquots drawn at 45, 60, 75 and 90 min (Right).....	37
Figure 17: The PXRD pattern of nanoparticles synthesized in the method described in the section above. The black dotted line shows a Gaussian fit to only 101 signal to find out crystallite size	37
Figure 18: A)TEM image of InN TMED aliquot at 75 min (Avg. size = 4.4 nm) ; B) HRTEM image of the same ; C) Lattice fringes in the nanoparticles are 0.549 nm apart (consistent with the lattice parameter obtained from the wurtzite phase) , D) TEM image of InN TMED aliquot at 90 min (Avg. size = 5.62 nm) ; E) HRTEM image of the same	38
Figure 19: Scheme: Schematics of the reaction using TMED and n-BuLi	40
Figure 20: (Left) Aliquots taken at 25, 35, 50, 70 and 90 min . (Right) NIR absorption spectra of colloidal InN nanoparticles, showing the lowest excitonic transition for different average particle diameters	41
Figure 21: PXRD pattern of the sample agrees well to wurtzite phase of InN	42
Figure 22: (Left) Scherrer analysis to find out size of the nanocrystal, (Right) HRTEM image of a nanoparticle from the final sample.....	42
Figure 23: Raman spectra of InN nanoparticles. Both $A_1(\text{LO})$ and E_{2h} peaks, which are related to a longitudinal optical phonon mode and a doubly degenerated mode, respectively, were observed at 596cm^{-1} and 495cm^{-1}	43
Figure 24: Size-dependence of the first absorption peak of nanometer-sized InN colloidal particles. The dashed line corresponds to the trend expected from the Brus equation	44
Figure 25: Magnified TEM images of InN nanoparticles. From these images it looks like the particles actually have a propensity to acquire platelet or disc like profiles	46
Figure 26: (Left) Lattice fringes in a HRTEM image shows the 101 facet. (Right) AFM image of the particles synthesized by this process	47
Figure 27: (Left) Absorption spectra of aliquots taken out of the reaction mixture synthesized with OLA:OA ratio 5:1. (Right) Size-dependence of the first absorption peak of these samples. The dashed line corresponds to the trend expected from the Brus equation	49
Figure 28: PXRD pattern of the TEM images synthesized by OLA:OA = 5:1 and HRTEM image showing (A) 101 plane and (B) 100 plane	50
Figure 29: TEM images of the two other aliquots drawn at 30 (left) and 45 min (right) from InN sample aliquots made with 5:1 ligand ratio	51

Figure 30: AFM image of nanoparticles prepared using OLA:OA = 5:1 ratio. Average height comes out to be as ~7.5 nm	52
Figure 31: (Left) Absorption spectra of aliquots taken out of the reaction mixture synthesized with OLA:OA ratio 5:1. (Right) Size-dependence of the first absorption peak of these samples	53
Figure 32: PXRD pattern of the sample is consistent with wurtzite crystal structure	54
Figure 33: Scherrer analysis (Left) and HRTEM image showing 101 plane (Right)	54
Figure 34: TEM (Left) and AFM (Right) image of the final aliquot	55
Figure 35: (Left) Absorption spectra of aliquots taken out of the reaction mixture synthesized with OLA:OA ratio 10:1. (Right) Size-dependence of the first absorption peak of these samples.....	56
Figure 36: PXRD pattern of the sample consistent with wurtzite crystal structure	57
Figure 37: Scherrer analysis of 101 signal of the PXRD pattern	58
Figure 38: TEM images of nanocrystals from aliquot 3 (radius ~ 3.82 nm) (Left) and final aliquot (radius ~ 5.98 nm) (Right)	59
Figure 39: AFM images of the nanoparticles from same aliquot (left- aliquot 3) and (right- final aliquot)	59
Figure 40: (Left) 101 plane with a d value of 0.270 nm, (Right) a) 100 plane with a d value of 0.308 nm) 101 plane with a d value of 0.271 nm	60
Figure 41: TEM image and selected area diffraction pattern of the the sample of In metal nanoparticles	62
Figure 42: XPS data of the In 3d _{5/2} of aliquots taken out at 30 min (A) and 60 min (B) from the reaction mixture using molar ratio of InBr ₃ , TMED, <i>n</i> -BuLi taken as 1:3:3 which shows relative concentration of In (III) and In (0)	63
Figure 43: : XPS data of the In 3d _{3/2} and In 3d _{5/2} of aliquots taken out at 90 min (A) from the reaction mixture using molar ratio of InBr ₃ , TMEDA, <i>n</i> -BuLi taken as 1:3:3 (B) shows relative concentration of In (III) to In (0) in the sample	64
Figure 44: XPS data of the In 3d _{5/2} of aliquots taken out at different time from the synthesis using excess TMED	66
Figure 45: Absorption spectra of aliquots from synthesis using excess TMED	67

Figure 46: PXRD pattern of InN quantum dots synthesized with excess TMED confirm the wurtzite nature of the crystal structure 68

Figure 47: Absorbance and PL Spectra of an aliquot of InN (A5) from the synthesis using OLA:OA ratio of 10:1 70

Figure 48: PL spectra of five aliquots of the sample from the synthesis using OLA:OA ratio 10:1 70

Figure 49: PL spectra of three aliquots of the InN sample synthesized using 3:1 ratio of OLA:OA 72

Figure 50: PL Lifetime decay of InN sample from two different synthesis using OLA:OA ratio of 10:1 and 3:1 respectively 72

Figure 51: Size vs. band gap plot for InN nanocrystals synthesized by using 3:1 OLA:OA ratio (Left), 10:1 ratio (Right) 78

KEY TO ABBREVIATIONS

AFM : Atomic force microscopy

Al : Aliquot

AlN : Aluminium Nitride

Avg : Average

CB : Conduction band

CBM : Conduction band minimum

CD : Compact disc

CHN : Carbon hydrogen nitrogen

CdSe : Cadmium Selenide

DVD : Digital video disc

EDS : Energy-dispersive X-ray spectroscopy

FTIR : Fourier transform infrared

FWHM : Full width at half maximum

GaAs : Gallium Arsenide

GaN : Gallium Nitride

GaP : Gallium phosphide

GaSb : Gallium Antimonide

HD : Hexadecane

HEMT : High electron mobility transistor

HRTEM : High resolution Transmission electron spectroscopy

ICP-AES : Inductively coupled plasma atomic emission spectroscopy

ICP-OES : Inductively coupled plasma optical emission spectroscopy

ICP : Inductively coupled plasma

InGaN : Indium gallium nitride

InN : Indium nitride

InP : Indium phosphide

InSb : Indium Antimonide

IR : Infrared

JCPDS : Joint Committee for Powder Diffraction Standards

LED : Light emitting diode

MBE : Molecular beam epitaxy

MOCVD : Metal organic chemical vapor deposition

NC : Nanocrystal

NIR : Near infrared

OA : Oleic acid

ODE : Octadecene

OLA : Oleylamine

PbS : Lead Sulfide

PbSe : Lead Selenide

PDF : Powder diffraction file

PL : Photoluminescence

PXRD : Powder X-ray diffraction

QD : Quantum dot

QY : Quantum yield

RF : Radiofrequency

RPM : Revolutions per minute

SAED : Selected area electron diffraction

SI : Supporting information

SPR : Surface plasmon resonance

TBA : Tributylamine

TCE : Tetrachloroethylene

TCSPC : Time-correlated single photon counting

TEM : Transmission electron microscopy

TMED : N,N,N',N'' tetramethylethylenediamine

TOA : Trioctylamine

TOP : Trioctylphosphine

UV : Ultra violet

VB : Valence band

VEELS : Valence electron energy loss spectroscopy

YSZ : Ytria-stabilized zirconia

XRD : X-ray diffraction

XPS : X-ray photoelectron spectroscopy

ZnS : Zinc Sulfide

CHAPTER 1 : INTRODUCTION

GROUP III-V SEMICONDUCTOR NANOMATERIALS

Quantum dots(QDs) are semiconductor nanocrystals with typical dimensions in the range of 1-100 nm that exhibit size-dependent optical and electronic properties.¹⁻⁴ With the absorption of a photon of energy equal or larger to the band gap (E_g), the excitation of an electron leaves an orbital hole in the valence band. The negatively charged electron and positively charged hole constitute an electro-statically bound electron-hole pair, known as the exciton. Recombination of the electron and hole annihilates the exciton and might be accompanied by the emission of a photon, a process known as radiative recombination. The exciton has a finite size within the crystal characterized by the excitonic Bohr radius (a_{exc}), which can vary from one to few hundreds of nanometers depending on the type of semiconductor material. If the size of a semiconductor nanocrystal is comparable or smaller than the size of the exciton, the charge carriers become spatially confined giving rise to size-dependent optical properties (quantum confinement). QDs are constrained in all three dimensions. It is the exciton size that delineates the transition between the bulk and confined regime. The electronic properties of QDs are intermediate between those of bulk semiconductors and of discrete molecules and show absorption features corresponding to discrete electronic transitions. These discrete transitions are reminiscent of atomic spectra and have led to QDs also being known as artificial atoms.⁵ The electronic properties of QDs are dependent on the size and shape of the individual crystals. The main advantage of QDs is the ability to obtain different electronic properties by tuning the size of the dots which make them so important for many applications. Owing to their nanoscale dimensions, they have very sharp density of states and excellent transport and optical properties. QDs have been applied in photodetectors,⁶ lasers⁷, sensors, displays and amplifiers.⁸

Semiconductor materials composed of elements from group III and group V (or, group 13 & 15) of the periodic table are termed as III-V semiconductors and include materials aluminium nitride (AlN), indium nitride (InN), gallium nitride (GaN), gallium arsenide (GaAs) and indium phosphide (InP). These have advantages over other semiconductor materials such as enhanced carrier mobility and ability to create ternary and quaternary materials that have fine-tunable electronic and optical properties based on the composition of material. III-V materials can also be utilized for specialized growth phenomena such as sacrificial layers or strained layers in novel nanostructures such as semiconductor nanotubes,⁹ nanowires,¹⁰ and self assembled QDs.¹¹ As far as semiconductor physics is concerned, properties such as high electron mobility in some III-V semiconductors give them edge over elemental semiconductors for utilization in high speed devices.¹²

Many III-V semiconductors have direct energy gaps (AlN, GaN, GaAs, GaSb, InN, InP, InSb, InAs) making them useful for optoelectronics. The feature that distinguishes these III-V materials from other traditional semiconductors is their direct band gap. In semiconductors like Si or Ge, the conduction band minima and valence band maxima do not share the same point in k-space. Consequently, a conduction band electron can only radiatively recombine with a valence band hole through the involvement of a phonon, where the phonon momentum equals the difference between the conduction band and valence band momentum. The involvement of the phonon makes this process much less probable, leading to slower radiative recombination in indirect band gap materials than direct band gap ones. This results in radiative recombinations being only a small proportion of total recombinations, with most of them being non-radiative in nature. A great amount of light conversion efficiency is lost in indirect band gap materials due to these non-radiative recombination such as the Auger effect or phonon emission.¹³ This is not the case

with direct band gap semiconductors since they do not require intermediate phonon involvement step and hence have much higher light conversion efficiencies, making them the choice materials for optical devices.

GROUP III-NITRIDE SEMICONDUCTORS

AlN, InN, GaN and their alloys are main components of the III-nitride semiconductor series. These prove to be very promising materials for multiple electronic and optoelectronic applications. Using these materials, a wide range of band gaps can be accessed (Fig. 1). For instance AlN has a band gap of 6.2 eV, whereas GaN has 3.4 eV (ultra violet (UV) region) and InN 0.7 eV (near infrared (NIR) band gap). III-V materials also possess very high decomposition temperatures; making them suitable for application in high-temperature electronics.¹⁴ These are usually resistant to traditional fabrication technique but on the other hand these materials offer appreciable chemical stability, one of the most desirable properties for fabrication in devices. GaN has a very large breakdown field (electric field that a pure material can withstand) of $\sim 3 \times 10^6$ V/cm¹⁵ and InN is known to have quite high electron mobility (4400 cm²/Vs).¹⁶ These exceptional properties make these III-V materials desirable in high-frequency and high-power applications. Alloys of these materials can be tuned to have possible combination of both the aforementioned properties.

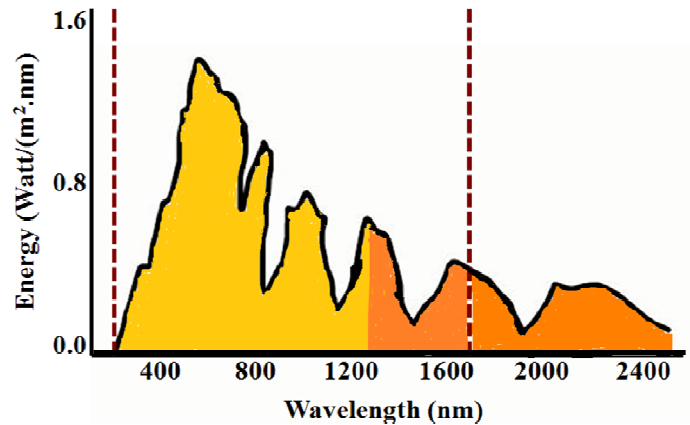


Figure 1: Plot of the solar spectrum. The range between the dotted lines indicate the portion of the spectrum that can be achieved by InGaN¹⁷

SIGNIFICANCE AND APPLICATION OF III-V MATERIALS AND INDIUM NITRIDE (InN)

III-V semiconductor materials have been utilized in many devices and instruments that have huge contribution in transforming our everyday life. These materials are largely responsible for ground-breaking advancements such as the internet, wireless communications, mobile phones and data storage media like CD, DVD etc. These also have been utilized in important technological applications, such as solar cells, light emitting devices (LED) for displays, significant improvements in healthcare sector in bio-imaging and also anti-terrorist activities (by IR-laser detection of explosives and weapons).

Some very distinct properties make these III-V semiconductors effective towards these particular applications. These materials possess high carrier mobility, they are mostly direct band gap materials and some of them have very narrow band gap making them versatile for use over a

huge range of energies. With efficient synthetic methods they can be highly crystalline and are expected to exhibit striking optoelectronic properties.

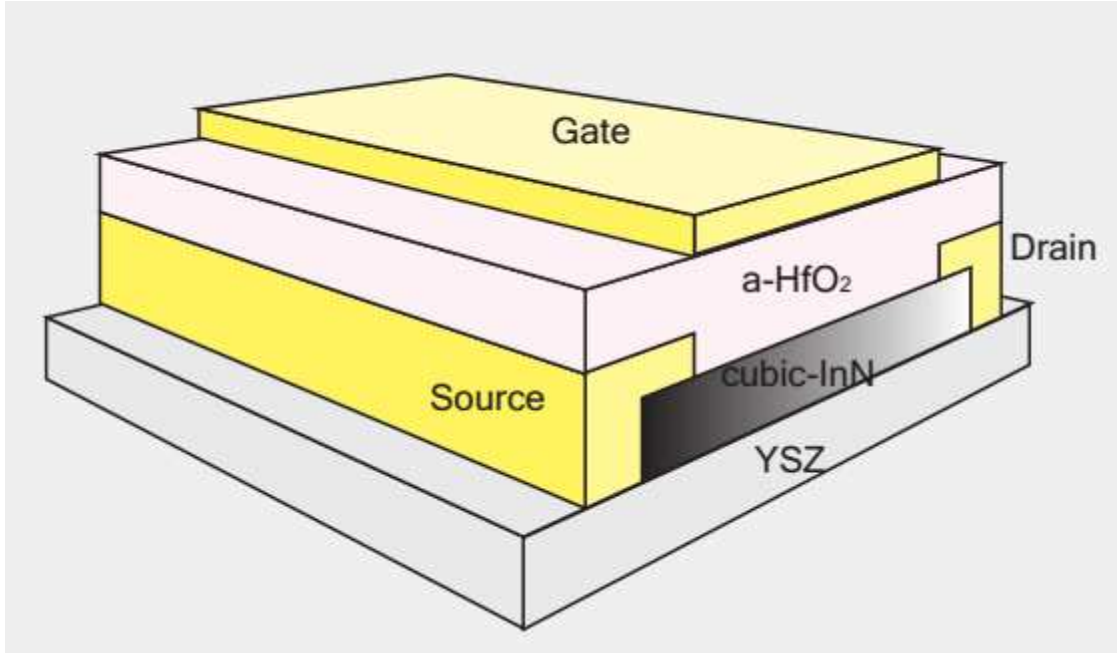


Figure 2: Schematic image of a InN-based field-effect transistor. InN was epitaxially grown on YSZ (Yttria-stabilized zirconia) substrates. This was performed using conventional photolithography and dry etching. The cubic InN channel layers were covered with Au (source and drain electrodes) and amorphous HfO_2 (gate insulator).¹⁸

InN is a direct band gap III-V semiconductor. The prospect of InN having a band gap ~ 0.7 eV has caused a great deal of excitement because devices that can utilize the entire visible spectrum and parts of the infrared spectrum have been envisioned based on the $\text{In}_x\text{Ga}_{1-x}\text{N}$ system. Such a material system would hold great promise for applications in solar cells and optoelectronics.¹⁹ In Fig. 2 we see the demonstration of first field effect transistor (FET) device which uses InN. In this device ultrathin InN is epitaxially deposited on insulating oxide yttria-stabilized zirconia

substrates. With various other applications, InN remains a potential material for applications in high electron mobility transistors (HEMT), and as dilute magnetic semiconductors.

DIRECT AND INDIRECT BAND GAP

The band gap depicts the energy difference between the valence band maxima and the conduction band minima. However, these do not always occur at the same value of electron momentum and this has massive impact on properties of crystal. In a direct band gap semiconductor, the top of the valence band and the bottom of the conduction band have the same momentum as shown in Fig. 3 (left). On the other hand, in an indirect band gap semiconductor, the valence band maxima and the conduction band minima do not align (they have different values of electron momentum) as shown in Fig. 3 (right).

For a transition between the valence band and the conduction band to occur the energy supplied must be greater than or equal to the band gap and the momentum must be conserved. In a direct band gap semiconductor, a photon of energy E_g (where E_g is the band gap energy) can lead to the transition of an electron from the valence band to the conduction band resulting in the formation of a bound electron-hole pair because the the top of the valence band and the bottom of the conduction band have the same momentum. However, in an indirect band gap semiconductor, this transition requires the addition or subtraction of momentum in order to satisfy conservation of momentum condition. The transition in indirect band gap semiconductor occurs via interaction of the electron with a photon as well as a phonon (lattice vibration) in order to gain/lose momentum. The indirect transition generally has lower excitation probability than the direct one because the former one involves three-particle interaction.

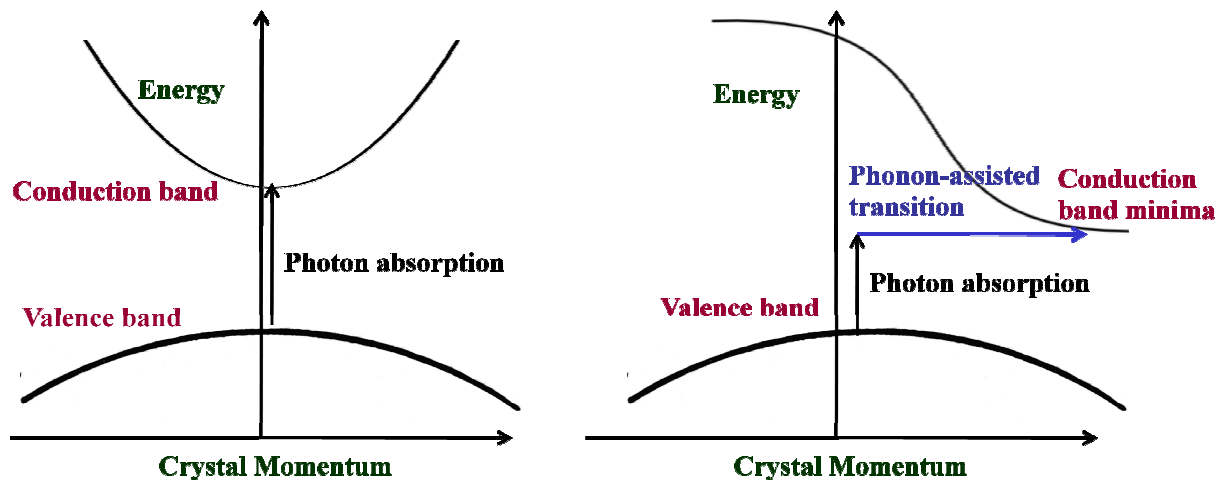


Figure 3: Demonstration of direct (left) and indirect band gap (right)

PREVIOUSLY REPORTED SYNTHETIC METHODS FOR INDIUM NITRIDE (InN)

This thesis will mainly focus on synthetic strategies to prepare colloidal indium nitride. The first report of III-nitrides synthesis was in 1938 by Juza *et al.* who synthesized GaN and InN crystallites.²⁰ Various groups have attempted the synthesis of InN nanocrystals using solution-phase routes, including hydrothermal,²¹ solvothermal,²²⁻²⁴ and thermal decomposition of molecular precursors.²⁵⁻²⁹ The outcomes of these approaches are generally large agglomerations of nanocrystalline InN, with non-uniform size and morphology distribution of nanocrystals. There are still no reports of high-yield or colloidal solubility of these nanocrystals in organic or aqueous solvents. The precise control over the size and shape of the nanomaterials is often not achievable by other methods. However, the chemistry behind the formation of III-V compounds is rather different than that of the more conventional II-VI semiconductor nanocrystals. The reason behind this is the greater covalent nature of the III-V materials and hence the organometallic precursors often used for their synthesis are not stable and can form complexes

with the solvent.³⁰ The nucleation and growth events which need to be separated in order to achieve monodispersity become high-energy processes and tend to occur simultaneously in the synthesis of these materials.³¹⁻³³ Other techniques for synthesis of indium nitride nanocrystals include ammonolysis,³⁴ dc-arc plasma,³⁵ reactive laser ablation³⁶ and vapor-phase methods.³⁷ In these methods, nanocrystals often tend to agglomerate and exhibit poor size distribution and crystallinity. Recently, by molecular beam epitaxy (MBE) process, some groups have been able to grow high-quality crystalline InN which has wurtzite lattice type and a band gap of ~0.65-0.7 eV.³⁸⁻⁴¹ However a low cost, straightforward method with readily available precursors was yet to be developed. Hsieh *et al.*¹⁷ and Xie *et al.*²² have reported synthetic methods to prepare InN nanocrystal by a simple blend of solution route and thermal decomposition method. However, no effect of quantum confinement have been demonstrated in these nanocrystals and superior size distribution has not been achieved either.^{41,42} Very recently Chen *et al.* has successfully prepared monodispersed InN nanoparticles by combining solution- and vapor-phase methods under silica shell confinement. These nanocrystals are reported to have cubic lattice type and band gap around 0.58 eV.⁴³ In this particular report too, the matter of control over size has not been addressed. We have attempted to resolve these significant concerns by developing a new synthetic approach that produces monodispersed InN nanocrystals with uniform size distribution and better colloidal solubility in organic media. Recently Nathan R. Neale, *et al.*⁴⁴ have modified a colloidal synthesis of 4-10 nm diameter indium nitride (InN) nanocrystals that exhibit both a visible absorption onset (~1.8 eV) and a strong localized surface plasmon resonance absorption in the mid-infrared (~3000 nm). This material was prepared keeping the goal in mind to make a nanostructure which will combine both metal and semiconductor properties which is believed to be of importance in the field of telecommunication and optical tuning of plasmonic devices.

They were able to change the absorption onset and the Plasmon energy by oxidation-reduction technique which does not alter the chemical composition of the substance but pushes the Fermi level of the semiconductor material. Thus we can see that though so far several attempts have been made to synthesize optically tuned colloidal InN nanocrystal much success has not been achieved in controlling these properties from fundamental aspect that is by manipulation of the size and morphology of the material. In our work we would like to shed some light on this area.

MOTIVATION FOR MOVING TO THE NANO REGIME

The origin of quantum confinement in QDs arises from the spatial confinement of electrons within the crystallite boundary. This effect is observed when the size of the particle is comparable to the wavelength of the electron. With decrease in size of material to nano-dimensions, the decrease in confining dimension make the energy levels discrete; which in turn leads to an increase of the band gap energy. Qualitatively the quantum confinement effect is analogous to the problem of a particle in a box and efforts to quantify confinement effects have been topic of considerable research for more than three decades now.^{45,46,47} In this regard, exploring the properties of InN and other III-V materials in nanoregime would be really interesting. Other than studying quantum physics in these small structures; another urge that boosted a lot of attention in this field was the necessity to miniaturize devices. The advantage of small devices being the higher density of integration, faster response, lower cost and low power consumption. The increasing demand for faster computer processors and high-capacity memory devices has been motivating the microelectronics industry to decrease the size of individual parts and components.

COMPARISON TO THE BULK MATERIAL

Bulk semiconductors are characterized by a composition-dependent band gap energy (E_g). With the absorption of a photon, an exciton is created. The minimum energy required to excite an electron from the valence band into the conduction band is $E_g - E_b$ (where E_b is the binding energy of the exciton). The exciton has a finite size within the crystal characterized by the Bohr excitonic radius (distance between the electron-hole pair a_{exc}), which can vary from less than 1 nm to more than 100 nm depending on the material.

$$a_{exc} = \frac{\epsilon_s m_0}{\mu} a_B \dots\dots\dots(1)$$

where a_{exc} is the Bohr excitonic radius of the semiconductor material

ϵ_s = static dielectric constant of the material

m_0 = mass of the free electron

a_B = Bohr radius of the hydrogen atom

$$\mu = \frac{m_e m_h}{m_e + m_h} \dots\dots\dots(2)$$

μ = reduced mass of the exciton

$m_{e(h)}$ = effective mass of electron (hole)

If the size of a semiconductor nanocrystal is smaller than the size of the exciton, the charge carriers become spatially confined, which raises their energy due to the inclusion of the confinement energy term (energy required to confine the exciton to a radius smaller than the

Bohr exciton radius). Dimension(s) of this confinement in the case of spherical nanoparticles refers to the diameter of the nanocrystal which needs to be comparable or less than twice the Bohr radius of excitons in the bulk material.³

The energy of the exciton in a QD is greater than the bulk semiconductor as shown in (Equation 3) where $E_{confinement}$ is the confinement energy of the exciton and $E_{coulombic}$ is the coulombic energy term resulting due to the attraction between the electron-hole pair. Thus, the smaller the size of the crystal, the greater the quantum confinement and greater the difference in energy between the highest valence band (VB) and the lowest conduction band (CB) energy levels, and thus greater energy is required to excite the electron from VB to CB.

$$E_{exciton} = E_{bandgap}(bulk) + E_{confinement} \dots\dots\dots(3)$$

It is a well known fact that when charge carriers (electrons and holes) are restricted by a potential barrier leading to quantization effect they manifest exciting properties like size-tunable absorption and emission wavelengths, discrete electronic transitions (Fig. 4), high quantum yield.^{1,2} The radiative recombination rate constants of semiconductor QDs are substantially larger than those of their bulk counterparts because of the localization of the exciton in the QDs compared to the bulk semiconductors.^{4,48} Narrow band gap semiconductors, including III-V compounds are emerging as an important class of materials and are attracting lot of attention because of their potential as emitters in the infrared region, and thus possible applications in telecommunication and biomedical fields.⁴⁸⁻⁵⁰ The prospect of generating multiple excitons induced by spatial confinement in narrow band gap semiconductor nanocrystals like InN results in considerable enhancement in the performance of optoelectronic devices, such as solar cells and low-threshold lasers.^{51,52} It is very important to note that owing to their covalent nature, the

III-V semiconductor nanocrystallites generally have smaller effective mass and larger dielectric constant which results in a larger Bohr excitonic radius (Equation 1) compared to II-VI or IV-VI materials. This can potentially lead to some phenomenal, unprecedented quantum confinement properties.^{1,48-50,53}

This makes the III-nitrides and their respective alloys a very interesting class of materials to explore. However, these are among one of the least studied class of materials primarily due to the challenges encountered in synthesis of high quality, crystalline, monodispersed InN nanoparticles.^{41,54} InN is chemically quite inert and is a direct band gap semiconductor with the band gap $\sim 0.65-0.7$ eV.^{41,55,56}

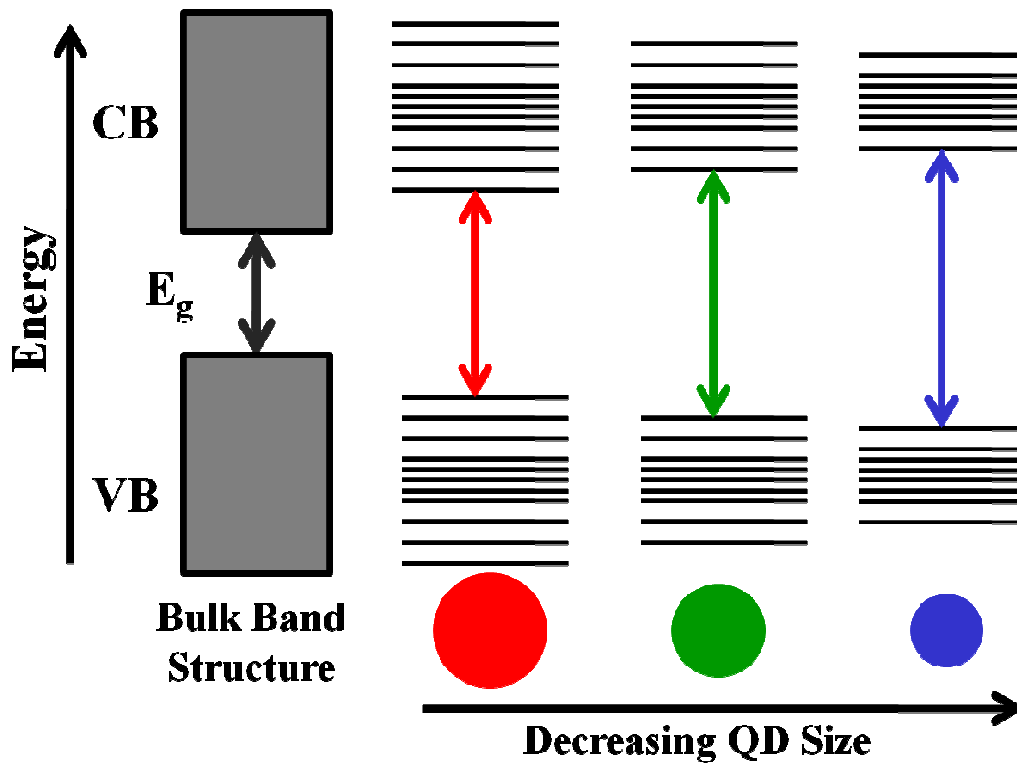


Figure 4: Increase in band gap with decrease in size of the semiconductor nanomaterial or quantum dot due to the quantum confinement effect

However, the band gap of InN was once thought to be 1.9 eV for quite some time; until it was found to be incorrect in 2001 reported by Davydov et. al and following studies.⁵⁷⁻⁶¹ This controversy regarding the band gap of InN will be addressed in details in the next section. By alloying with other III-nitride material, InN can be transformed into an excellent candidate for broad-spectrum solar cell⁶² and equally promising as nanocrystalline phosphors spanning a wide range of the optical spectrum. Thus, exploring the synthetic possibilities of InN and understanding its intrinsic material properties has provided a great deal of motivation to develop a method to prepare size tunable indium nitride nanoparticles.

THE BAND GAP CONTROVERSY OF INDIUM NITRIDE

The optical band gap value of InN was first traced in 1986. For the first time a distinct optical absorption feature at ~ 1.9 eV was observed by Tansley and Foley.⁵⁹ The InN samples showing that particular absorption edge were grown by radio frequency (RF) sputtering of a metallic indium target in nitrogen atmosphere. Optical analysis was conducted by optical absorption and electrical measurements were performed on photo lithographically defined clover leaf contacts. These polycrystalline InN films were found to be *n*-type in nature and these films were reported to exhibit a maximum mobility of $5000 \text{ cm}^2/\text{Vs}$ at 150 K and room temperature electron mobility of $2700 \text{ cm}^2/\text{Vs}$.⁶³ The value 1.9 eV was accepted as an official band gap for a while; as other reports supported this finding.^{58,64,65} With increasing sophistication in MOCVD and MBE techniques it was possible to grow epitaxial InN films. In a short communication published in 2001; Davydov *et al.* claimed to observe a prominent absorption peak as well as strong photoluminescence (PL) signal located below 1 eV (close to 0.9 eV) for InN single crystal grown by MBE.⁶⁶ This was subsequently supported by different publications from Wu *et al.*⁶⁷ and Matsuoka *et al.*⁵⁵ who also found evidence in InN grown by MBE and MOCVD methods with a band gap near 0.7 eV. These reports triggered re-evaluation of InN properties and progressively lower optical band gap in the range of 0.65-0.80 eV was confirmed and other crucial parameters were naturally re-investigated.

There are several issues that can be identified as reasons for the wide range in reported values for the InN band gap. GaN and AlN are two other nitride semiconductors known to show evidence of absorption onsets and PL feature. These properties originate from deep traps within the band gap.⁶⁸ In some cases these effects can play a significant role in governing optical measurements. Thus a similar phenomenon seemed very possible for InN. Within some InN films traces of

metallic indium were found and Shubina *et al.* argued that the luminescence from InN films increased to a great extent in regions around these metallic clusters.⁶⁹ This raises the possibility that the emission ~ 0.7 eV could be a result of Mie resonances. Later, Specht *et al.* used valence electron energy loss spectroscopy (VEELS) technique to demonstrate that InN could apparently show an absorption onset near 1.7 eV. After this; additional doubts were raised that this process could induce electron damage on the sample its resulting effect.⁷⁰ Even the ratio of In:N in the InN cluster can affect the band gap of the material which has been illustrated by Butcher *et al.* They have shown that the stoichiometry of indium and nitrogen in InN films can be different and not 1:1 necessarily. Their work suggests that InN with excess In metal in the cluster or a different In:N ratio (other than unity) can be considered as In_xN_y alloys with varying composition and could be possible explanation behind wide variety of results in determining the band gap.^{68,71} Davydov *et al.* and Wu *et al.* have however claimed that the higher absorption features observed can be described in terms of the Burstein-Moss effect.^{72,73}

The Burstein-Moss effect :

When all states close to the conduction band of a semiconductor material become populated (by electrons) and as a result the apparent band gap of a semiconductor is increased by driving the absorption edge towards higher energy, the phenomenon is known as Burstein-Moss effect. In some cases where degenerate semiconductors (a semiconductor with such a high level of doping that the material starts to act more like a metal than a semiconductor) are involved (in this case InN with the presence of excess In metal) degenerate electron distribution is found to take place and it is called Burstein-Moss shift (Fig. 5).

This kind of shift takes place when the electron carrier concentration surpasses the conduction band edge density of states. This factor actually happens to depend on the degenerate doping level in semiconductors. Semiconductors, that are doped by a small amount, for those the Fermi level lies between the conduction and valence bands. As the doping concentration is increased, electrons populate states within the conduction band. This results in pushing the Fermi level higher in energy and in the case of degenerate level of doping, the Fermi level lies inside the conduction band. In these cases the "apparent" band gap of a semiconductor can be determined using various spectroscopic methods. If we consider a degenerate semiconductor, the Fermi level lies in conduction band and all the states below the Fermi level are occupied. An electron from the top of the valence band can only be excited into conduction band above the Fermi level. Since the Fermi level resides inside the conduction band Pauli's exclusion principle forbids excitation into these occupied states. For this reason an increase in the apparent band gap is observed. So the new band gap that we see is the sum of actual band gap + Moss-Burstein shift (as shown in Fig. 5).

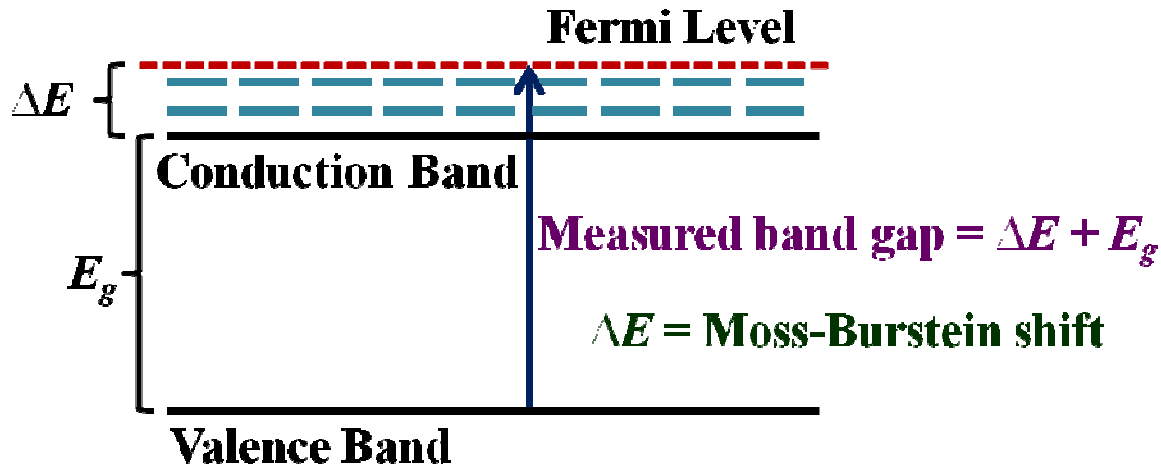


Figure 5: Origin of the Burstein-Moss shift

Effect of oxygen impurity :

It is known that indium oxide (In_2O_3) is an indirect gap material with a band gap near 3.75 eV.⁷⁴ In several cases InN films have been found to possess oxygen contamination. Some of them were due to drawbacks of the synthetic procedure whereas some were due to oxidation of the sample after preparation or while performing measurements. Though it has been known for a while that InN films are prone to oxidation at the surface; yet how this influences the outcome of the electrical and optical properties is still an unresolved puzzle. It has been previously suggested that the higher oxygen concentration in these films results from sputtering and is the inherent reason behind the higher band gap that is observed during the characterization of this material. This is simply because InN- In_2O_3 alloys will definitely have wider absorption edge than InN.^{73,75,76} This theory is indeed supported by the fact that many polycrystalline films exhibit strong correlation between oxygen content and absorption onset which has been shown by Yoshimoto *et al.*⁷⁵ Later, Bhuiyan *et al.* used different growth techniques to produce films of

variable oxygen content and it was found that absorption edges again appeared to correlate with oxygen composition.⁷⁶ However, it has been suggested by Monemar *et al.*,⁶⁹ that the measured oxygen content in these films appears to be inadequate to account for a shift from 0.7 eV to 1.9 eV assuming common levels of band gap bowing. It has also been noted that some reports show that In₂O₃ in fact separate out within the InN lattice and do not form alloy. If that is the scenario then additional absorption feature should be observed near 3.75 eV which happens to be the band gap of In₂O₃ and not 1.9 eV. Davydov *et al.* also entertained the possibility of oxygen inducing background electron concentration that results in occupied states well above the conduction band minimum (CBM). In such cases, absorption transitions to empty conduction band states occur at energies larger than the band gap energy value which lead to Burstein-Moss effect. Theoretical simulation has predicted that the Moss-Burstein occupation can extend the absorption energy as much as 2 eV for InN.⁷²

SCOPE OF THE THESIS

Despite the prospect of utilizing InN in many interesting applications, this material is still in its infancy in terms of our understanding of the preparation and optoelectronic properties of this material. The highest quality epitaxial layers prepared to this date still have high dislocation densities and heavy *n*-type conductivity. Understanding the origin of this *n*-type conductivity and eventually producing *p*-type InN will be a major step forward. On the other hand, resolving the band gap controversy would reveal the utility of this material for infrared optics and high power HEMTs. This thesis considers all these aspects of InN in details. Particular emphasis has been given on developing a very easy, scalable, inexpensive method to synthesize high quality

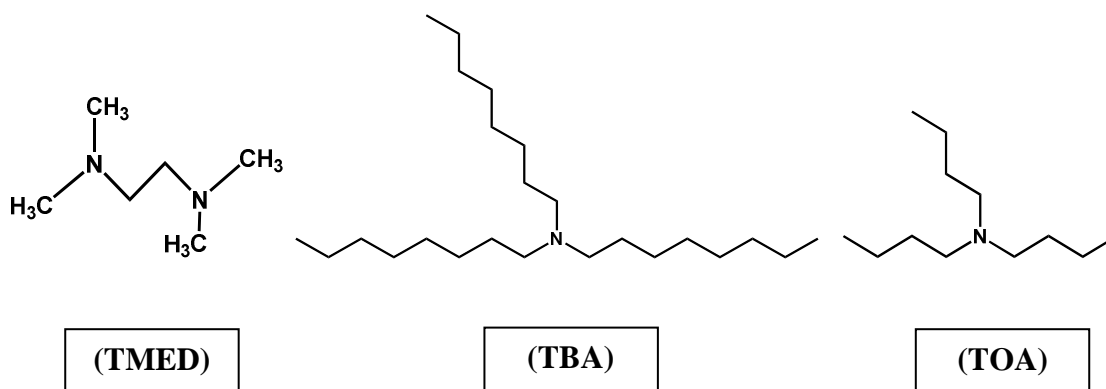
crystalline colloidal InN QDs. This has been attempted by different research groups all over the world without much success until now. Attempts have been made to address the band gap query by using the traditional techniques like absorption and photoluminescence (PL) spectroscopy. A number of techniques like transmission electron microscopy, electron diffraction, X-ray photoelectron spectroscopy have been used to characterize the synthesized materials and to find out the size, shape, crystallinity and further relate them to the electronic band structure.

The enormous synthetic challenge to prepare a good quality material was the biggest inspiration to work in this area. The greater covalent nature of the III-V material makes these more difficult to prepare. The list includes InN, InP and InAs. In order to achieve a narrow size distribution in colloidal particle synthesis, temporal separation between particle nucleation and particle growth is necessary. This can be easily obtained with II-VI materials by rapid introduction of the required precursors (usually discrete ions) into a solvent of choice, which results in immediate nucleation followed by slow particle growth.⁷⁷ The III-V materials being more covalent, it often becomes really difficult to find precursors that can achieve similar results like the II-VI nanocrystal synthesis. The organometallic precursors often used in the preparation of III-V materials are not stable enough and can complex with the solvent instead.⁷⁸ The nucleation and growth steps in these cases have individual high energy barriers and separating them from each other become rather difficult. The materials prepared by such methods are generally of a lower quality unlike the II-VI analogues. Despite the difficulties in preparation, the III-V materials seem ideal candidates to examine size quantization effects, as the excitonic Bohr radius is much larger than for the analogous II-VI compounds. This means that particles should display phenomena such as the 'blue shift' in the band edge at relatively large crystal sizes, making investigations into strongly confined nanostructures achievable.

CHAPTER 2: EXPERIMENTAL SECTION

MATERIALS

The following chemicals were used for the different synthesis protocols. Indium (III) bromide, (InBr_3), anhydrous (99.999% In; Strem Chemicals) [MW: 354.530 g/mol]; sodium amide (NaNH_2)(94%; Alfa Aesar) [MW : 39.01 g/mol], oleylamine (OLA) (min. 40% assay; VWR), (min. 70% assay Sigma Aldrich) [MW: 267.49 g/mol, density : 0.813 g/mL], octadecene (ODE) (90%; Sigma Aldrich) [MW: 252.48 g/mol, density: 0.789 g/mL], oleic acid (OA) (90%; Alfa Aesar) [MW: 282.47 g/mol, density: 0.8946 g/mL], *N,N,N',N'*-tetramethylethylenediamine (TMED) (99%; Sigma Aldrich) [MW : 116.20 g/mol, density : 0.775 g/mL], tributylamine (TBA) (98.5%; Sigma Aldrich) [MW: 185.35 g/mol], trioctylamine (TOA) (98%; Sigma Aldrich) [MW : 353.67 g/mol], n-Butyllithium solution; 2.5 M in hexanes [density of solution 0.693 g/mL at 25 °C, MW of butyllithium 64.06] and lithium dimethylamide $\text{LiN}(\text{CH}_3)_2$ (95% ; Sigma Aldrich). All the chemicals were used as received.



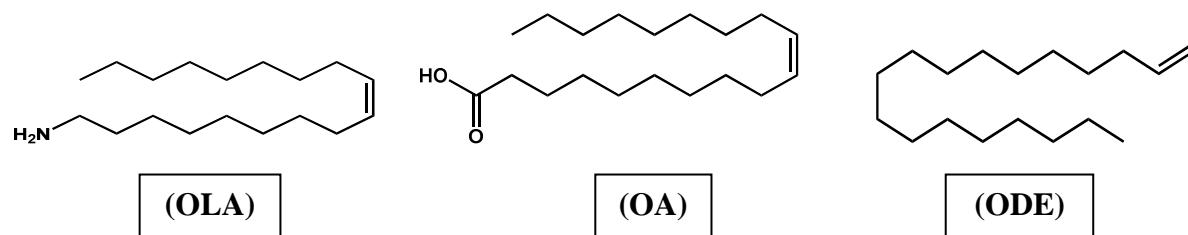


Figure 6: Molecular structure of some chemicals used for different synthesis

INSTRUMENTS

The Powder X-ray diffraction (PXRD) pattern was recorded on the Bruker Davinci Diffractometer ($\text{Cu K}_\alpha = 0.154 \text{ nm}$). The QD solution was drop-cast on zero-background silica plates for PXRD measurements. The Transmission electron microscopy (TEM) images were recorded on a JEOL2200FS transmission electron microscope operating at 200 keV. Formvar-coated copper grids were used as nanocrystal supports for TEM. Absorption spectra were measured on a Hitachi U-4001 spectrometer and a OLIS17 UV/VIS/NIR spectrometer. The Perkin Elmer Phi 5600 ESCA system was used for X-ray photoelectron spectroscopy (XPS) analysis with a magnesium K_α X-ray source at a take-off angle of 45° . Raman spectra were measured with a Labram ARAMIS Horiba Jobin Yvon Raman spectrometer, equipped with an Ar^+ ion laser as a light source. Argon ion lasers emit at 13 wavelengths through the visible, ultraviolet, and near-visible spectrum, including: 351.1 nm, 363.8 nm, 454.6 nm, 457.9 nm, 465.8 nm, 476.5 nm, 488.0 nm, 496.5 nm, 501.7 nm, 514.5 nm, 528.7 nm, 1092.3 nm. For the PL experiments, the emission of the QDs was monitored using a Horiba Jobin Yvon Fluorimeter with a InGaAs array (IGA-1024*1-25-1700-3LS). The grating used is 300 grooves/nm, blazed at

2000 nm. The lifetime measurements were recorded using a Time-correlated single photon counting (TCSPC) set up. The acquisition electronics is Pico-Harp 300 from Picoquant. The detector is a single photon detector from AUREA for infrared range (900-1700 nm). The laser used for the experiment is a 405 nm laser from Opto Engine LLC (MLL-III-405nm-100mW) and 532 nm laser from LASOS Lasertechnik GmbH (GLK-3250 T01). ICP-OES was done using 710-Axial ICP instrument.

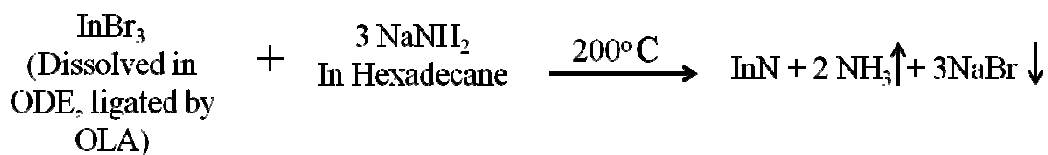
SYNTHESIS USING INDIUM NITRIDE NANOPARTICLES USING SODIUM AMIDE

Based on previous reports it seemed that formation of indium metal as a by-product of InN nanoparticle synthesis is a common occurrence.⁷⁹⁻⁸¹ Some researchers have deliberately avoided the use of InBr₃ as a precursor stating the weaker covalent bond nature of InBr₃ (lower melting point than the chloride and fluoride) to be responsible for formation of In metal.^{82,83} Belcher *et al.* attempted to synthesize InN from thermolysis of In(NH₂)₃ complex and had some success, though it was not a stable colloidal solution and the samples did not exhibit any quantum confinement effects.⁴¹ We have revisited this synthetic method as a starting point towards our goal of synthesizing high quality crystalline colloidal InN nanoparticles. The added advantage of this synthetic method was the commercial availability and relatively inexpensive nature of the precursors used in this procedure. It has been observed that the indium metal impurities could be easily removed by oxidizing the mixture using dilute nitric acid (~4%). Following this process with slight modifications in the synthetic procedure, colloidal InN nanocrystals were successfully obtained.

In this synthetic procedure 1 mmol (0.3543 g) of InBr₃ is taken in 7.59 mmol (2.5 mL) OLA and 5.0 mL ODE (both degassed with nitrogen gas). This mixture is stirred and heated at 150°C until a clear mixture is obtained; indicating that InBr₃ has been solvated in the nonpolar solvent. 3 mmol (0.127g) NaNH₂ is taken in 10 mL hexadecane (HD) and heated up to 220°C. The sodium amide salt which is melted and dissolved in the hexadecane, results in a homogeneous dispersion of the reactive amide anion (⁻NH₂). The InBr₃ solution is then injected into the amide solution using a glass syringe at 180°C and the temperature is slowly ramped to 250°C over a period of two hours. The solution remained at this temperature for 4 hours and then was slowly cooled down to room temperature over a time period of 2 hours. The transparent solution starts turning

grey over time and after about two hours of heating turns completely black. The product is centrifuged at 3000 rpm and washed with 5.0 mL hot ethanol (~50°C) several times to get rid of bromide salt and then redispersed in 5.0 ml hexane. At this point the product contains some In metal impurities which are oxidized to soluble nitrate form by adding 2 ml dilute (4%) nitric acid. The sample is washed with 5 mL ethanol and then sonicated and if colloidal suspension is not obtained then the sample is heated and stirred with 5.0 mL OLA (min. 40% assay from VWR) at ~40°C to effectively ligate the surface of the nanocrystals. The InN nanocrystals are finally dispersed in toluene. It is important to make sure that during the washing procedure only the sodium bromide and indium nitrate is removed and not the indium nitride particles. In order to avoid removal of indium nitride particles controlling the centrifugation rate is crucial. Indium nitride particles do not precipitate out if the centrifugation is done at 3000 rpm or at a lower speed.

The reaction pathway can be described by the following (Equation 4):



We have adopted the above method in order to bring the effect of hot-injection method in the reaction media and to have most of the precursor materials react at once. The hot injection method involves the injection of a “cold” (room temperature) solution of one precursor molecules into hot solution of another precursor. The temperature of injection (the temperature of the hot solution at which the other solution is injected) should be high enough for the nucleation to occur. Thus, the injection leads to the “instantaneous” formation of nuclei of the desired product. Due to a drop in temperature on addition of the cold component, the formation

of new nuclei is prevented. The result is a suspension of reasonably monodispersed nuclei together with considerable amounts of free precursors. Increasing the temperature to higher values, but maintaining it below the nucleation temperature, results in slow growth of the existing nuclei. The greatest advantage of this method is that the nucleation and growth events are well-separated resulting in a very reasonable size dispersion of the nanocrystals.

Though, by using this procedure we are able to synthesize pure InN nanocrystals, the main drawback of this procedure is that despite carrying out several variations in the solvent used in synthesis, reaction temperature, post-synthesis treatments and washing procedures we could not obtain good quality absorption data. We thought, this can be result of two factors, either the nanocrystals were so large in size that it is not possible for them to stay dispersed in the solvent or the polar nature of the surface of the nanocrystals which prevents them from being efficiently solubilized in the nonpolar media. The structure of these materials obtained from Powder X-ray diffraction (PXRD) measurement correspond to wurtzite phase InN with crystallite size over 20 nm (obtained through Scherrer analysis). This is consistent with that observed in the transmission electron microscopy (TEM) images as shown respectively in Figs 7 and 8.

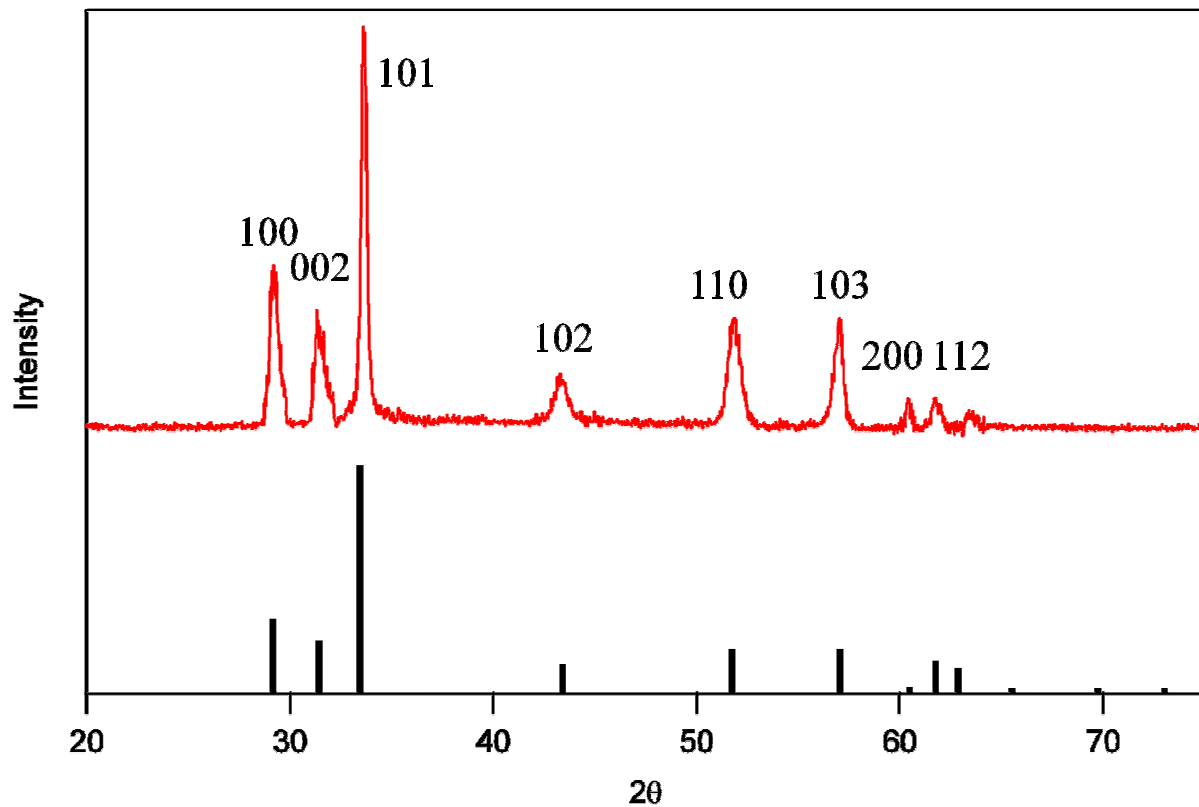


Figure 7: PXRD pattern of InN nanoparticles; Crystallite Size ~20 nm Structure: Wurtzite; System: Hexagonal; PDF: 01-074-0244; Space Group: $P6_3mc$

The PXRD pattern of the synthesized nanocrystals matches very well with previously published wurtzite phase bulk InN semiconductor and InN nanostructures.^{83,84} The first three d values are 3.162, 2.954, 2.528 Å corresponding to [100], [002] and [101] plane with lattice parameters $a = b = 3.558\text{Å}$, $c = 5.752\text{Å}$. From the TEM images; the size of the nanoparticles were confirmed to be around 15~20 nm. The crystal fringes were not visible due to the large size of particles but selected area electron diffraction (SAED) pattern confirmed the presence of crystalline InN.

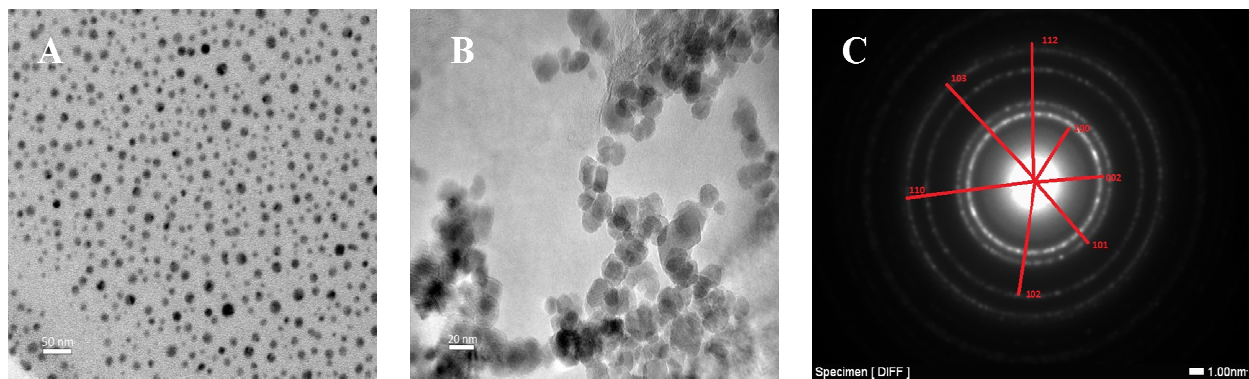


Figure 8: TEM image of InN nanoparticles in hexane (A), (B). The Selected Area Electron Diffraction pattern corresponding to the wurtzite phase of the nanocrystals (C)⁵⁵

To obtain good quality colloidal nanoparticles an additional ligand which can also act as a proton scavenger is introduced to strip off the protons from the surface of the particles which presumably should make them more soluble in non polar solvents. So, we included 5 mmol (1.25 mL) tributylamine (TBA) in the synthesis which has the possibility of acting also as a ligand. Post synthetic procedure for this experiment was carried out the same way as described for the previous experiment. The product of this method seems to be more stable in non polar solvents and methylene chloride (CH_2Cl_2) appears to work as the most efficient one to successfully solubilize the nanoparticles. The absorption spectra are recorded in tetrachloroethylene (TCE) and the excitonic feature is observed at 0.873 eV which is the first direct evidence of quantum confinement in InN nanocrystals (Fig. 14). As we can see in Fig. 9, the PXRD pattern of the sample prepared by this method confirms the wurtzite phase of the lattice. The energy-dispersive X-ray spectroscopy EDS (Fig. 10) acts as an evidence for the presence of the element In in the material. From the TEM images (Fig. 11) we can see that the average diameter of these particles

are around 8 nm which is smaller than the Bohr radius of InN, generally considered to be ~10 nm.^{85,86}

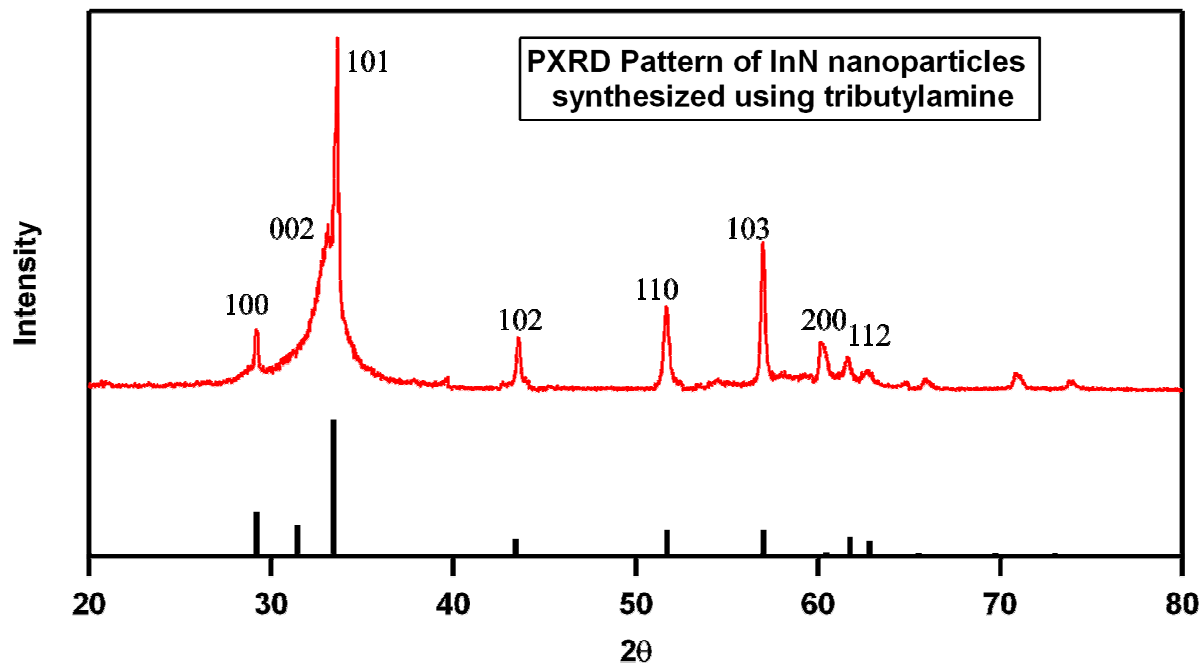


Figure 9: The PXRD pattern of the InN sample using tributylamine, agrees to wurtzite phase of InN

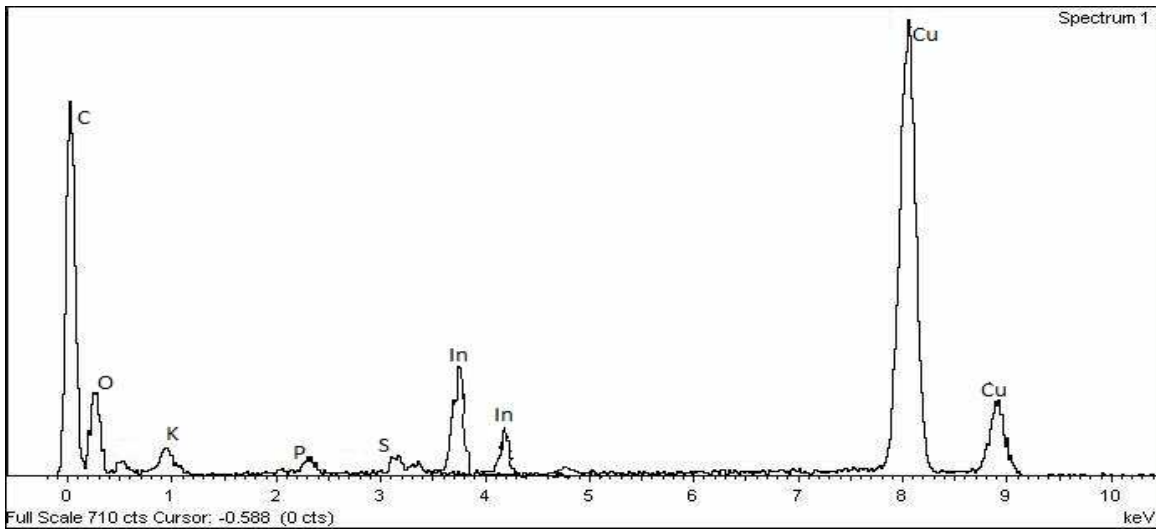


Figure 10: The EDS pattern of the sample prepared with TBA which shows presence of Indium

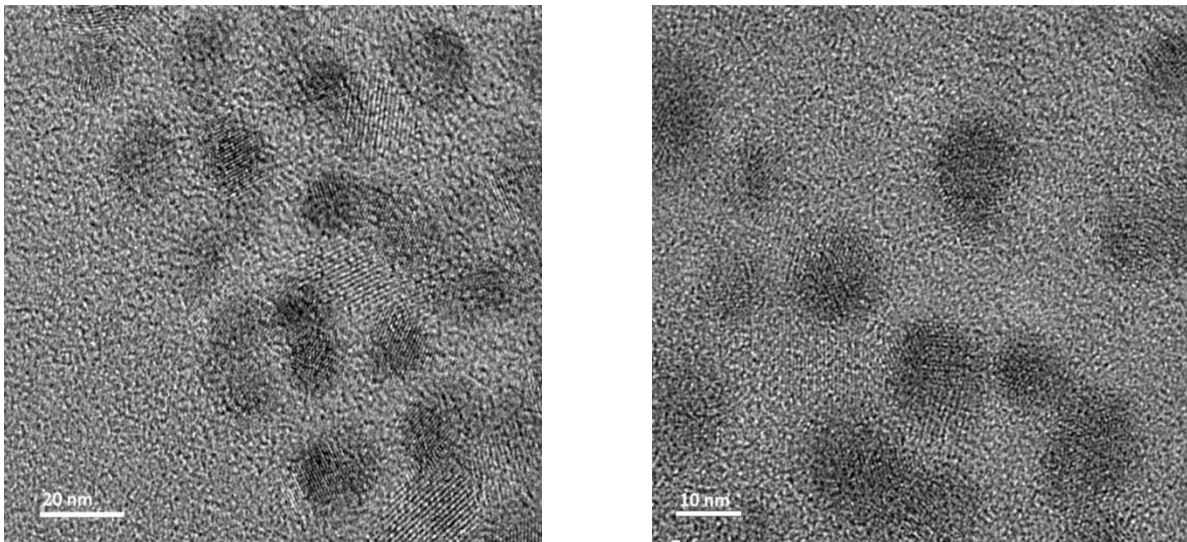


Figure 11: TEM images of InN nanoparticles synthesized using TBA

CRYSTAL SIZE ANALYSIS

The Scherrer Equation is a popular method to estimate crystallite size of nanoparticles.^{87,88} This equation relates the size of sub-micrometre particles, or crystallites, in a solid to the broadening of a peak in a diffraction pattern. Here, in Fig. 12 the peak corresponding to 110 plane (at $2\theta = 51.9^\circ$) is chosen for Scherrer analysis. The following formula is used to calculate crystal size.

$$B = \frac{K\lambda}{L \cos \theta_B} \dots\dots\dots(5)$$

L = Size or thickness of crystallite

K = constant dependent on crystallite shape (0.89)

λ = x-ray wavelength (0.154 nm)

B = FWHM (full width at half max) or integral breadth (in radian); $0.79^\circ = 0.014$ radian

θ_B = Bragg angle ($51.874^\circ / 2 = 25.937^\circ$)

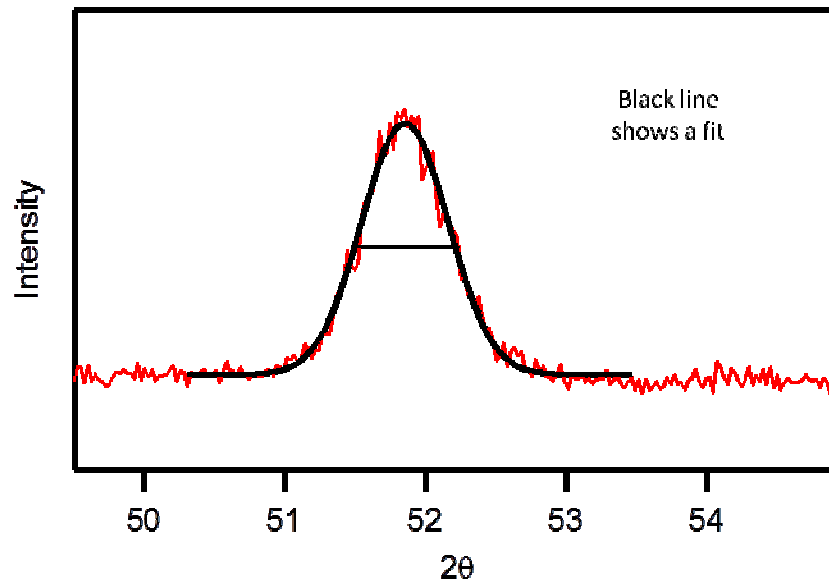


Figure 12: Scherrer analysis to find crystallite size. Plugging in the values above the size of the nanocrystal is calculated to be 10.9 nm.(However this kind of analysis can give us 20%-30% accuracy at best)

One of the limitations of scherrer formula is that it provides lower bound on the particles size. Various factors contribute to the broadening of the peak, out of which most important ones are inhomogeneous strain and crystal lattice imperfection.

SYNTHESIS OF INDIUM NITRIDE BY THERMOLYSIS METHOD

In this method 1 mmol (0.3543 g) of InBr_3 is taken in 7.59 mmol (2.5 mL) OLA and 5.0 mL ODE and 3 mmol (0.153 g) of lithium dimethylamide, $\text{LiN}(\text{CH}_3)_2$ was taken in 15.0 mL hexane and stirred at room temperature (r.t.) for 2 days and 7 days in two different experimental setup. Then the supernatant solution from this mixture was carefully taken out and was heated at 200°C under inert atmosphere (nitrogen gas) for 48 hours. The transparent colorless solution which contains the indium precursor turns black almost after a day of heating and the color turns deeper with time indicating formation of InN nanoparticles. In this process it is considered that $\text{In}(\text{N}(\text{CH}_3)_2)_3$ is formed and then it dissociates at high temperature to form crystalline InN. Aliquots were taken during the process to see any observable change. After the reaction was complete the reaction mixture was cooled down to room temperature. Then the aliquots were added to 5 ml hexane. The suspension of particles did not seem to be stable in hexane or any other usual non-polar solvent such as toluene or methylene chloride. PXRD was taken by drop casting the hexane solution containing the particles on a silica plate. The PXRD (Fig. 13) corresponds to wurtzite phase and TEM images (Fig. 15) shows crystallite size to be around 15-20 nm. We thought the particles were too large to be suspended in a solvent for long. The absorption spectra was taken by suspending these particles in tetrachloroethylene (TCE). Though it does not result in a good quality colloidal suspension, In the absorption spectrum (Fig. 14) we did see some feature but could not be convincingly assigned to any excitonic signature from the semiconductor. Since if a trace of the reactants used was left in the solution to be measured they could absorb in that region as well. If these were peaks from InN semiconductor then band gap of the material would determined to be $\sim 0.77\text{-}0.79$ eV; which is very close to the bulk InN in wurtzite phase.

The reaction scheme can be represented by the following equation. (Equation 6):

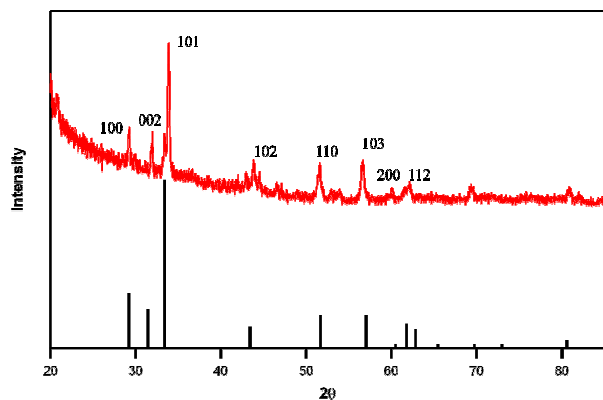
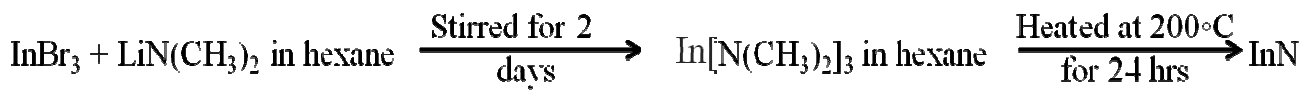


Figure 13: PXRD pattern of InN sample prepared by thermolysis method

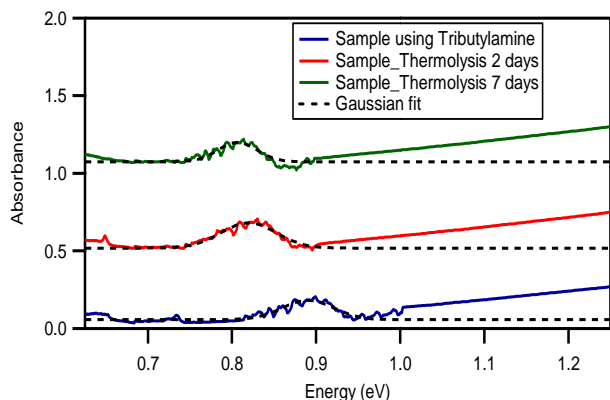


Figure 14: Absorption spectra of InN samples in TCE (Solvent)

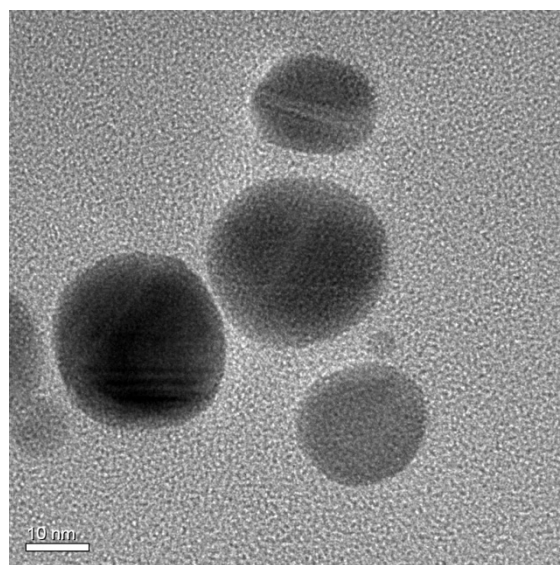
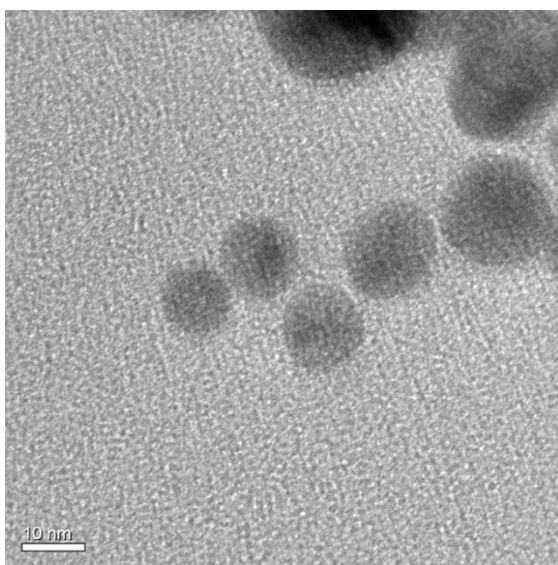


Figure 15: TEM images of InN sample prepared by thermolysis method

NEW APPROACH : SYNTHESIS OF INDIUM NITRIDE USING

TMED AS NITROGEN SOURCE

As it is quite evident, all the previous methods attempted have residual N-H bonds on the surface of the nanoparticles which leads to *n*-type doping of the material. This makes these particles more polar in nature and makes them unstable in colloidal suspension using non-polar solvent. We also hypothesized that absence of these polar extensions could be the reason for not having enough control over the nucleation and growth process. So, we wanted to find a precursor which will not contain these –N-H bonds which hints towards substituted amides. This led us to a precursor Tetramethylethylenediamine (TMED) which is stable in non-polar media.

Recently research group led by Horst Weller⁸⁹ published a method to prepare III-V semiconductor nanocrystals by transmetallation route where *n*-butyllithium (*n*-BuLi) is used as a reducing agent to produce metal nanoparticle in-situ which forms an organometallic precursor and later produces the desired compound by dissociating at high temperature. In this method trioctylphosphine (TOP) was used as the phosphorous source which is hypothesized to form a complex with indium (In) metal and then later form indium phosphide via thermolysis. We tried to replicate this method to prepare InN and attempted the synthesis using tributylamine and trioctylamine as the nitrogen source which resulted in mostly formation of In metal particles. Since, tetramethylethylenediamine (TMED) is known to form complex with metals it seemed to be logical to use it as a starting material. With TMED we not only hoped to take care of the solubility issue but being a bidentate ligand it acts as an effective source for nitrogen. Besides, previously used amide precursors used to serve the purpose of both nitrogen source as well as the

reducing agent. Here, having TMED as the source of nitrogen and *n*-BuLi as the reducing agent we expected the method to be simpler as well as more controlled.

In this procedure 1 mmol (0.3543 g) of InBr_3 is taken in 2.5 mL OLA and 5 mL ODE and stirred at around 150°C until a transparent solution (homogenous) was obtained. 3 mmol (0.3 mL) TMED was taken in 3 mL ODE and mixed into the previous solution. This mixture is stirred for 1 hour and the temperature is ramped to 250°C ; in the meantime 6 mmol *n*-BuLi (2.4 ml 2.5(M) solution in hexane) was dissolved in 3.6 mL ODE and was then drop wise added to the mixture of InBr_3 and TMED over an hour at a rate of 6 ml/hour using a syringe pump. The mixture starts to turn brown after about 15-20 min and then black precipitate starts to form which is believed to be In metal. The concentration of this black precipitate increases with time and the solution gets darker. After the addition of *n*-BuLi is complete; the reaction mixture is heated and stirred for another half an hour and then cooled to room temperature.

The aliquots from reaction mixture is then precipitated and washed with 5 ml ethanol and dispersed in hexane several times. The product shows maximum stability in methylene chloride but does not result into a good quality colloidal suspension which might be due to the residual polar nature of the surface of the particles. So, these particles are stirred at a little elevated temperature of 50°C with excess OLA (~10 mL) which increases the solubility of these particles in non polar media. The excess OLA is removed by washing with ethanol and then the particles are dispersed in 5 mL TCE.

The PXRD pattern of the final sample corresponds to wurtzite phase of InN (JCPDS no.:PDF-01-070-2547) (Fig. 17) [Refer to SI Table 1]. In the absorption measurement of the first two aliquots taken at 10 min and 20 min after starting addition of *n*-BuLi; no signature of InN band

edge has been observed rather it manifests occurrence of In metal in solution (Fig. 16(Left)). Absorption at ~ 400 nm is due to surface plasmon resonance absorption of In metal nanoparticles.^{90,91} The aliquot taken after half an hour of beginning the addition first shows some near IR absorption which is probably indication of formation of InN. The SPR peak still subsists which notify co-existence of In and InN in the mixture.⁸⁹ The aliquot taken at 45 min shows clear absorption feature of InN and semiconductor nature of the material. The band edge absorption of the samples range from 0.86 to 1.0 eV(Fig. 16(Right)). The PXRD of the sample taken at 30 min was amorphous meaning predominant presence of In metal nanoparticles (Melting point 159°C , supposed to be even lower for nanoparticles)(SI-Fig. S1). Significant broadening is observed in the initial sample compared to the final one which is indicative of the growth of nanocrystals.(Fig. S2).

The size of nanocrystals range from 5-9 nm (Fig. 18). The size distribution of the synthesized particles is quite narrow (10-12 %) (Figure S3). From the SAED pattern and also by measuring the distance between lattice fringes (the spacing between two lines is 0.27 nm which 101 plane in the hexagonal lattice) we can confirm the presence of InN (Fig. S4). In the absorption spectra, a shift of λ_{max} towards higher wavelength (lower energy) is observed in the aliquots taken at increasing time intervals (with time the nanoparticles grow in size) (Fig. 16(Right)). This is a manifestation of quantum confinement in the synthesized nanoparticles.

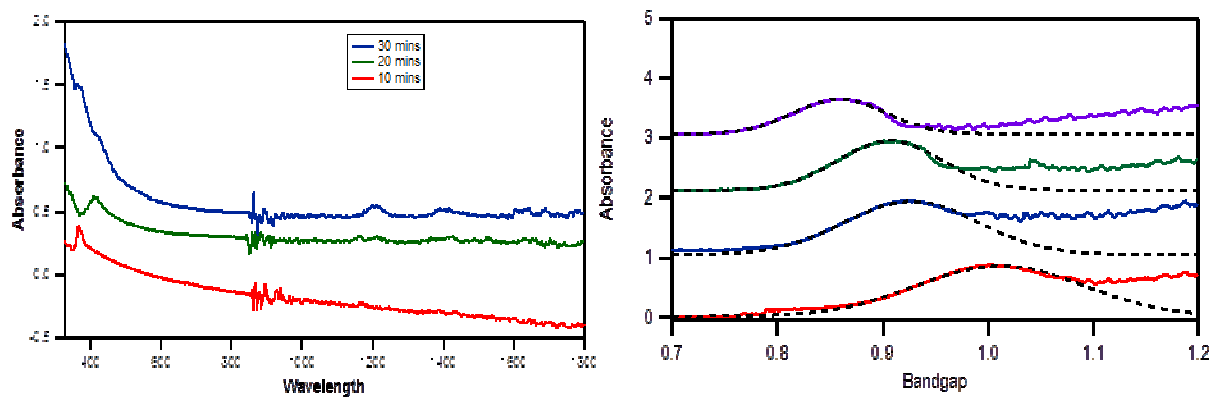


Figure 16: (Left) Aliquots drawn at 10, 20 and 30 min. (Right) Aliquots drawn at 45, 60, 75 and 90 min. The absorption spectra were measured with TCE as a solvent

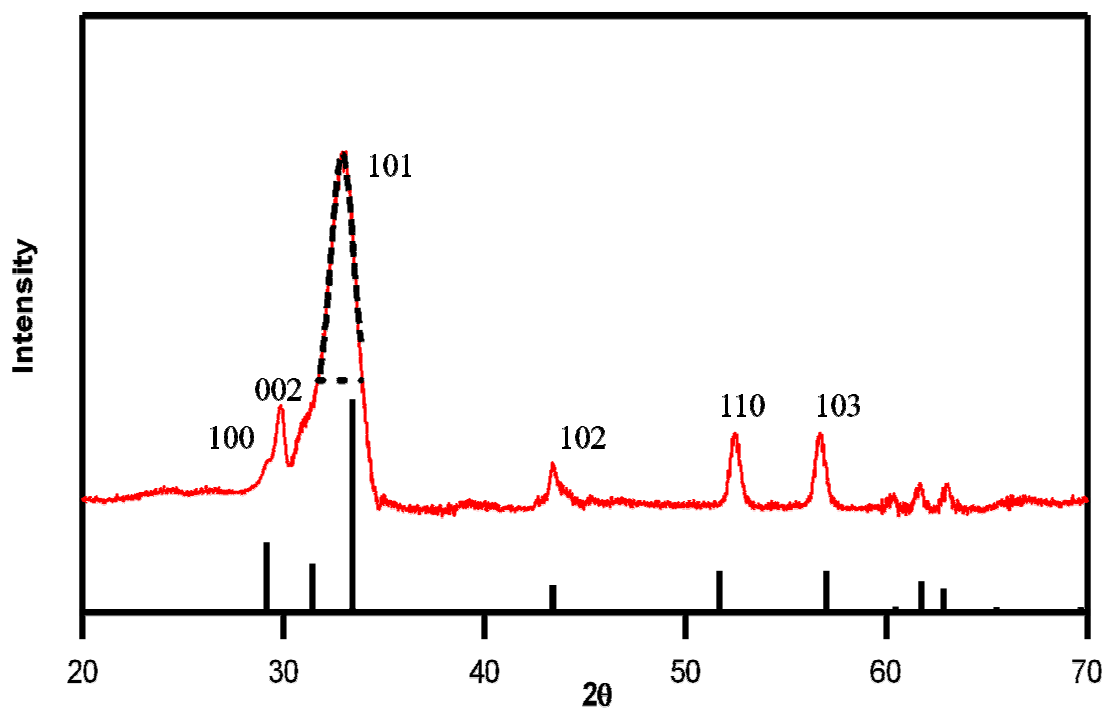


Figure 17: PXRD pattern of nanoparticles synthesized in the method described above. The black dotted line shows a Gaussian fit to only 101 signal to find out crystallite size

The two sets of three peaks at $28-34^\circ$ and $50-64^\circ$ correspond to wurtzite phase InN with lattice parameters $a = 3.543 \text{ \AA}$, $c = 5.752 \text{ \AA}$ and grain sizes of 12 nm. The lattice values are close to previously published values for InN nanopowders. The 101 peak contains a shoulder from the 002 signal which results in broadening of the 101 signal.

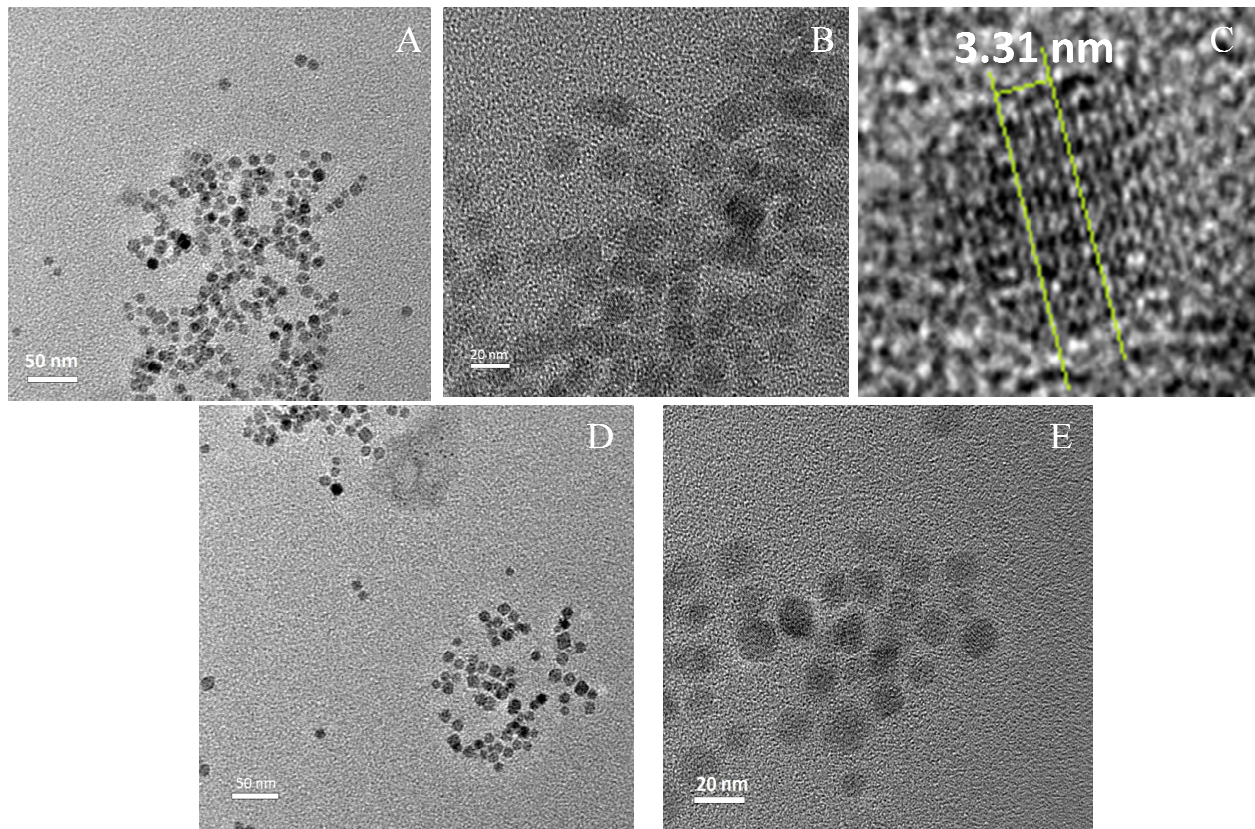


Figure 18 : A) TEM image of InN TMED aliquot at 75 min (Avg. size = 4.4 nm); B) HRTEM image of the same C) Lattice fringes in the nanoparticles are 0.27 nm apart (consistent with the lattice parameter obtained from the wurtzite phase), D) TEM image of InN TMED aliquot at 90 min (Avg. size = 5.62 nm); E) HRTEM image of the same

MODIFICATIONS TOWARDS IMPROVED QUALITY COLLOIDAL NANOCRYSTALS

The primary problem that we encountered with this synthetic method was obtaining stability of the nanoparticles in a solution as a colloidal suspension. It seemed hard to have these InN particles stabilized in the non-polar media. So, we tried different surfactants and different ratios as the passivating media. The composition that seemed to work a bit efficiently for the first time was a 3:1 ratio of OLA and OA while dissolving the InBr₃. This combination made dispersing the particles in the desired organic solvent; in our case TCE comparatively easier. The colloidal stability of the particles increase which is the foremost requirement for study of optical properties.

In a typical synthesis(Fig. 19), 1 mmol of InBr₃ (0.354 g) is solubilized in a mixture of oleic acid (OA, 2 mL), oleylamine (OLA, 6 mL, min. 70% assay from Sigma-Aldrich) and octadecene (ODE, 5 mL) under air free conditions (N₂ Schlenck line) by heating to 150 °C. The nitrogen precursor, tetramethylethylenediamine (TMED, 3 mmol, 0.45 mL) in 3 mL ODE, is then added to the main solution. The mixture is stirred for about 1 hr, at which point the temperature is raised to 250 °C. A mixture of *n*-butyllithium (*n*-BuLi, 1.2 mL of 2.5 M hexane solution) dissolved in 3 mL ODE is then added slowly at a rate of 4.2 mL/hr to the InBr₃/TMED solution using a syringe pump. The mixture starts to darken about 20 min after the beginning of the *n*-BuLi addition, indicative of formation of InN (*vide infra*). Once the addition is over, the reaction is kept under heating/stirring for half an hour, and then cooled down to room temperature. The colloidal suspension is crashed out and washed several times with ethanol, and dispersed in tetrachloroethylene (TCE). During the washing procedure the centrifugation to crash the particles out needs to be done at a speed of 2500 rpm or lower for about 4-5 minute. At this speed only larger In metal impurities crash out along with the bromide salt. After removing

the impurities to the supernatant TCE solution about 2 mL of ethanol is added and the centrifugation is done at 4500 rpm or higher. This usually crash out the larger InN nanoparticles. These crashed out particles then undergo surface treatment. The quality of the colloidal suspension is generally improved substantially by treating the sample in excess OLA at 40 °C for 120-480 min. (2-8 hours). To crash out and then re-suspend the smaller particles ethanol is added to the rest of the solution and the speed for centrifugation was increased up to 5700 rpm. The time for centrifugation was varied accordingly.

NIR-Vis absorption spectroscopy measurements were done by transferring the colloid particles into 5 mL tetrachloroethylene. After washing, as we can see in Fig. 20 (left) the color of the aliquots drawn with time is becoming darker. The aliquot taken at 25 min is light brown in color where the final one is completely black. The absorption spectra also show that the excitonic feature of the aliquots drawn with increasing time; shifts to lower energy (Fig. 20; right). This suggests that the aliquots that were drawn later contain larger particles. Larger particles being less confined their band gap energy is not much higher than the bulk material whereas the smaller particles exhibit higher amount of confinement and their band gap energy can be 0.4 eV higher than the bulk material.

The reaction pathway can be described as following scheme:

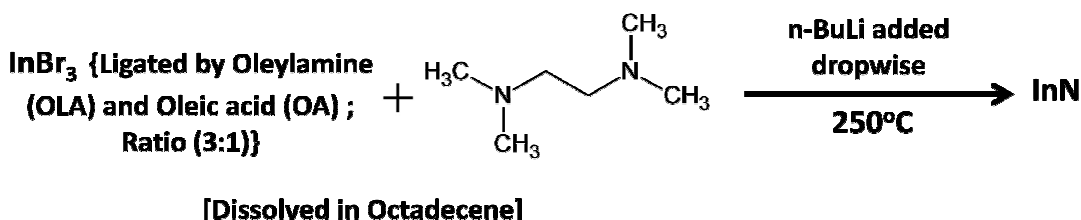


Figure 19 : Schematics of the reaction using TMED and n-BuLi

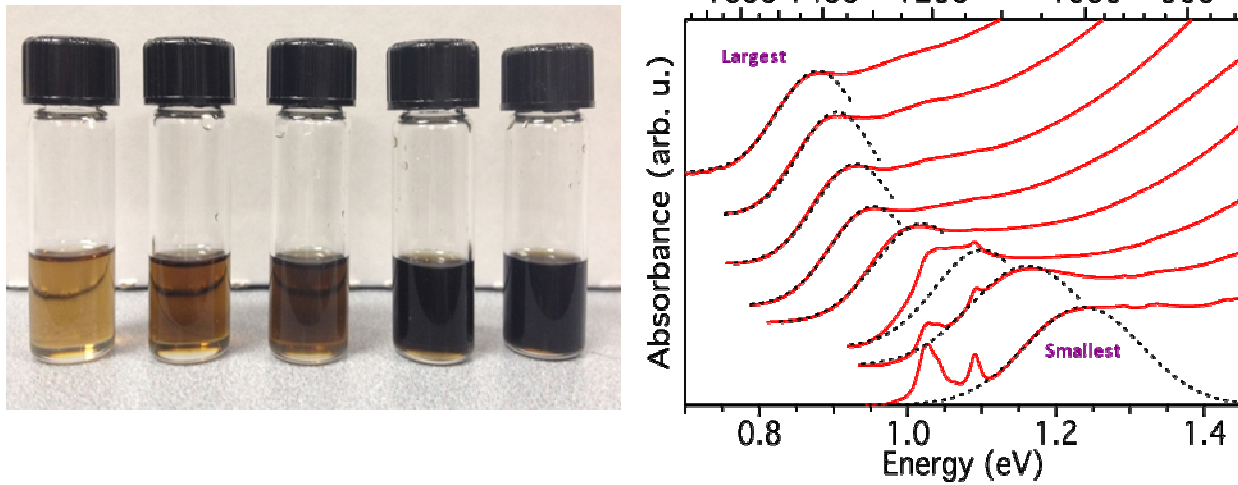


Figure 20: (Left) Aliquots taken at 25, 35, 50, 70 and 90 min. (Right) NIR absorption spectra of colloidal InN nanoparticles, showing the lowest excitonic transition for different average particle diameters

The gradual increase in the darkness of the color can actually come from two factors. Firstly, due to the increase in size of the particles their inherent band gap energy becomes lower as the quantum confinement becomes less prominent. Secondly, larger particles can absorb more visible light than the smaller ones (they have higher extinction coefficient) which also contribute towards the darker color of the aliquots.

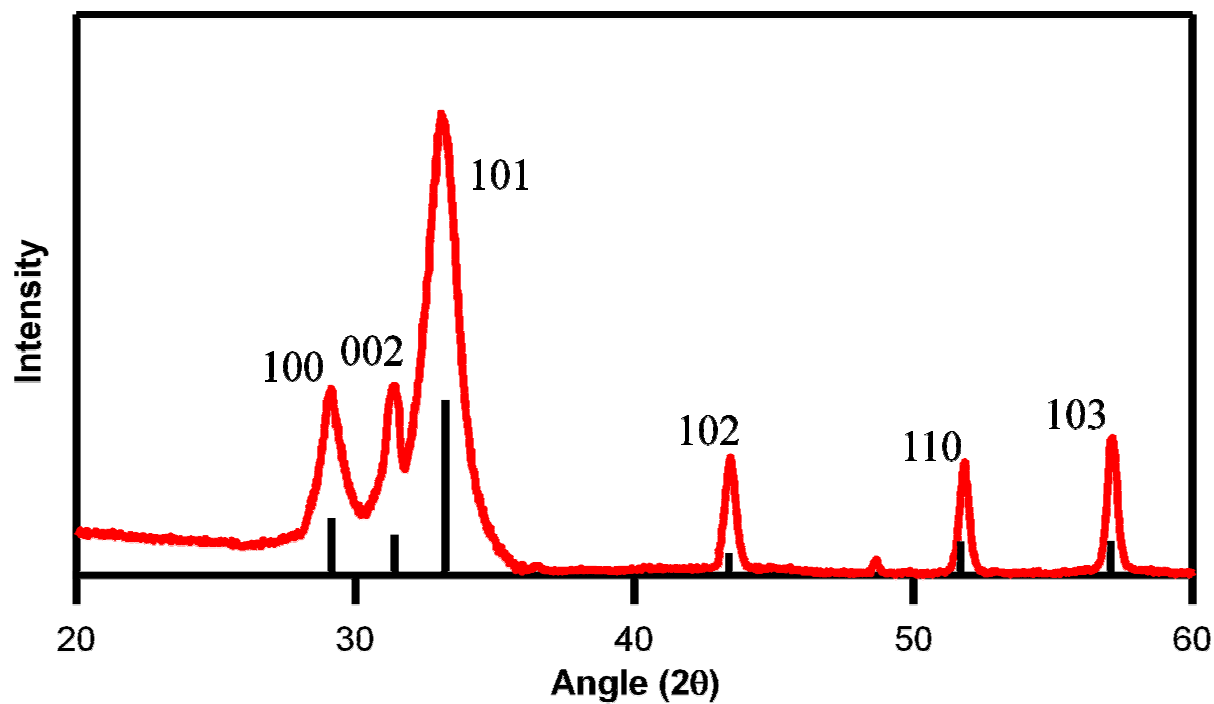


Figure 21: PXRD pattern of the sample drawn from final aliquot agrees well to wurtzite phase of InN

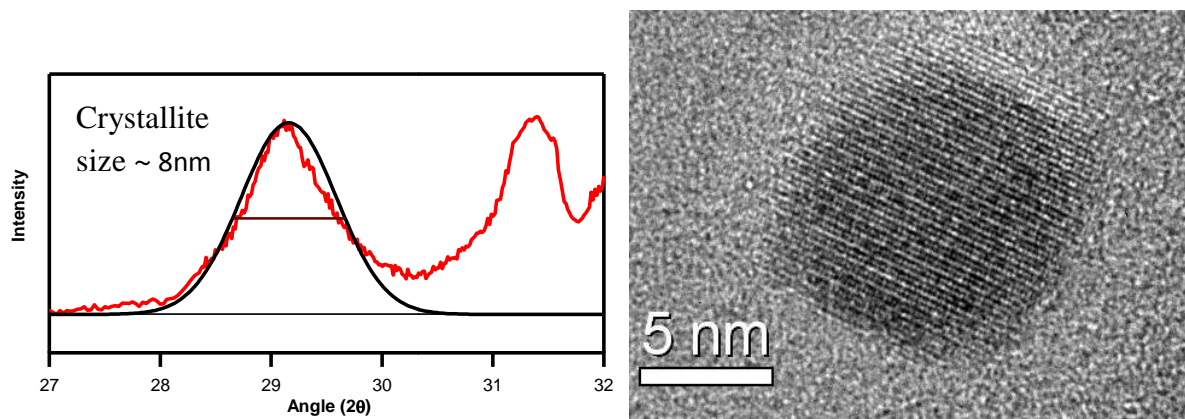


Figure 22: (Left) Scherrer analysis to find out size of the nanocrystal, (Right) HRTEM image of a nanoparticle from the sample taken from final aliquot of InN

The PXRD pattern (Fig. 21) of the sample is in good agreement with the wurtzite phase InN. Taking into account the width of the peak corresponding to the 100 plane the we see that at the angle $2\theta = 29.16^\circ$, full width at half maxima (FWHM) is 1.015° . From this data we can calculate the crystallite size of the material using scherrer formula (Eqn. 5), which comes out to be ~ 8 nm (Fig. 22). The HRTEM image (Fig. 22) shows the lattice fringes which corresponds to the 101 planes of InN. The distance between two planes is 0.308 nm which again is in agreement with (PCPDF- 01-074-0244).⁸³

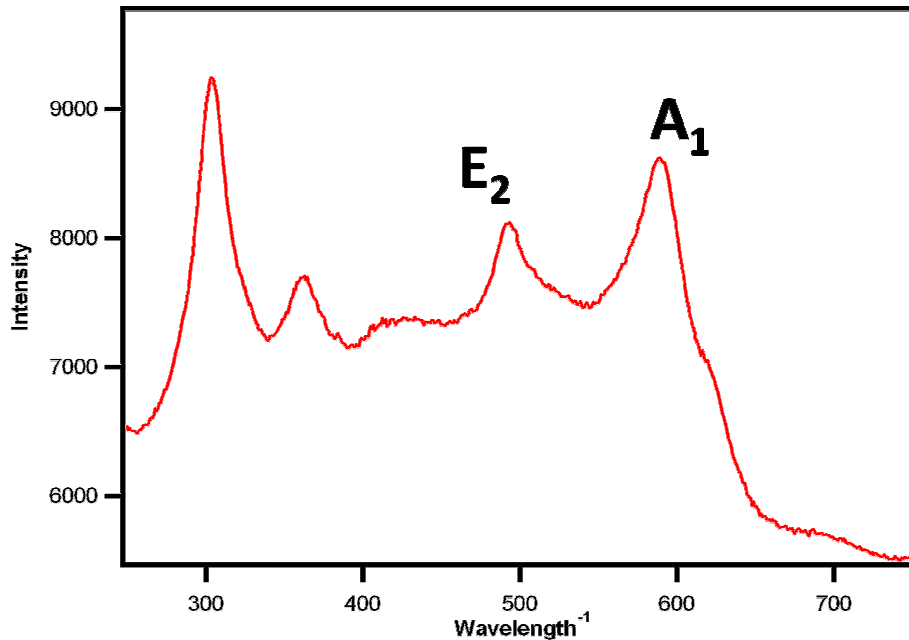


Figure 23: Raman spectra of InN nanoparticles. Both $A_1(\text{LO})$ and E_{2h} peaks, which are related to a longitudinal optical phonon mode and a doubly degenerated mode, respectively, were observed at 596cm^{-1} and 495cm^{-1} .^{92,93}

The Raman spectrum (Fig. 23) provide additional characterization information for InN. The data from Raman spectra proves the existence of In-N bond and also verifies the nature of the crystal structure to be wurtzite. The intense peak at 300cm^{-1} correspond to some internal deformation of

the lattice.⁸⁹ Raman spectra were taken with a Labram ARAMIS Horiba Jobin Yvon Raman spectrometer, equipped with an Ar⁺ ion laser as a light source operating at a wavelength of 514 nm and focused on the sample through an optical microscope. The infrared spectrum was recorded in the wavenumber range of 4000-400 cm⁻¹ with a Fourier transform infrared (FTIR) spectrometer.

Size of these InN nanocrystals has been determined by TEM and HRTEM images (see SI) taken from different aliquots of this synthesis and we will relate the average size of these particles to the band gap of those nanocrystals.

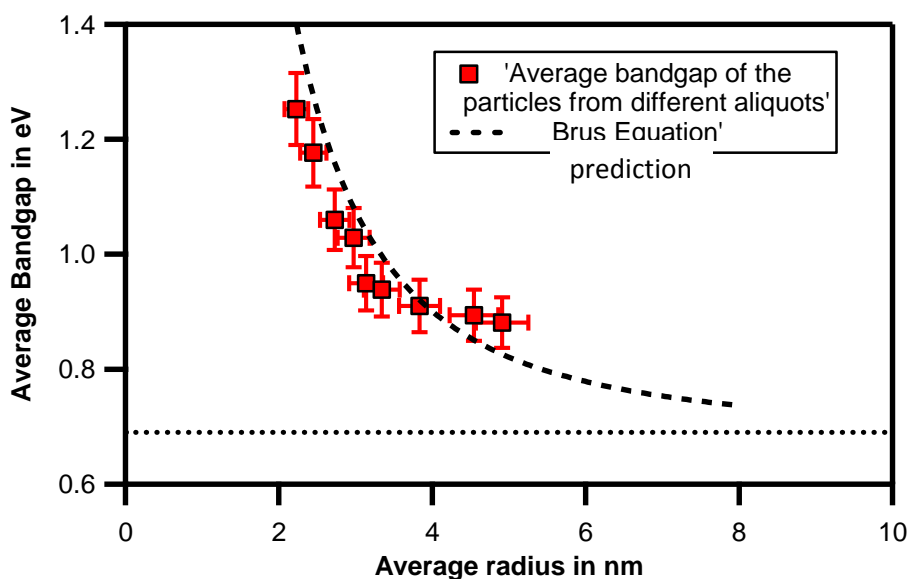


Figure 24: Size-dependence of the first absorption peak of nanometer-sized InN colloidal particles. The dashed line corresponds to the trend expected from the Brus equation

The lowest-energy feature in the NIR spectrum is definitely an excitonic transition here because this transition directly depends on the size of the nanocrystal (Fig. 24). As we have seen earlier, this is expected for quantum confined systems, as the excitonic transition is supposed to shift to

larger energies as the particle size is decreased from 9.2 nm to 4.5 nm diameters. The system becomes gradually more confined as we tend to decrease the size of the particles which actually results into restricting the movement of the electrons. The entire shift in this spectrum extends to 350 meV which happens to be 50% of the bulk band gap of InN. This significantly manifests the magnitude of quantum confinement effects in these InN nanoparticles. Brus predicted this behavior for nanocrystals as they experience confinement by having a smaller size than their Bohr radii.⁹⁴ In this case for InN we see that it follows the expected trend quite well even in strong confinement regime.

REVELATION OF SHAPE OF PARTICLES

Though we can see the material exhibiting excitonic feature and confinement behavior very evidently, there were some facts during the characterization process which raised some questions in our mind about the shape of the nanoparticles. The relation between the size and the excitonic feature does not seem to follow the nature predicted by Brus properly as the material close to hit the bulk band gap value. It seems that band gap of the particles do not tend to change after obtaining a certain size of around 8 nm. Ideally it should reach progressively for the bulk band gap as the size come close to the Bohr radii of that substance. But from Fig. 24 it's very evident that after reaching radii of about 4 nm the band gap of the particles still stays pretty much at the same energy level. Some PXRD pattern and TEM images also indicated in the same way.

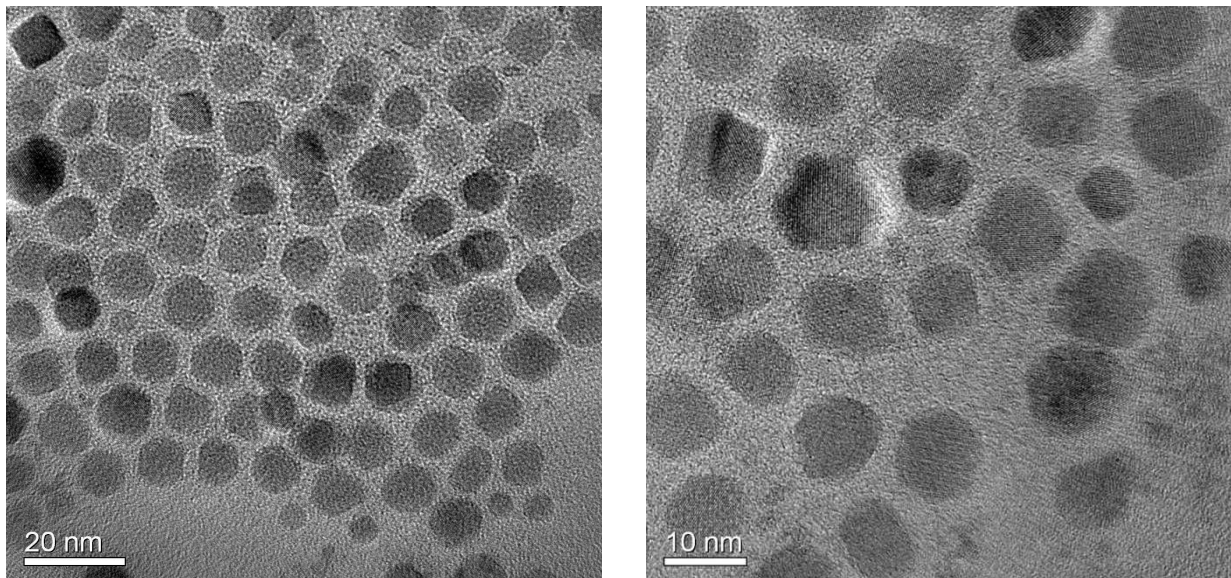


Figure 25: Magnified TEM images of InN nanoparticles. From these images it looks like the particles actually have a propensity to acquire platelet or disc like profiles

The 002 peak in the PXRD stays a bit hidden under the strong 101 feature and in some of the PXRD data actually cannot distinguish the 002 signal from the 101 (Fig. 20). Looking carefully at the TEM images we see that the boundaries of the particle can be seen inside another particle. This means that the particles are probably stacked on one another and this is easily visible in some cases. Had all these crystals have the equal dimension it'd be very unlikely as a sphere can not be piled on the other. It would be a very unstable structure and boundaries of them also should not be this evident. The other reason to think about the irregular shape is the HRTEM images (Fig.s 20 and 25) which show preference towards one particular plane i.e. the 101 plane. So, we performed AFM analysis on these particles and it turned out they were really very flat as predicted.

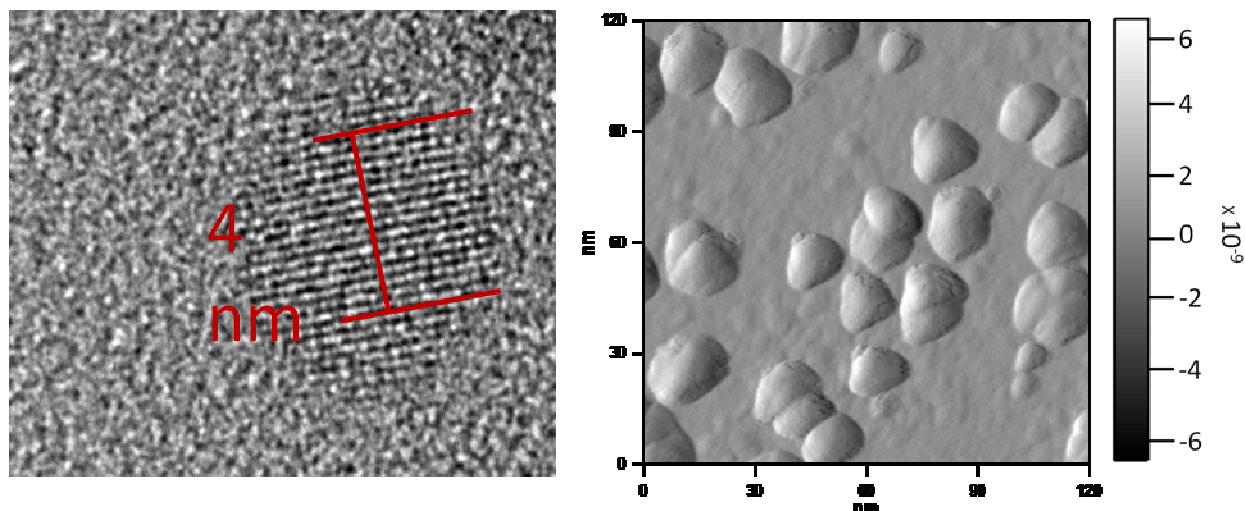


Figure 26: (Left) Lattice fringes in a HRTEM image shows the 101 facet. (Right) AFM image of the particles synthesized by this process

From this AFM image (Fig. 26) of a sample from the final aliquot of the product InN, we can get the average height of the nanoparticles which in this case is about ~ 6 nm. However, the TEM images show that the average size of these nanocrystals is 9.2 nm. That clearly shows that the height of the nanomaterials is smaller than their average diameter. Quantum confinement thus strongly depends on direction and it plays a dominant role in this case. The electron will experience confinement in the smallest dimension available and that will play the most fundamental role in deciding the extent of confinement in a certain particle. This phenomenon supports the saturation of band gap after a certain size in the size vs. E_g (band gap energy) plot.

Oleic acid as a ligand or surfactant is known to facilitate growth of particles in a uni-directional manner.⁹⁵⁻⁹⁸ Here, introduction of OA might have administered a similar effect. In that case growth in a particular facet of crystal is more favored than others or in other way on plane the

growth is more restricted. In most cases the crystal plane with highest amount of surface energy undergoes preferential growth and which helps it to stabilize.⁹⁹ There has not been enough study to investigate the growth process of different crystal planes of wurtzite phase nanomaterials. We wanted to explore this which actually provided us with an opportunity to alter the shape of particles.

CHAPTER 3: CONTROLLING THE SHAPE OF NANOPARTICLES

Keeping in mind the ability of the ligands to influence the shape of nanomaterials we wanted to see if by changing the ratio of them we can actually maneuver the shape of these particles. If our assumption were true putting different amount of ligands in the synthesis should have a variable effect on the morphology of the product. Also, the other objective was eventually to reach the bulk band gap by increasing the effective Bohr radius of the material. So, we decided to vary the ratio of OLA and OA and see what effects it bring to the morphology. Since OLA-OA mixture was proven to be an efficient surfactant system we wanted to proceed with that first. For the previous method we had a ratio of OLA to OA as 3:1. It was varied to 5:1, 7.5:1 and 10:1. Since, OA is the component which favors growth on a certain facet it's ratio to OLA was decreased gradually to observe the resulting effects.

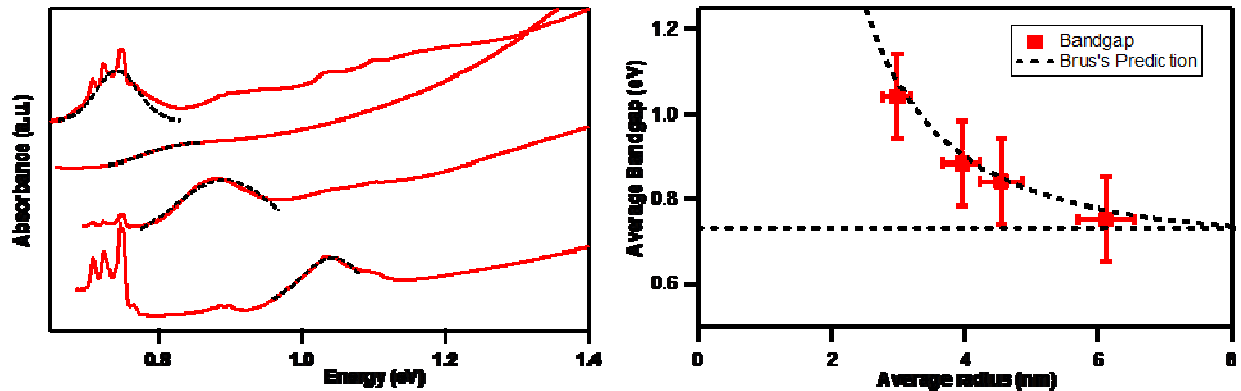


Figure 27: (Left) Absorption spectra of aliquots taken out of the reaction mixture synthesized with OLA:OA ratio 5:1. (Right) Size-dependence of the first absorption peak of these samples. The dashed line corresponds to the trend expected from the Brus equation (Equation 10)

In this method total 8.0 mL of ligands i.e. 6.6 mL of OLA and 1.4 mL of OA were used. The aliquots were drawn from the reaction mixture at 30, 45, 60 and 75 min. From our previous experience it has been observed that growth of the nanocrystals cease after about 60-70 min after initiation of adding the reducing agent *n*-BuLi. As we can see here the final sample has a diameter of about 12 nm which is confirmed by the TEM image analysis (Fig. 29).

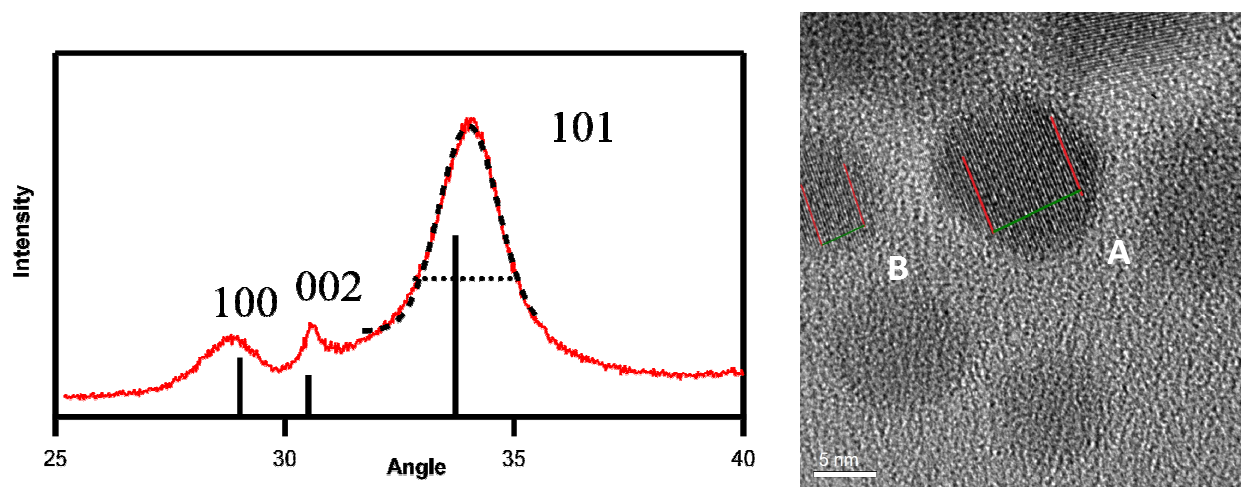


Figure 28: PXRD pattern of the TEM images synthesized by OLA:OA = 5:1 and a HRTEM image showing (A) 101 and (B) 100 plane

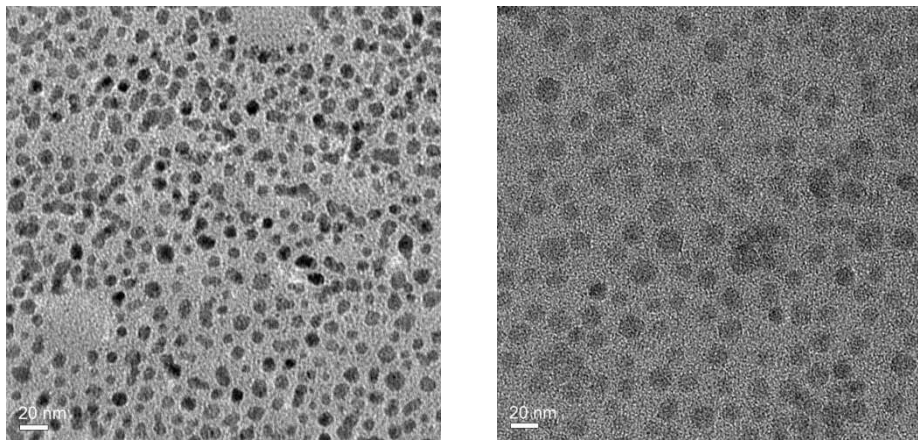


Figure 29: TEM images of the two other aliquots drawn at 30 (left) and 45 min (right) from InN sample aliquots made with 5:1 ligand ratio.

As we see in the absorption spectra the excitonic feature shows up at different energies due to formation of different size particles in the aliquots drawn in time interval. It seems to follow the trend predicted by Brus more closely and we can also reach the bulk band gap value using these particles. From the PXRD data we can see that with the OLA:OA ratio 5:1 we can get very similar quality nanocrystals with same crystalline phase (Fig. 28). The particles possess a diameter of ~ 12.2 nm and they also have good size distribution (Fig. 29) which is clear from the TEM images. An interesting fact is in the HRTEM image (Fig. 28) we can see two different types of planes though which was very rare in case of the particles synthesized using 3:1 OLA:OA ratio. However the preferred orientation effect still remains and it can be observed in the PXRD pattern of the material. The 002 feature is not very distinct and associated with the peak from 101 plane (Fig. 28). From the AFM images (Fig. 30) also we can see that the average height of the particles is ~ 7.5 nm which is still smaller than their diameter. The AFM images also

reveal the disc like structure of the particles. So, we kept on investigating effects of changing ratio of the ligands in the synthesis.

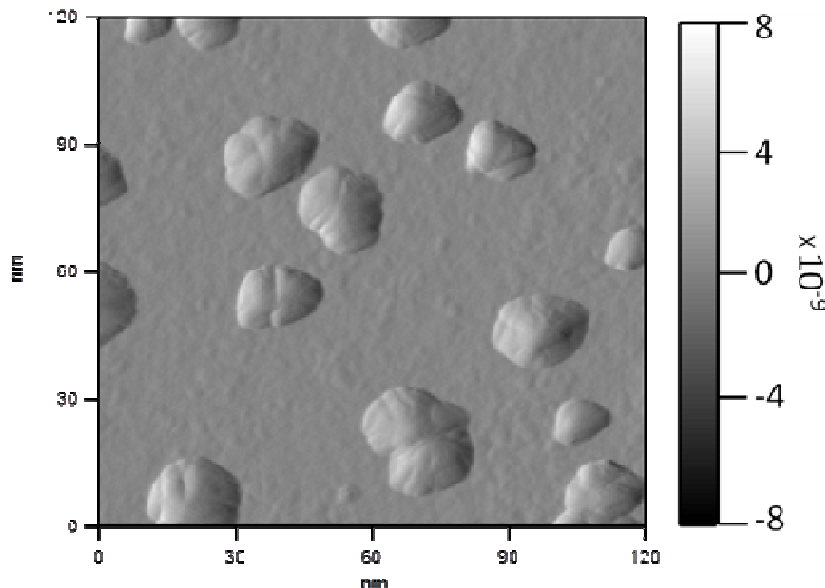


Figure 30: AFM image of nanoparticles prepared using OLA:OA = 5:1 ratio. Average height comes out to be as ~ 7.5 nm

Since increasing the ratio of OLA:OA led us to the right direction the next step was exploring further raised proportion of OLA in the mixture. So, we went on with OLA:OA 7.5:1 and 10:1.

In these methods we kept everything same apart from the amount of OLA and OA introduced. For 7.5:1 ratio the amount of OLA used was 7 mL and 1 mL of OA was included. As we can notice in the absorption spectra very similar trend is observed. The aliquots were drawn at 30 min, 45 min, 60 min, 75 min. We can find the average size of the particles from the TEM images (see SI) and band gap of each particle size from their optical absorption. The plot of average

band gap vs. radius tag along the nature suggested by the Brus model and we do not see any saturation at a certain size. PXRD of the sample confirms it to be InN (Fig. 32).

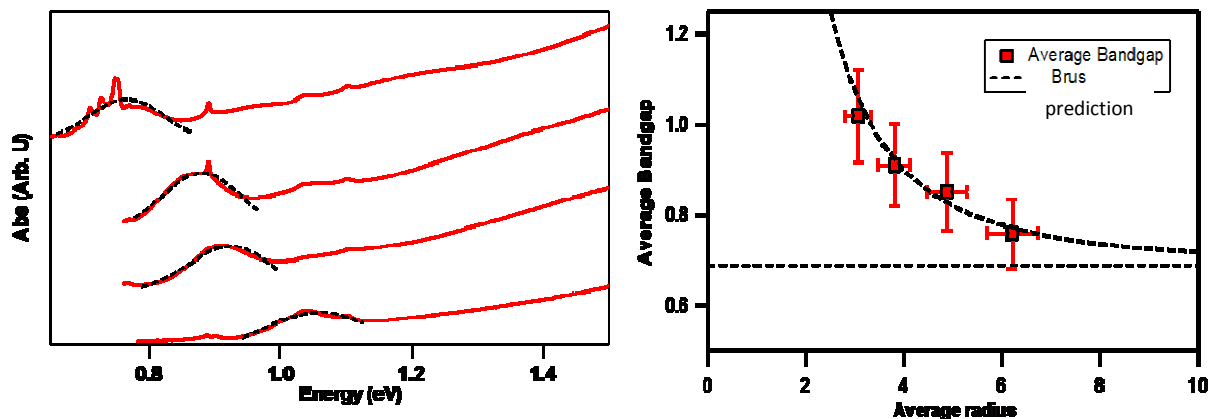


Figure 31: (Left) Absorption spectra of aliquots taken out of the reaction mixture synthesized with OLA:OA ratio 5:1. (Right) Size-dependence of the first absorption peak of these samples.

In order to compare the morphology of these InN nanocrystals synthesized we want to know the average diameter and average height of the particles. In the PXRD pattern (Fig. 32) of the material we don't see 002 plane as a shoulder of 101 plane in this case. Rather, very distinct features are present for both signals. As mentioned earlier, preferred orientation could be the reason for the XRD signals to pile up.

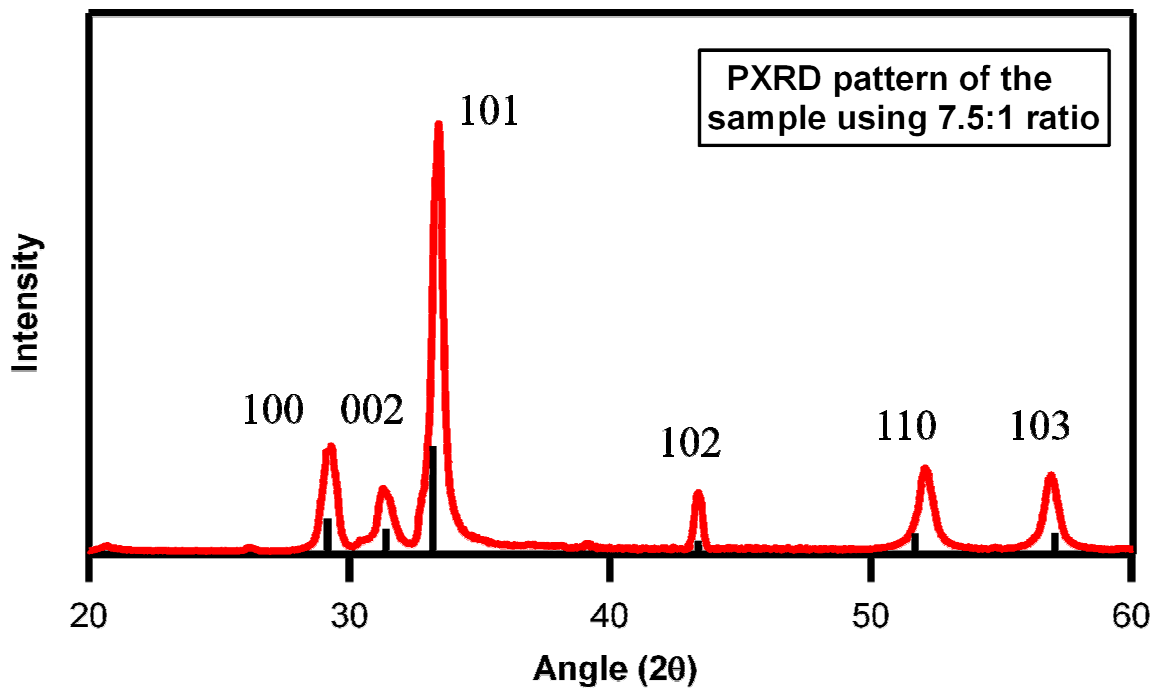


Figure 32: PXRD pattern of the sample is consistent with wurtzite crystal structure

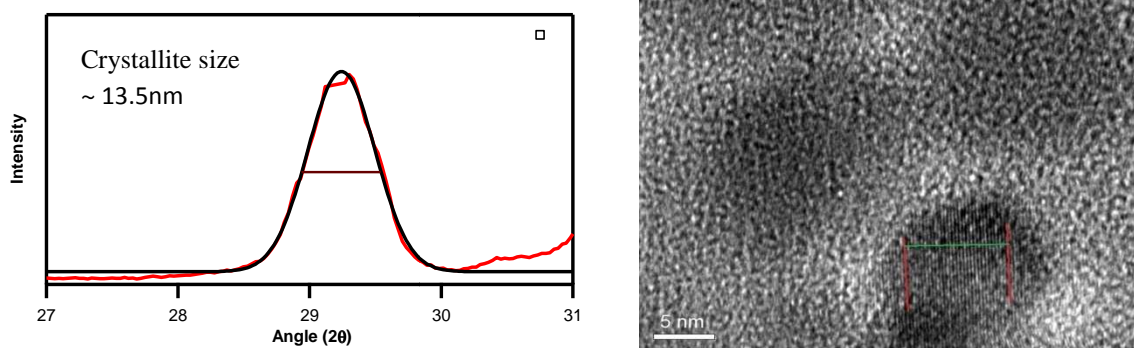


Figure 33: Scherrer analysis (left) and HRTEM image showing 101 plane (right)

So, we see that the average size of the particles in the final aliquot for this method is ~ 12.25 nm (Fig. 34). The Scherrer analysis (Fig. 33) also supports this number because from the peak width we get the average size to be 13.53 nm. This can be explained as during the sample preparation the solution of nanoparticles is drop casted on the sample holder. It is very likely that when the solvent is evaporated the nanoparticles form an agglomerate which would be much larger in size than usual nanoparticles. Since in the Scherrer analysis a collection of quantitative data is calculated the average size that comes up as the result is larger.

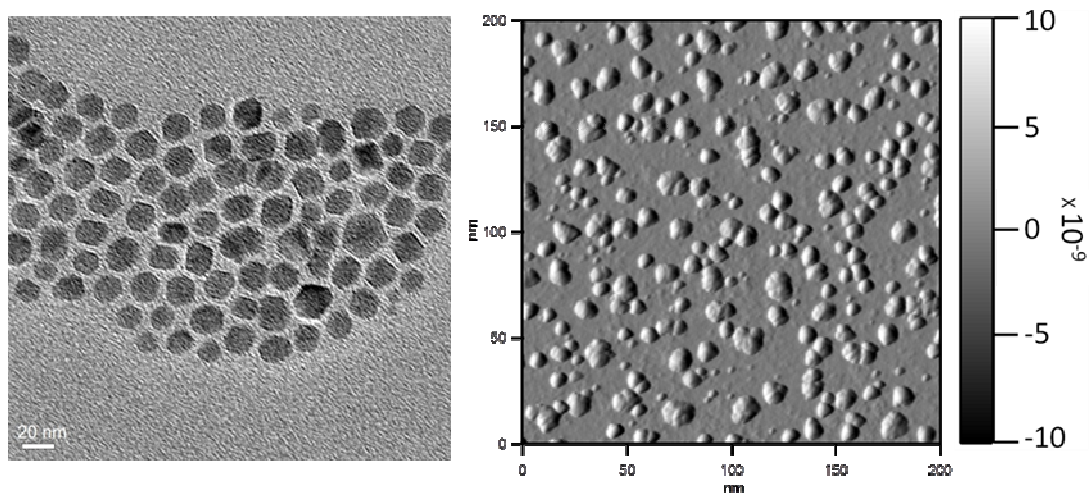


Figure 34: TEM (left) and AFM (right) image of the final aliquot

In the AFM image taken using the same sample aliquot we see that the average height for this particle is ~ 8.5 nm. This still points toward the fact that all the dimensions are equal for the nanomaterial. Though in the AFM image the particles don't look like platelets and in the PXRD pattern also, there's no indication of preferred orientation it seems that we have not obtained quite spherical particles this time as well. The very small spots on the AFM image are believed to be residues from organic solvents. The HRTEM image (Fig. 33) exhibit presence of lattice fringes which correspond to 101 plane. We did not have enough HRTEM data to draw a

conclusion on whether this can be attributed to a preferred orientation effect. So, we decided to look further with a different ligand ratio.

However, as we can see, in case of 5:1 and 7.5:1 both the final sample shows excitonic feature very close to the band gap of the bulk material. So, the first objective of reaching the size featuring bulk band gap is completed. This would be very useful to pin-point the Bohr radius of InN which has not been yet experimentally determined.

In the next procedure everything was kept the same except for the amounts of ligands introduced. 7.2 mL OLA and 0.8 mL of OA were used in this attempt. The aliquots shown in the absorption spectra were drawn at 25, 35, 45, 60, 75 and 90 min (Fig. 35).

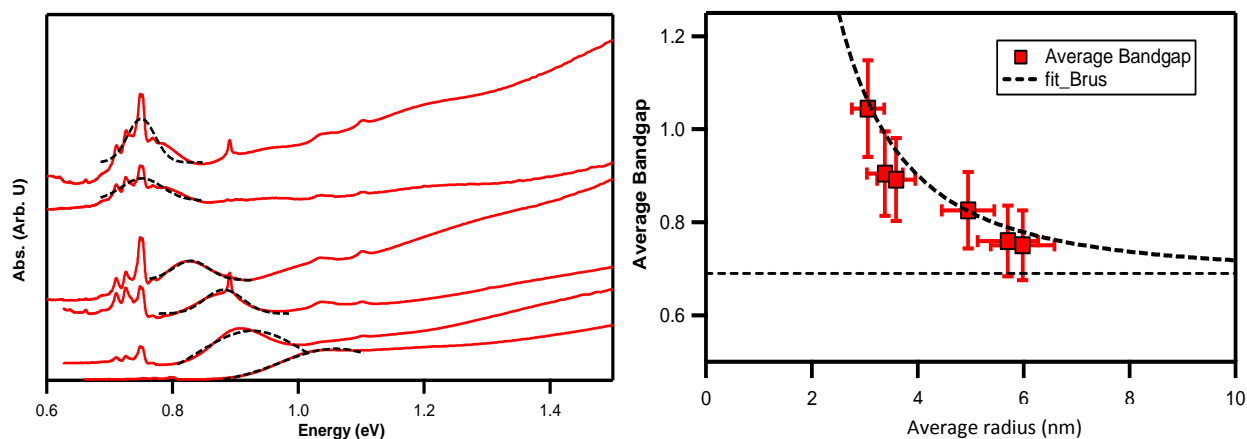


Figure 35: (Left) Absorption spectra of aliquots taken out of the reaction mixture synthesized with OLA:OA ratio 10:1. (Right) Size-dependence of the first absorption peak of these samples.

The colloidal quality of the nanocrystals was substantially good. The band gap energy was found from their absorption spectra and the TEM images (see SI) gave us the information about their size. As we look into the average band gap vs average size plot it seems to follow the trend predicted by Brus. In the PXRD pattern (Fig. 36) we do not really see any interference due to preferred orientation which means the crystals must be regularly shaped and the incident x-ray gets equivalent treatment in all directions. It also falls in very good agreement with the wurtzite crystal structure of InN.

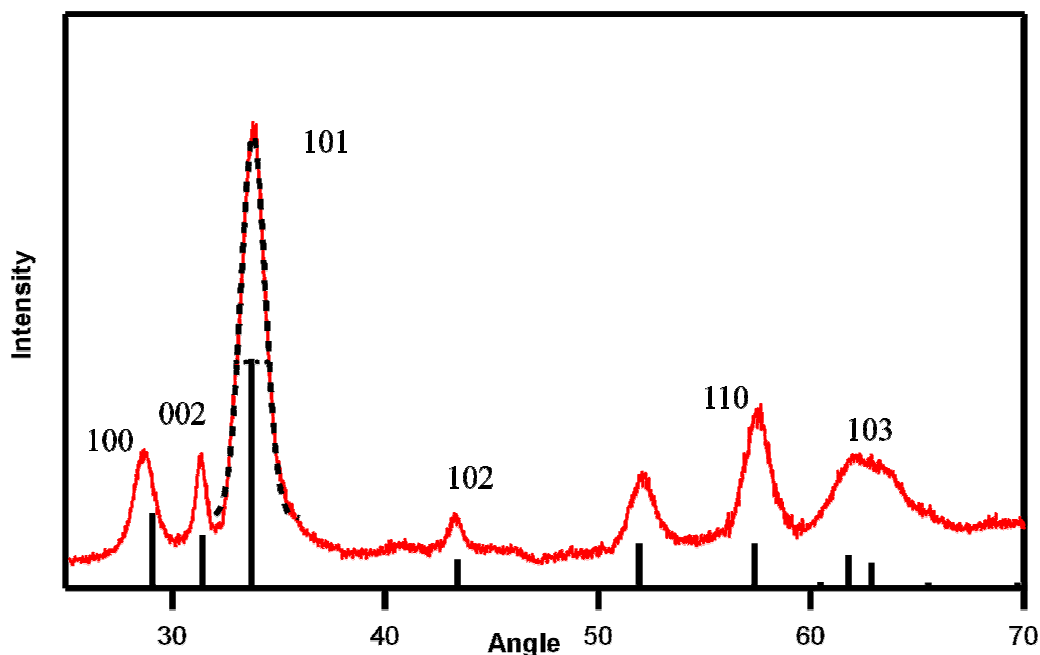


Figure 36: PXRD pattern of the sample is consistent with wurtzite crystal structure

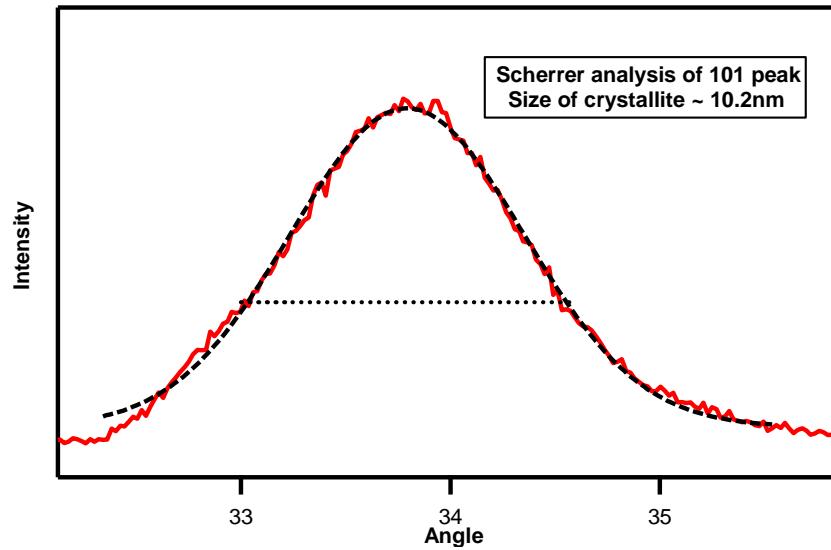


Figure 37: Scherrer analysis of 101 signal of the PXRD pattern shown above

So, from both Scherrer analysis and TEM images, the size of nanoparticles were found to be ~11 nm. Here we see a set of TEM and AFM showing sample particles from the same aliquot so we can compare their morphology.

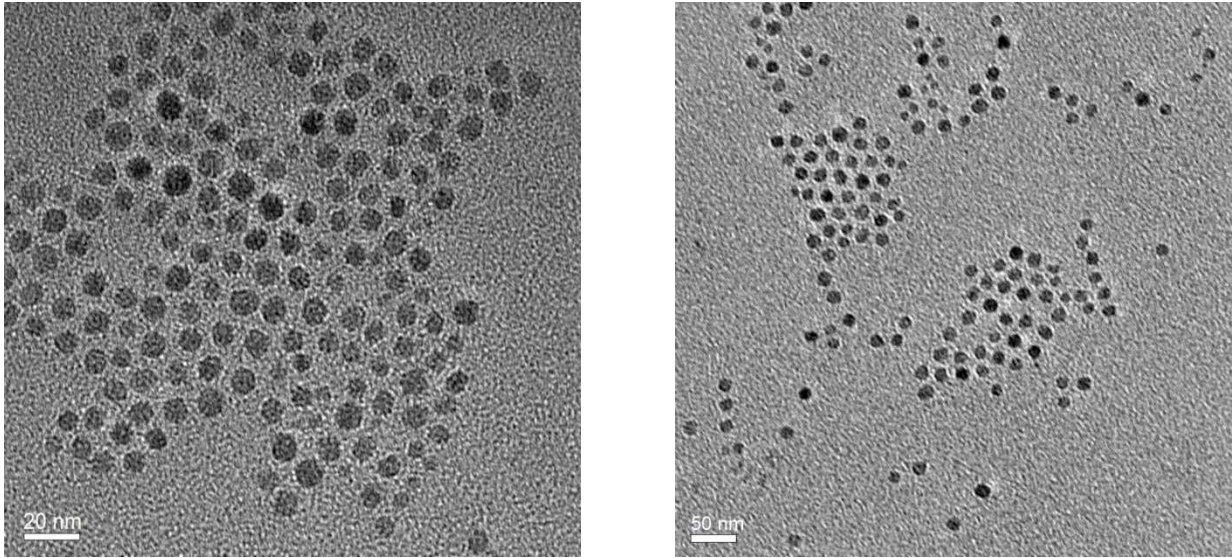


Figure 38: TEM images of nanocrystals from aliquot 3 (radius ~ 3.82 nm) [left] and final aliquot (radius ~ 5.98 nm)

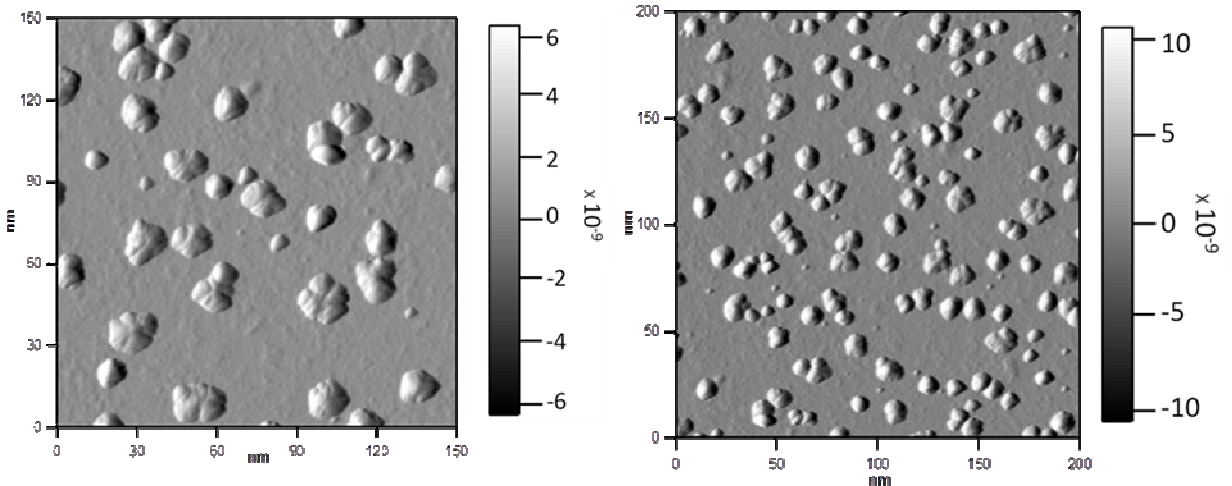


Figure 39: AFM images of the nanoparticles from same aliquot (left- aliquot 3) and (right- final aliquot)

The average height for the particles taken from aliquot 3 of this synthesis is ~7 nm and for final sample (right) is ~10 nm (Fig. 39) which complement the diameter of these particles found from TEM image analysis (Fig. 38). This means that the particles formed by this method have more regular spherical shape. As for the HRTEM images we can see different crystal planes present as we analyze the lattice fringes showing up.

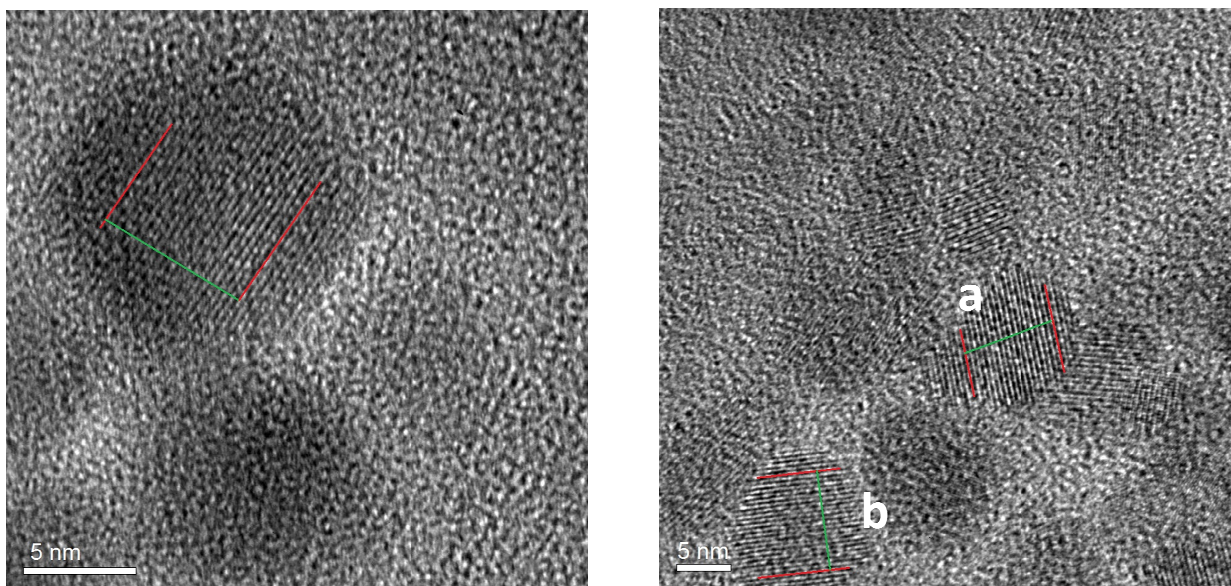


Figure 40: (Left) 101 plane with a d value of 0.270 nm, (Right) a) 100 plane with a d value of 0.308 nm) 101 plane with a d value of 0.271 nm

Considering all above mentioned evidences, they all indicate toward the fact that the particles synthesized in this case are very spherical in nature. Unidirectional growth does not play a big role in this case.

CHAPTER 4: INSIGHT INTO REACTION MECHANISM

Since, the reaction scheme is not exactly a hot injection method we tried to investigate the mechanism of the reaction. Initially it was assumed that In metal is formed as an intermediate and TMED forms a complex with In metal which is later reduced by *n*-BuLi to produce InN. There are a set of experiments we did which supports this hypothesis.

SYNTHESIS OF INDIUM NITRIDE USING INDIUM METAL AS THE STARTING MATERIAL

If In metal were the constituent complexing with TMED to form the precursor complex In metal should be an efficient source of In in the reaction. So, In metal was synthesized in situ using *n*-BuLi as reducing agent and then TMED was added to it. Despite raising the temperature to the desired point and continuous heating the reaction for over an hour any sign of evolution of InN was not observed. The In metal nanoparticles are black in color after addition of TMED and raising the temperature beyond the melting point of In metal nanoparticles the solution starts to turn little translucent and it does not exhibit any further precipitation indicating development of InN nanocrystals. However when small amount of *n*-BuLi was added to the solution black color appears within 2 minutes which might be due to formation of small quantity of InN in the solution or due to further reduction of an oxidized state.

The PXRD pattern does not match with any traditional InN phase (See SI) and amorphous SAED (Fig. 41) pattern suggests those particles were not crystalline in nature meaning most of them

were left as unreacted In metal nanoparticle. The TEM images (Fig. 41) show that 10-15 nm particles are formed as product.

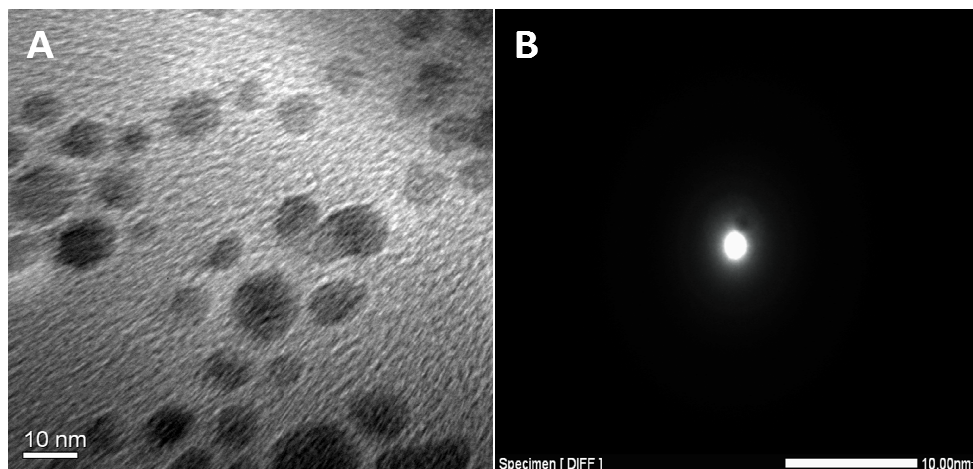


Figure 41: TEM image AND selected area diffraction pattern of the sample of In metal nanoparticles.

XPS (X-RAY PHOTOELECTRON SPECTROSCOPY) STUDIES TO INVESTIGATE THE REACTION PATHWAY

To confirm our proposition about the reaction mechanism XPS studies and ICP-OES measurement was done on the aliquots obtained from different reaction mixture. It turned out in the XPS studies that in the initial aliquots concentration of In(0) predominates and in the consecutive aliquots concentration of In (III) which is a component of InN, grows continuously. To inspect the effect of TMED, InN was synthesized with varying amount of TMED. In the first case 1, 3 and 3 mmol of InBr₃, TMED, *n*-BuLi and in the other one 12 mmol of TMED was

used. In Fig. 42 we see the XPS data of two aliquots taken at 30 and 60 min. for the first synthesis mentioned in the previous paragraph. In the aliquot taken at 30 min concentration of In(0) is predominant where as in the 60 min aliquot the opposite is observed.

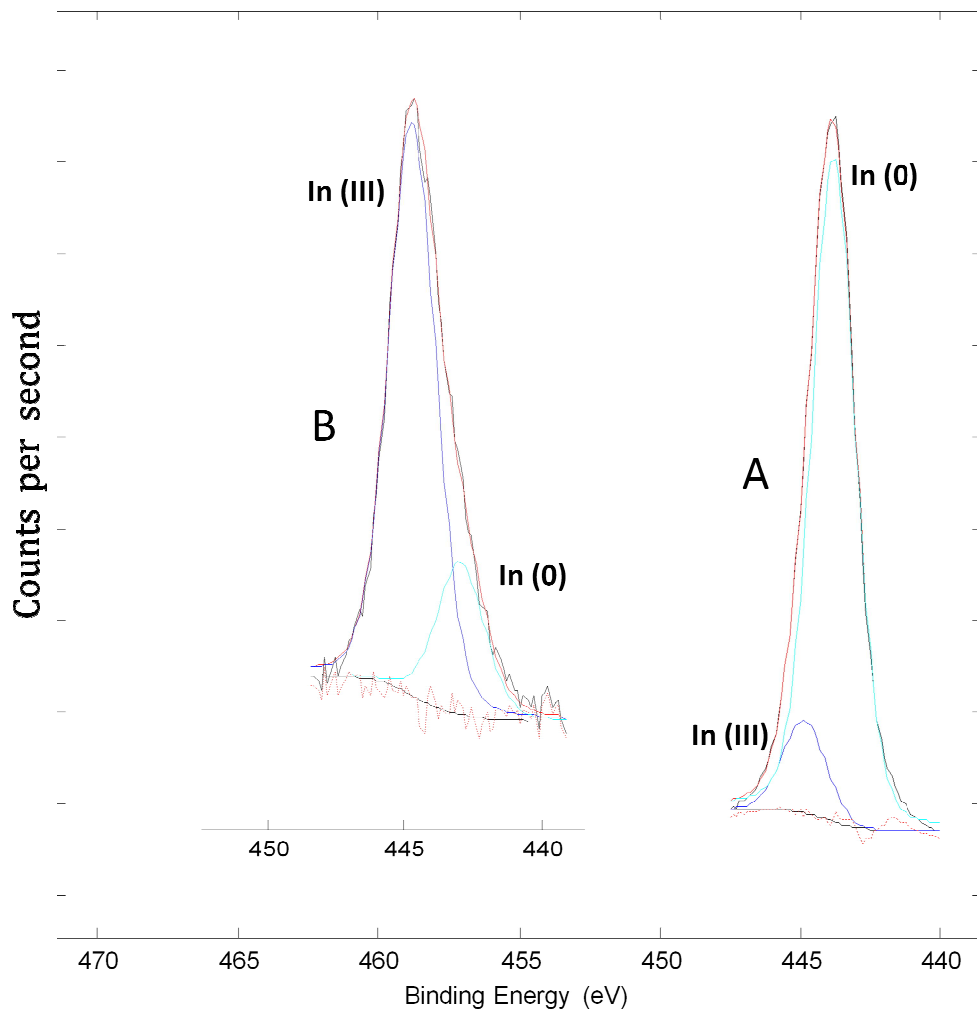


Figure 42: XPS data of the In 3d_{5/2} of aliquots taken out at 30 min (A) and 60 min (B) from the reaction mixture using molar ratio of InBr₃, TMED, *n*-BuLi taken as 1:3:3 which shows relative concentration of In (III) and In (0)¹⁰⁰

In the aliquot drawn at 90 min (Fig. 43) the relative ratio of In(III) increases even more compared to that of In metal or In(0). The gradual rise in the relative concentration of In(III) in Fig. 42 suggests that, most likely an In-intermediate was formed during the process. Initially addition of the reducing agent transforms InBr_3 into In metal which contributes to the high concentration of In(0) at the beginning.

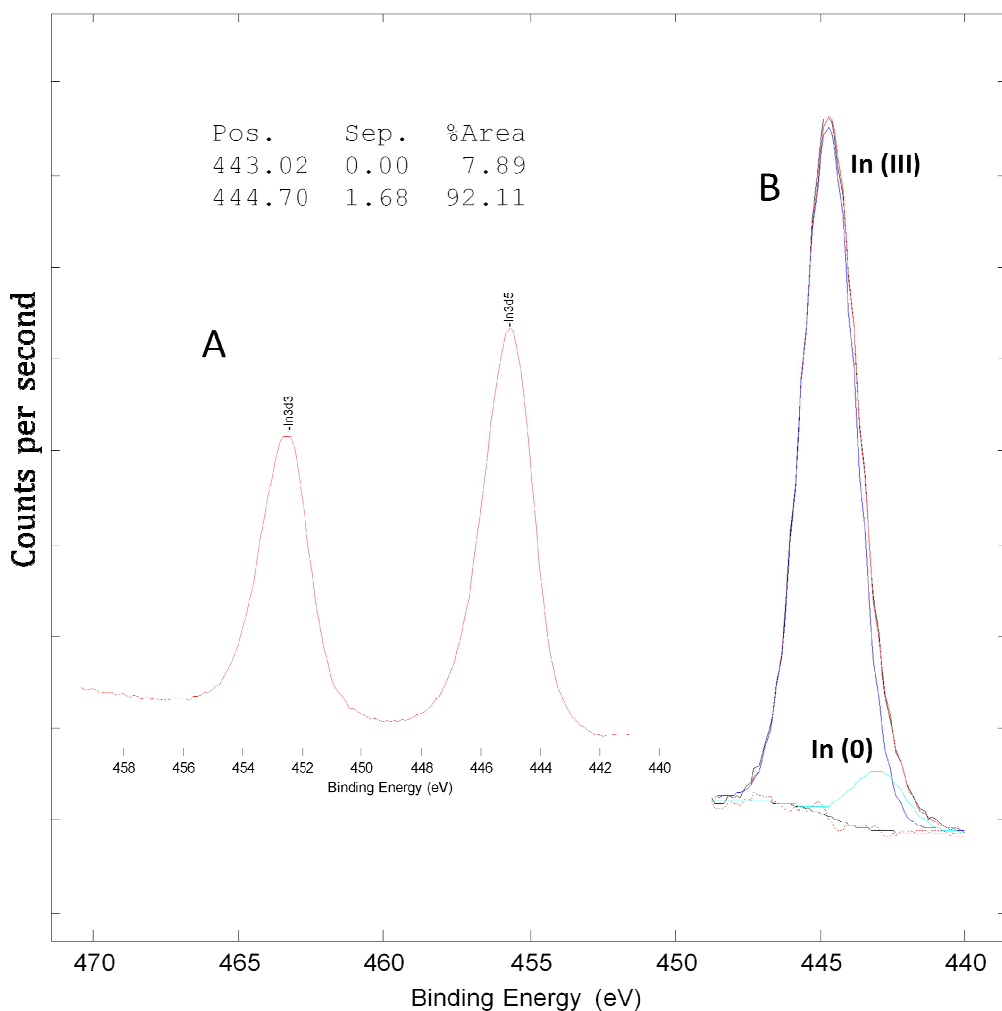


Figure 43: XPS data of the In $3d_{3/2}$ and In $3d_{5/2}$ of aliquots taken out at 90 min (A) from the reaction mixture using molar ratio of InBr_3 , TMEDA, *n*-BuLi taken as 1:3:3 (B) shows relative concentration of In (III) to In (0) in the sample

Later, when InBr_3 and TMED forms enough amount of the intermediate and its concentration reaches a threshold value. At this point this intermediate dissociates to form InN which boosts the relative concentration of In(III) in the solution. This intermediate now becomes the source of formation of InN hence In(III) and the dissociation becomes the dominant process. With time by more conversion into In(III) the relative ratio of the In(III) to In metal continues to grow higher.

SYNTHESIS OF INDIUM NITRIDE WITH EXCESS TMED

In this case the ratio of InBr_3 , TMED, *n*-BuLi was taken as 1:12:3. The Aliquots were drawn at 30, 45 and 75 min intervals. It is found that at same rate of addition of the reducing agent and at same time interval, the particles formed were larger in size. The average size of the nanoparticles from TEM was ~6.14 nm with reasonably good size distribution. The XPS data shows lower percentage of In metal component in these aliquots. A portion of the final sample was treated with dilute 0.2 mM nitric acid and this helps to get rid of most of the In metal part. PXRD of the washed nanoparticles agrees to the wurtzite phase of InN (Fig. 46).

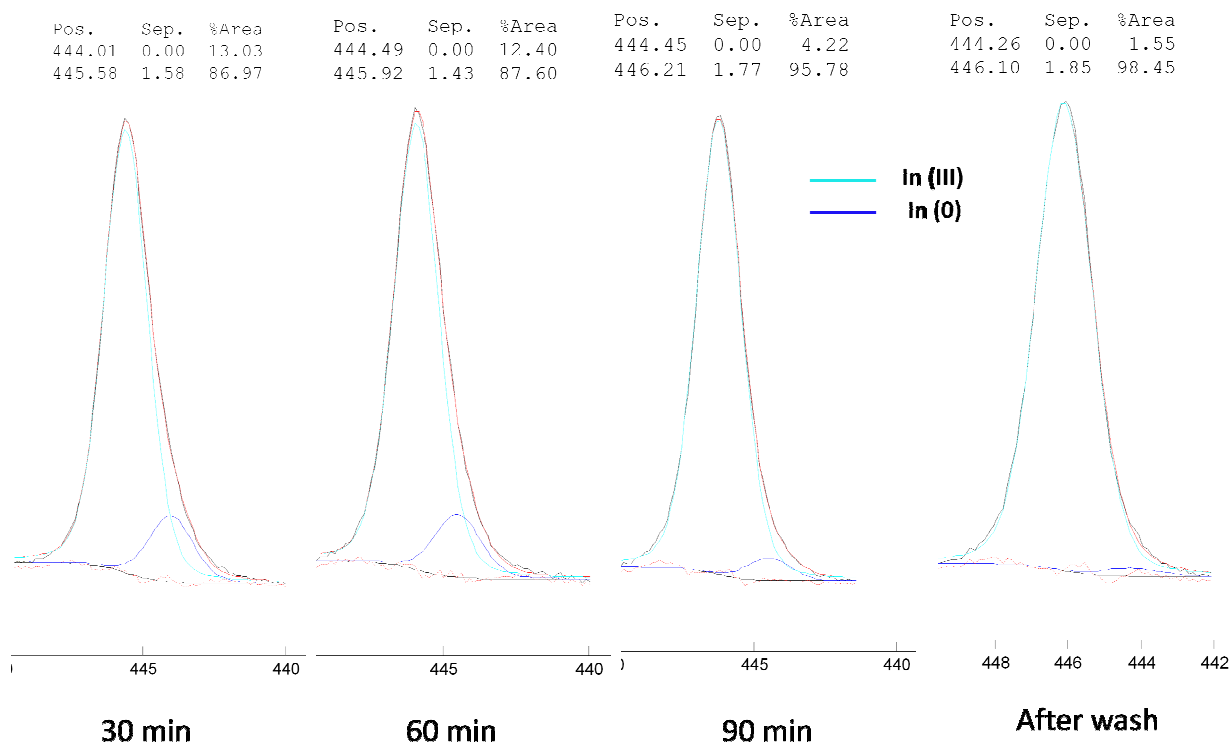


Figure 44: XPS data of the In $3d_{5/2}$ of aliquots taken out at different time from the synthesis using excess TMED

So, from these XPS data (Fig. 44) it has been observed that in this case even at 30 min excess concentration of In(0) is not found. We suppose the reason for this is favorable condition for formation of the intermediate producing InN. TMED is known to form stable complexes with metals.¹⁰¹⁻¹⁰⁴ This leads to the fact with more conversion rate of InBr_3 into this intermediate and later to InN, there is not much left to be reduced to In(0). This supports the very low concentration of In(0) at the start and almost nil at the end. This favors the assumption that InBr_3 probably forms some kind of complex with TMED which is more favored in presence of excess

reactant whereas when there's more unreacted InBr_3 , $n\text{-BuLi}$ reduces it directly to form more $\text{In}(0)$.

Also from the absorption spectra of the sample prepared with excess TMED we see that aliquots taken out at the same time as other reaction mixtures comprised of lower InBr_3 to TMED ratio incorporates smaller nanocrystals. Keeping everything same by increasing relative quantity of TMED produced larger size particles (Figure S10). This means the rate of formation of InN nanocrystals is faster in presence of excess TMED. This also supports the idea that most likely TMED complexes well with the In(III) component and thus forms InN faster upon addition of $n\text{-BuLi}$. Also the PXRD pattern (Fig. 46) matches very well with wurtzite InN .

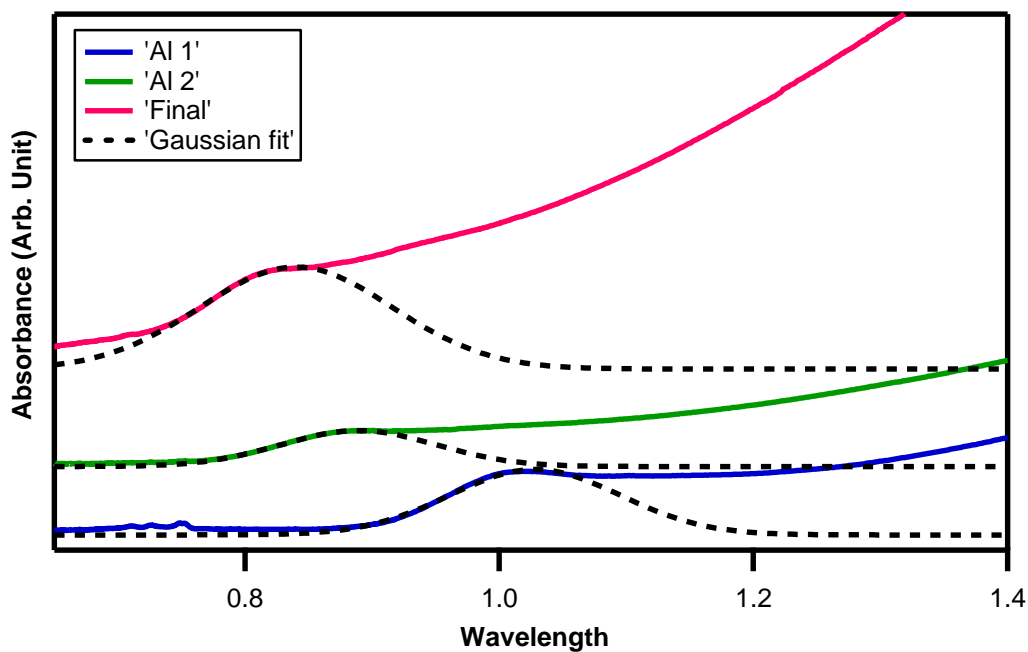


Figure 45 : Absorption spectra of the aliquots taken during synthesis with excess TMED

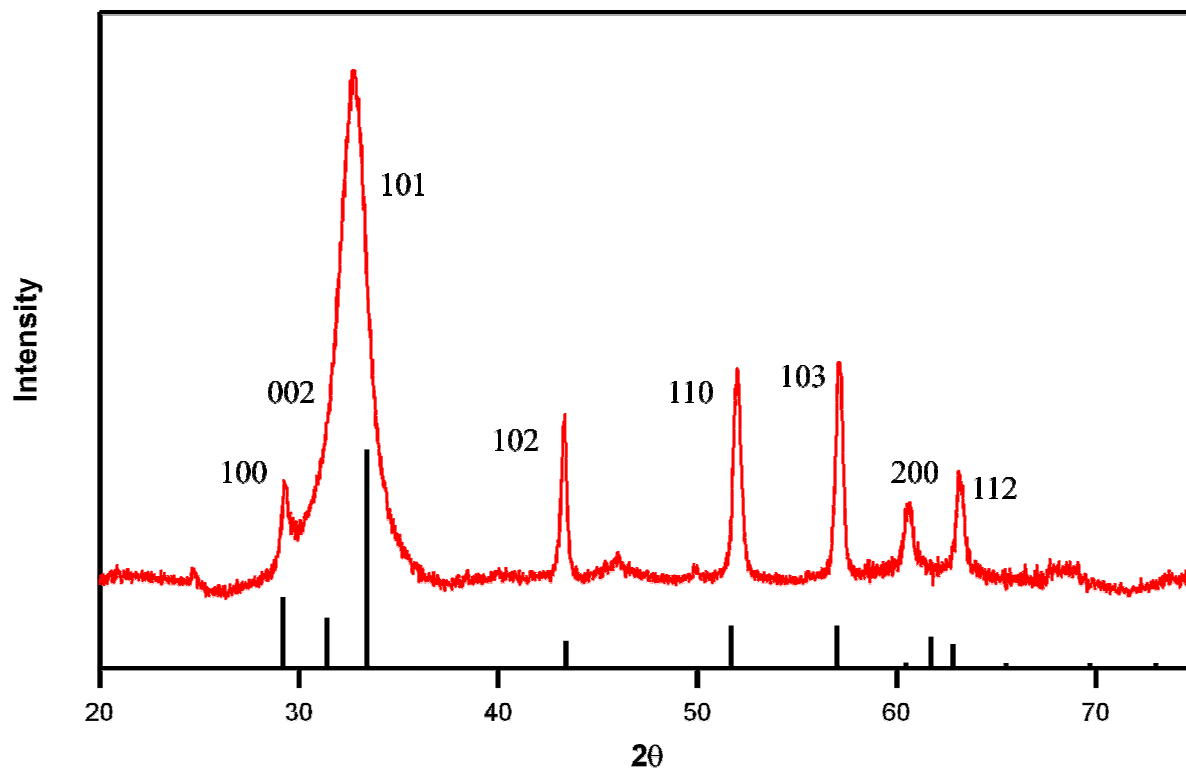


Figure 46: PXRD pattern of InN quantum dots synthesized with excess TMED confirm the wurtzite nature of the crystal structure

So, it occurred to us that if In metal itself cannot act as an efficient precursor leading to high yield of InN, it's probably not an intermediate towards the end product. The other option would be then if InBr_3 forms some kind of complex with TMED which is then reduced to InN by the reducing agent as TMED is known to form stable complexes with metals. There are several instances of TMED being used as a chelating or complexing agent in literature. If there is a complex intermediate involved the rate of formation of that complex should be higher in presence of excess TMED. So, by monitoring the rate and yield role of TMED was investigated.

CHAPTER 5: STUDY OF OPTICAL PROPERTIES

PHOTOLUMINESCENCE (PL) FROM INDIUM NITRIDE NANOCRYSTALS

As we were able to determine the band gap of InN using the techniques of optical absorption, photoluminescence was next to be explored. In a recent work Neale *et al.*⁴⁴ claimed that InN is very unlikely to demonstrate any photoluminescence due to its electronic structure. In all the previous reports, it has been shown that InN exhibits luminescence in visible region. This was explained considering the previously reported band gap of 1.9 eV. With more research and development in this field; the actual band gap of this material has been determined to be close to 0.7 eV;⁵⁵ so now these explanations do not seem justified any more.

We have been able to demonstrate luminescence of these materials in NIR region and it can be varied by tuning the size of InN. This seems much more reasonable because we can show that the optical band gap as well as the wavelength of emission is related to the nanocrystal size due to quantum confinement effect. The photoluminescence quantum yield (QY) of the material has been found to be reasonably high considering the fact that we have not yet explored all the possibilities to increase the emissive properties of these materials. The fact that these materials (without additional surface treatments to enhance the emissive property) tend to show quite high QY of emission (detailed calculations shown later) implies that the surface of these particles do not accommodate very large number of trap states. Thus the colloidal nature and superior optical quality of these nanocrystals makes them an incredibly appealing subject to study. In the following discussion, the PL efficiency of these materials will be investigated. The PL efficiency of materials from different synthetic methods will also be compared.

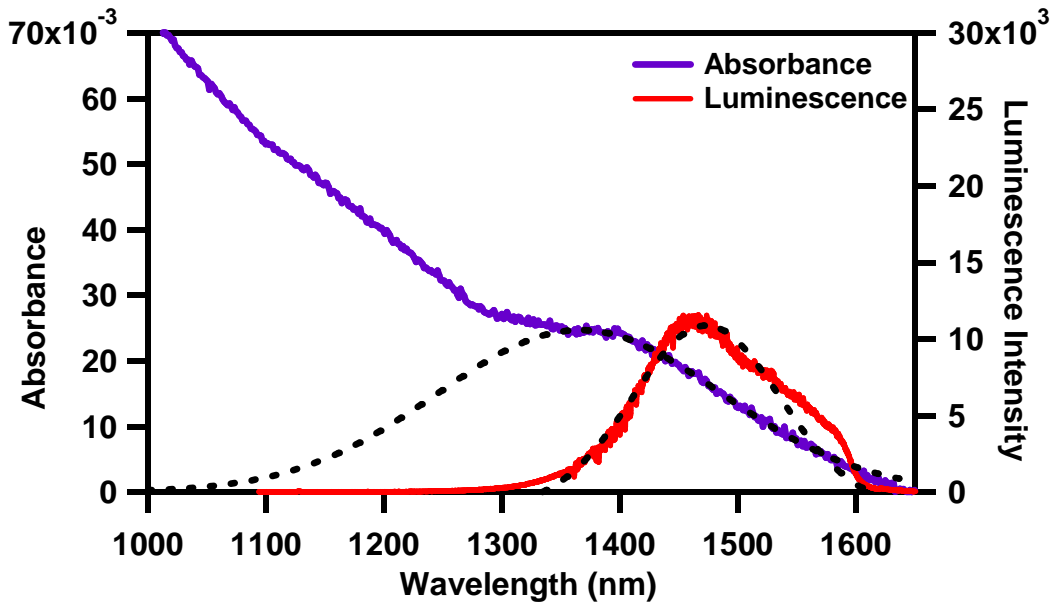


Figure 47: Absorbance and PL Spectra of an aliquot of InN (A5) from the synthesis using OLA:OA ratio of 10:1

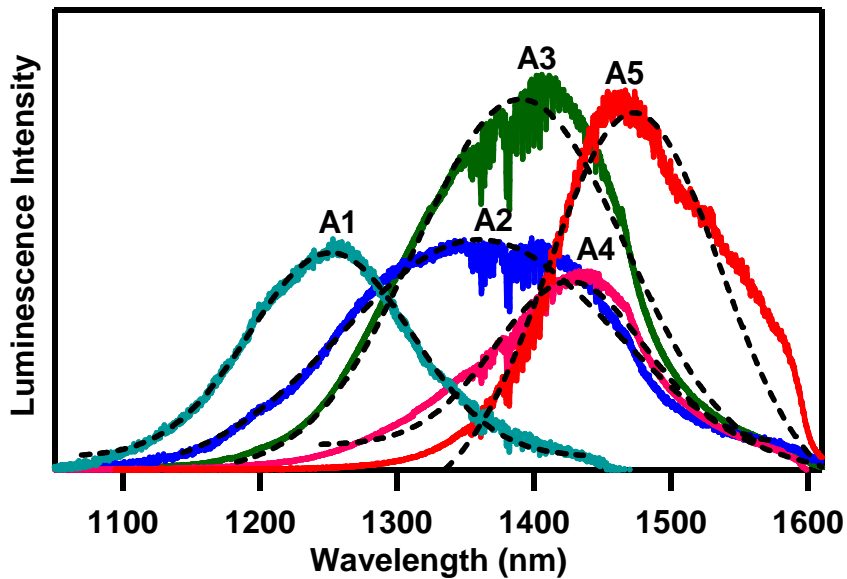


Figure 48: PL spectra of five aliquots of the sample from the synthesis using OLA:OA ratio 10:1

Fig. 47 compares the absorbance and PL spectra of an aliquot of InN from the synthesis using OLA: OA in 10:1 ratio as described in chapter 3. The dotted lines in the figure are the Gaussian fits of the absorbance and the emission peaks. The abrupt drop ~ 1600 nm is due to the limited detection capacity of the instrument above this wavelength range. Figs 48 and 49 depict the dependence of the PL position on the average QD size. The width of the luminescence peak is correlated to the size distribution of the nanocrystals. The spectral bandwidth of the PL spectra in Fig. 47 is comparable to the absorption peak, suggesting that the emission is from a single excitonic state rather than an ensemble of trap states. Trapped state emission from a nanocrystal solution typically has a full width at half maximum (FWHM) significantly larger than the FWHM of the Gaussian fit of the band edge peak.¹⁰⁵

The shift between the lowest energy peak in the absorbance spectrum of the QD and the corresponding emission is termed as the “Stokes shift”. From Fig. 47 the Stokes shift of the InN (A5) is calculated to be ~ 106 nm. A larger Stokes shift is desirable for applications of QDs in LEDs because larger Stokes shift means a smaller overlap area between absorption and emission spectra because reabsorption reduces the total efficiency of the QDs.¹⁰⁶ The Stokes shift has also been reported to be strongly dependent on the QD size.¹⁰⁷ In our case too, a similar phenomenon has been observed.

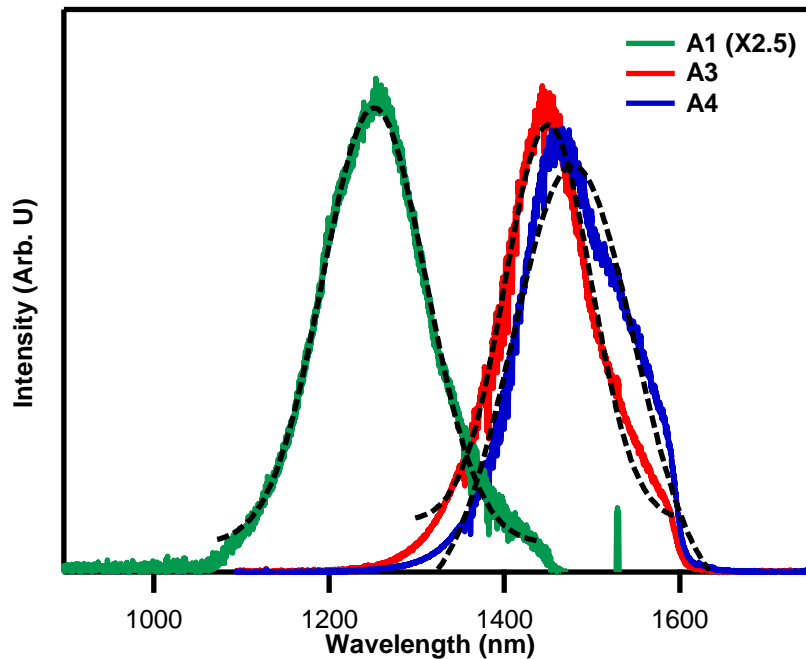


Figure 49: PL spectra of three aliquots of the InN sample synthesized using 3:1 ratio of OLA:OA

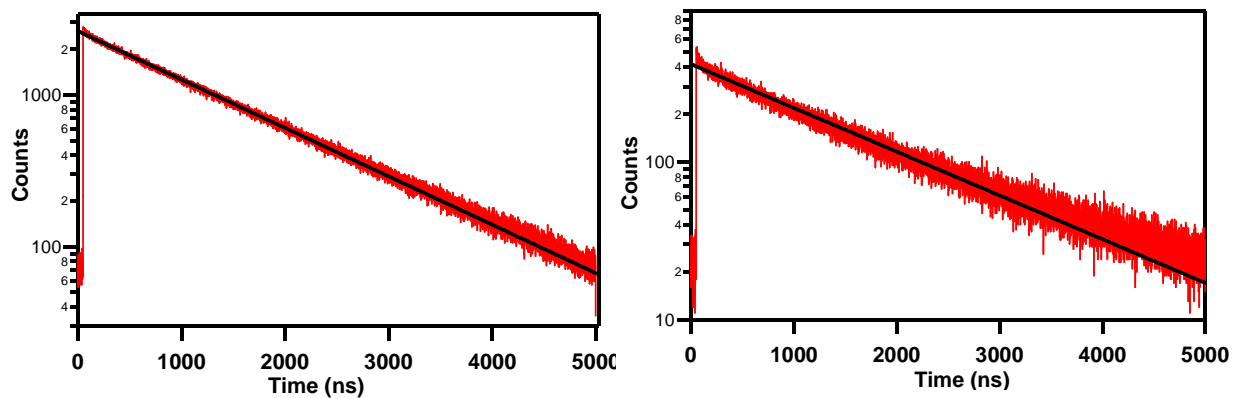


Figure 50: PL Lifetime decay of InN sample (final aliquot) from two different synthesis using OLA:OA ratio of 10:1 and 3:1 respectively

Fig. 50 shows the excited state decay of InN nanoparticles. The lifetime decay was found to be mono-exponential in nature. To extract the lifetime of the excited state, the decay was fit to single exponential function (black solid lines show the fit). The lifetimes of the nanoparticles have been calculated to be 1.4 μs and 1.6 μs respectively. PbS nanocrystals have been reported to show a single-exponential time constant measured to be $\sim 1 \mu\text{s}$ about two orders of magnitude longer than that reported for CdSe/ZnS nanocrystals.^{105,108} Colloidal PbSe semiconductor nanocrystals have also shown long fluorescence lifetimes of up to 0.88 μs .¹⁰⁹ The decay time of the InN reported here are similar to the IV-VI NCs and is longer than expected for a dipole transition (Fig. 50), but shorter than that expected for emission related to trap states.¹⁰⁹ The long radiative lifetime in the PbSe nanocrystals was attributed to the effects of dielectric screening. The screening of the radiating field inside the nanocrystal has the effect of weakening the internal field and consequently increases the radiative lifetime. Thus the long lifetimes of the InN QDs observed are consistent with the effect of dielectric screening for semiconductor nanocrystals with somewhat high dielectric constants. The lifetimes observed for these III-V materials and IV-VI materials studied before are found to be much longer than that of the more conventional II-VI nanocrystals which show lifetime in the range of $\sim 10\text{-}25 \text{ ns}$ owing to the higher dielectric constant of these materials. The highly mono-exponential nature of the excited state decay suggests that the surface of these nanomaterials were well-passivated and probably lack appreciable amount of trap states. Presence of surface traps generally leads to highly multi-exponential behavior of the excited state decay. Therefore, absence of such behavior clearly reflects the good surface property of these particles. II-VI QDs with really high quantum yields seldom show such mono-exponential behavior.

QUANTUM YIELD (QY)

The quantum yield (Φ) of photoluminescence emission is the number of photon emission occurrence for each photon absorbed by the system. QY is a measure of the emissive property of the particles and hence an important quantity to be determined in our case.

$$\phi = \frac{\text{No. of photons emitted}}{\text{No. of photons absorbed}} \dots\dots\dots (7)$$

Here, we calculate the relative quantum yield of some InN samples using a dye IR-26 (See SI for PL signal) (A commercially available dye emitting in the NIR region; QY 0.05%) as a standard.¹¹⁰

The QY of the nanoparticles are calculated using the following equation¹¹¹ :

$$\phi = 0.05 \times \frac{A_x}{A_s} \times \frac{F_s}{F_x} \times \left(\frac{n_x}{n_s} \right)^2 \dots\dots\dots (8)$$

Here, the subscripts x and s refer to the sample (InN) and the standard (IR26), respectively. ‘A’ refers to the integrated area under the emission spectrum, ‘F’ refers to the fraction of exciting light absorbed at the excitation wavelength (405 nm here) and n to the refractive index of the solvent (dichloromethane for IR26 and tetrachloroethylene for InN)

A sample QY calculation for Aliquot 2 (InN sample prepared using OLA:OA=10:1) by plugging in the absorbance and integrated PL intensity values in Equation 8 is shown below:

$$\phi = 0.1 \times \frac{2.18 \times 10^6}{6.42 \times 10^3} \times \frac{0.737}{0.277} \times 1.12 = 5.1\%$$

(QY calculations for other sample in SI)

For InN sample prepared using OLA:OA=3:1 the QY table is given below:

Aliquots	λ_{\max} (nm)	Calculated QY (%)
1	1350	4.77
2	1400	4.38
3	1425	4.28

Table 1: Calculated QY (relative) for the InN samples prepared using OLA:OA=3:1

The calculated QYs for the different InN aliquots from the synthesis using OLA:OA ratio 10:1 are listed here in the table below:

Aliquots	λ_{\max} (nm)	Calculated QY (%)
1	1350	2.2
2	1400	5.1
3	1425	2.6
4	1475	4.0

Table 2: Calculated QY (relative) for the InN samples using OLA:OA ratio 10:1

MANIFESTATION OF SIZE DEPENDANT OPTICAL PROPERTIES

THE BRUS EQUATION

An intuitive approach to understanding quantum dots utilizing the particle-in-a-box approach was performed by L.E. Brus.^{94,112} In the following section; the relationship between the size of the nanoparticles and the band gap will be demonstrated with the help of Brus equation.

$$E_g(r) = E_g(0) + \left(\frac{h^2}{8\mu}\right) \frac{1}{r^2} - \left(\frac{1.786e^2}{4\pi\epsilon_0\epsilon_\infty}\right) \frac{1}{r} \dots\dots\dots(8)$$

where $E_g(r)$ is the band gap of a quantum dot of radius r , $E_g(0)$ is the bulk band gap, h is Planck constant (6.626×10^{-34} J·s), e is the electrical unit charge (1.602×10^{-19} C), ϵ_0 is the permittivity of

vacuum ($8.854 \times 10^{-12} \text{ C}^2 \cdot \text{s}^2 \cdot \text{kg}^{-1} \cdot \text{m}^{-3}$), ϵ_{∞} is the optical dielectric constant of the material, and μ is the reduced mass of the electron-hole pair:

$$\mu = \frac{m_e m_h}{m_e + m_h} \dots\dots\dots (9)$$

where $m_{e(h)}$ is the effective mass of the electron/hole. The Coulomb term shifts E_g to lower energy as r , while the quantum localization (confinement) term shifts E_g to higher energy as r^2 . Thus the apparent band gap will always increase for small enough r .

The relevant empirical parameters of the bulk InN are listed in Table 3 below. These parameters have been used to relate the size dependence of the observed band gap of the synthesized InN nanocrystals to that predicted from the Brus equation.

Parameters	Value	Reference
$E_g(0)$	0.69 eV	113
ϵ_{∞}	6.0	114
m_e	$0.1 m_0$	115
m_h	$1.63 m_0$	116

* m_0 is the rest mass of the electron, $9.109 \times 10^{-31} \text{ kg}$.

Table 3: Empirical data of bulk wurtzite InN.

Converting the units from joules to electron-volts and meters to nanometers, and substituting the above parameters in Equation 8, we get the following relationship for the band gap of the quantum confined InN (Equation 10):

$$E_g(r) = E_g(0) + \frac{3.99 \text{ eV} \cdot \text{nm}^2}{r^2} - \frac{0.07 \text{ eV} \cdot \text{nm}}{r} \dots\dots\dots(10)$$

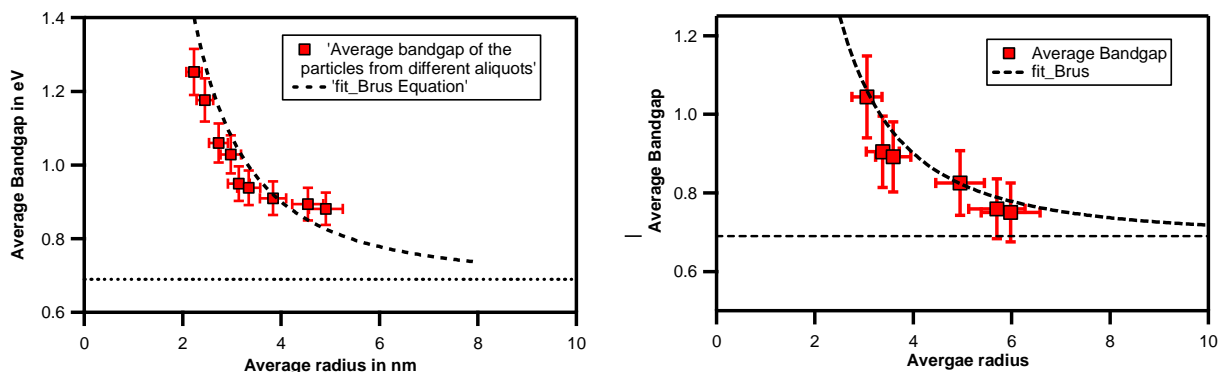


Figure 51: Size vs. band gap plot for InN nanocrystals synthesized by using 3:1 OLA:OA ratio (left), 10:1 ratio (right)

The curved line (dotted) shows the size predicted by the Brus equation (Equation 10). The agreement is really good, considering the limits of Brus equation.

As explained in the previous discussion there is subtle difference between the ways the two synthesized materials follow the trend predicted by Brus. Due to their platelet like shape the QDs synthesized by using 3:1 molar ratio reaches a minimum in the band gap energy whereas the QDs synthesized via 10:1 ratio of ligands can reach the band gap energy of the bulk material (Fig. 51).

ELEMENTAL ANALYSIS

We carried out some elemental analysis to find out the composition of the nanocrystals or the relative molar ratio of In:N. According to the work carried out by Nathan R. Neale *et al.*,⁴⁴ they claim that this ratio had a big impact on how the semiconductors behave. We tried to figure out if the materials synthesized with different methods had any difference in their relative composition and how significant this ratio is as far as their electronic properties are concerned. For this purpose the amount of In was found out by a technique called inductively coupled plasma atomic emission spectroscopy (ICP-AES) and the quantity of nitrogen was calculated from CHN analysis.

INDUCTIVELY COUPLED PLASMA ATOMIC EMISSION SPECTROSCOPY

Inductively coupled plasma atomic emission spectroscopy (ICP-AES), also referred to as inductively coupled plasma optical emission spectrometry (ICP-OES) is one of the most powerful and popular analytical tools for the determination of trace elements in a myriad of sample types.¹¹⁷ This technique is based upon the spontaneous emission of photons from atoms and ions that have been excited in a radiofrequency (RF) discharge. Liquid and gas samples can be injected directly into the instrument, while solid samples require extraction or acid digestion. The sample solution is converted to an aerosol and directed into the central channel of the plasma. At its core the inductively coupled plasma (ICP) sustains a temperature of approximately 10 000 K, which vaporizes the aerosol quickly and analytes are liberated as free atoms in the gaseous state. Further collisional excitation within the plasma imparts additional energy to the

atoms, promoting them to excited states. Sufficient energy is often available to convert the atoms into ions and subsequently promote the ions to excited states. Both the atomic and ionic excited state species may then relax to the ground state via the emission of a photon. These photons have characteristic energies that are determined by the quantized energy level structure for the atoms or ions. Thus the wavelength of the photons can be used to identify the elements from which they originated and the total number of photons is directly proportional to the concentration of the originating element in the sample.

CHN ANALYSIS

CHN analysis is a form of elemental analysis concerned with determination of only Carbon (C), Hydrogen (H) and Nitrogen (N) in a sample. The most popular technique behind the CHN analysis is combustion analysis where the sample is first fully combusted and then the products of its combustion are analyzed.¹¹⁸ The complete combustion is usually achieved by providing abundant oxygen supply during the combustion process. In this method, the carbon, hydrogen and nitrogen atoms of the product under analysis oxidize and form carbon dioxide, water and nitrogen oxide, respectively. Then these combustion products are carefully collected and weighed. The weights are used to determine the elemental composition, or empirical formula, of the analyzed sample.

Findings from the ICP-AES Studies:

Yield of reaction for 3:1 system = 31%; Conc. of In from ICP-AES = 15.68g/L

Yield of reaction for 10:1 system = 38%; Conc. of In from ICP-AES = 19.20g/L

From CHN analysis, the percent quantities of these elements were established to be as following:

Sample	C	H	N	In	In:N
Expected value	0.1-10%	0-0.25%	10-11%	80-90%	
OLA Only	3.12	--	12.72	84.16	0.733:0.9 = 0.81:1
3:1 (A)	1.57	--	10.55	87.88	0.765:0.75 = 1.015:1
3:1 (B)	2.31	0.10	11.07	86.62	0.75:0.79 = 0.948:1
5:1 (A)	1.47	--	10.97	87.56	0.76:0.78 = 0.97:1
7.5:1 (A)	2.05	--	12.87	85.08	0.74:0.92 = 0.8:1
10:1 (A)	2.43	0.16	11.44	86.13	0.75:0.817 = 0.917:1
10:1 (B)	2.35	--	12.38	85.27	0.74:0.88 = 0.84:1

Table 4: CHN analysis of InN samples prepared using different OLA:OA ratio

As we can see the data from ICP-OES analysis and from CHN analysis support each other in the sense that amount of In found by both technique is almost equivalent. Also, this set of data shows that the In:N ratio is >1. The material synthesized by Neale et al.,⁴⁴ is reported to have

excess metal [In(0)] content; and this is suspected to be the reason behind the electron rich surface and the Burstein-Moss effect which is responsible for the absorption onset at ~ 1.8 eV. Due to this phenomenon, the excitonic feature of the semiconductor is not revealed and the band gap transition cannot be noticed in the InN nanocrystals synthesized by the Neale group. However, the InN nanocrystals synthesized by us do not have substantial In(0) content and is thus unlikely to show this effect.

CONCLUSION

In this report the synthetic methods and mechanistic details to obtain high quality, monodispersed, colloidal, wurtzite InN have been described and the size dependant optical properties of indium nitride nanocrystals have been illustrated for the first time. It has also been depicted that not only the size but the shape of these nanocrystals can have significant effects on the electronic structure and the optical properties of the semiconductor. We have been able to synthesize different sizes and the shapes of the InN nanocrystals by varying the reaction conditions and changing the ratio of surfactants respectively. These nanocrystals turned out to be emissive; which is an impressive breakthrough for technological applications. Lifetime measurements provide us vital insight towards the nature of the exciton. We have obtained a very precise idea about the Bohr radius of our material of interest and have also been able to study the correlation of the size dependence of the band gap with that predicted by Brus. An outline for the reaction mechanism has also been provided by identifying the undesired by-product which is In metal. Though we have not been able to isolate the complex formed as the intermediate during the synthesis but we have enough evidence to stand by the fact that a bi-dentate amine complex of In forms in the course of the reaction with TMED.

This technique produces nanoparticles with a reasonably high yield. This method can be applied to synthesize various nitride nanocrystals and also utilized to dope these nanocrystals. This report illustrates the technique to obtain high quality, size and shape controlled and emissive colloidal InN nanocrystals for the first time along with the detailed study of its electronic structure and optical properties.

FUTURE WORK

A number of new techniques have been developed for doping of nanocrystals and it'd be an interesting step to explore their effectiveness toward InN. Also, since we don't have very clear idea about the nature of the intermediate and the reaction pathway, it's our aim to find a more proficient way to decipher it. The material shows to be very promising as far as its emissive nature is concerned. It would be worth investing some time to look into ways of increasing the quantum yield of InN since that is highly desirable for several industrial applications. Synthesis of colloidal, monodispersed III-V nanocrystals, such as; gallium nitride (GaN), indium and gallium phosphide (InP, GaP) and study of their size dependant optical properties would be our next priority. These materials having very different band gap values could prove to be very useful in synthesis of alloy materials covering a wide range of spectrum. We also plan to investigate the effect of doping (transition metals) on the magnetic and electronic properties of these materials for photonics and spintronics application.

BIBLIOGRAPHY

BIBLIOGRAPHY

- (1) Ekimov, A. I.; Efros, A. L.; Onushchenko, A. A. *Solid State Comm.* **1985**, *56*, 921.
- (2) Rossetti, R.; Brus, L. J. *Phys Chem.* **1982**, *86*, 4470.
- (3) Ekimov, A. I.; Onushchenko, A. A. *Sov. Phys. Semicon.* **1982**, *16*, 775.
- (4) Alivisatos, A. P. *Science* **1996**, *271*, 933.
- (5) Schaller, R. D.; Klimov, V. I. *Phys. Rev. Lett.* **2004**, *92*, 1886011.
- (6) Martyniuk, P.; Rogalski, A. *Prog Quant Electron* **2008**, *32*, 89.
- (7) Lagatsky, A. A.; Leburn, C. G.; Brown, C. T. A.; Sibbett, W.; Zolotovskaya, S. A.; Rafailov, E. U. *Prog Quant Electron* **2010**, *34*, 1.
- (8) Harbold, J.; Plisch, M. *The Quantum Dot*, Cornell University, 2008.
- (9) Su, C. I.; Xiuling, L. *IEEE Transactions on Nanotechnology* **2008**, *7*, 493.
- (10) Fortuna, S. A.; Wen, J.; Chun, I. S.; Li, X. *Nano Letters* **2008**, *8*, 4421.
- (11) Petroff, P. M.; DenBaars, S. P. *Superlattices and Microstructures* **1994**, *15*, 15.
- (12) InJo, O.; Kim, H.; Zhang, M.; Lee, T.; Zhu, F.; Yu, L.; Koveshnikov, S.; Tsai, W.; Tokranov, V.; Yakimov, M.; Oktyabrsky, S.; Lee, J. C. *International Electron Devices Meeting* **2006**, 1.
- (13) Pankove, J. I. *Optical Processes in Semiconductors.* ; Dover: New York, NY, 1975.
- (14) Neumayer, D. A.; Ekerdt, J. G. *Chem. Mater.* **1996**, *8*, 9.
- (15) Dmitriev, V. A.; Irvine, K. G.; Carter, C. H.; Kuznetsov, N. I.; Kainina, E. V. *Appl. Phys. Lett.* **1996**, *68*, 229.
- (16) Monemar, B. *Journal of Materials Science-Materials in Electronics* **1999**, *10*, 227.
- (17) Hsieh, J. C., MIT, 2004.
- (18) Oseki, M.; Okubo, K.; Kobayashi, A.; Ohta, J.; Fujioka, H. *Nature* **2014**, *4*, 39511.
- (19) Chichibu, S.; Azuhata, T.; Sota, T.; Nakamura, S. *Appl. Phys. Lett.* *69*, 4188 (1996) **1996**, *69*, 4188.
- (20) Juza, R.; Hahn, H.; Anorg, Z. *Allgem. Chem.* **1938**, *234*, 282.
- (21) Xiong, Y.; Xie, Y.; Li, Z.; Li, X.; Zhang, R. *New J. Chem.* **2004**, *28*, 214.

- (22) Xiao, J.; Xie, Y.; Tang, R.; Luo, W. *Inorg. Chem.* **2003**, *42*, 107.
- (23) Sardar, K.; Deepak, F. L.; Govindaraj, A.; Seikh, M. M.; Rao, C. N. R. *Small* **2005**, *1*, 91.
- (24) Bai, Y.; Liu, Z.; Xu, X.; Cui, D.; Hao, X.; Feng, X.; Wang, Q. *J. Cryst. Growth* **2002**, *241*, 189.
- (25) Frank, A. C.; Stowasser, F.; Sussek, H.; Pritzkow, H.; Ambacher, C. R.; Giersig, M.; Fischer, R. A. *J. Am. Chem. Soc.* **1998**, *120*, 3512.
- (26) Sardar, K.; Dan, M.; Schwenzer, B.; Rao, C. N. *J. Mater. Chem.* **2005**, *15*, 2175.
- (27) Dingman, S. D.; Rath, N. P.; Markowitz, P. D.; Gibbons, P. C.; Buhro, W. E. *Angew. Chem., Int. Ed.* **2000**, *39*, 1470.
- (28) Liu, R. S.; Shen, C. H.; Chan, T. S.; Gundakaram, R.; Hu, S. F.; Lin, J. G.; Huang, C. Y. *Tamkang J. of Science and Engineering* **2002**, *5*, 59.
- (29) Bhaviripudi, S.; Qi, J.; Hu, E.; Belcher, A. M. *Nano Lett.* **2007**, *7*, 3512.
- (30) Baker, R. T.; Google Patents: 1992.
- (31) Heath, J. R.; Shiang, J. J. *Chem Soc Rev.* **1998**, *27*, 65.
- (32) Klimov, V. I. *Nanocrystal Quantum Dots*; 2nd ed.; CRC Press: Boca Raton, FL, 2010.
- (33) Allen, P. M.; Walkar, B. J.; Bawendi, M. G. *Angew. Chem., Int. Ed.* **2010**, *49*, 760.
- (34) Schwenzer, B.; Meier, C.; Masala, O.; Seshadri, R.; DenBaars, S. P.; Mishra, U. K. *J. Mater. Chem.* **2005**, *15*, 1891.
- (35) Li, H. Y.; Yu, S.; Zou, G.; Li, Y.; Liu, S.; Yang, S. *Appl. Phys. Lett.* **1996**, *69*, 1285.
- (36) Goodwin, T. J. L.; V. J.; Risbud, S. H.; Kennedy, I. M.; Lee, H. W. H. *Appl. Phys. Lett.* **1997**, *70*, 3122.
- (37) Bhaviripudi, S.; Qi, J.; Hu, E.; Belcher, A. M. *Nano Lett.* **2007**, *7*, 3512.
- (38) Chang, Y. L.; Li, F.; Fatehi, A.; Mi, Z. *Nanotechnology* **2009**, *20*, 345203.
- (39) Chang, Y. L.; Mi, Z. L.; F. *Adv. Funct. Mater.* **2010**, *20*, 4146.
- (40) Cesar, M.; Ke, Y. Q.; Ji, W.; Guo, H.; Mi, Z. T. *Appl. Phys. Lett.* **2011**, *98*, 202107.
- (41) Hsieh, J. C.; Yun, D. S.; Hu, E.; Belcher, A. M. *J. Mater. Chem.* **2010**, *20*, 1435.
- (42) Lei, L.; Hu, S.; Liu, Y.; Xie, Y. *New J. Chem.* **2005**, *29*, 1610.
- (43) Chen, Z.; Li, Y.; Xu, X.; Cao, C. *J. Am. Chem. Soc.* **2012**, *134*, 780.

- (44) Palomaki, P. K. B.; Miller, E. M.; Neale, N. R. *J. Am. Chem. Soc.* **2013**, *135*, 14142.
- (45) Yoffe, A. D. *Adv. Phys.* **42** (2) 1993, 173 **1993**, *42*, 173.
- (46) Kastner, M. A. In *Physics Today* 1993; Vol. 46, p 24.
- (47) Ashoori, R. C. *Nature* **1996**, *379*, 413.
- (48) Rogach, A.; Kershaw, S.; Burt, M.; Harrison, M.; Kornowski, A.; Eychmuller, A.; Weller, H. *Adv. Mater.* **1999**, *11*, 552.
- (49) Sargent, E. H. *Adv. Mater.* **2005**, *17*, 515.
- (50) Rogach, A. L.; Eychmuller, A.; Hickey, S. G.; Kershaw, S. V. *Small* **2007**, *3*, 536.
- (51) Nozik, A. J. *Chem. Phys. Lett.* **2008**, *457*, 3.
- (52) Nozik, A. J.; Beard, M. C.; Luther, J. M.; Law, M.; Ellingson, R. J.; Johnson, J. C. *Chem. Rev.* **2010**, *110*, 6873.
- (53) Liu, W.; Tallapin, D. *J. Am. Chem. Soc.* **2012**, *134*, 20258.
- (54) Taylor, P. N.; Heffernan, J.; Publication, U. S. P. A., Ed. 2011; Vol. US 2011/0272668 A1.
- (55) Matsuoka, T.; Okamoto, H.; Nakao, M.; Harima, H.; Kurimoto, E. *Appl. Phys. Lett.*, **2002**, *81*, 1246.
- (56) Davydov, V. Y.; Klochikhin, A. A. *Indium Nitride and Related Alloys*; LLC, Baton Rouge: FL, 2009.
- (57) Tyagi, V. A.; Eustigneev, V. A.; Krasilov, A. M.; Andreeva, A. F.; Malatidiou, V. Y. *Sov. Phys. Semicond.* **1977**, *11*, 1257.
- (58) Westra, K. L.; Lason, R. P. W.; Brett, M. J. *J. Vac. Sci. Technol. A* **1988**, *6*, 1730.
- (59) Tansley, T. L.; Foley, C. P. *J. Appl. Phys.* **1986**, *59*, 3241.
- (60) Morkoc, H. *Nitride Semiconductors and Devices*; Springer: Heidelberg, 1999.
- (61) Madelung, O. *Semiconductors: Data Handbook*; 3rd ed.; Springer, 2004.
- (62) Yamamoto, A.; Tsujino, M.; Ohkubo, M.; Hashimoto, A. In *7th International Photovoltaic Science and Engineering Conference (PVSEC-7)*; Elsevier Science: Nagoya, Japan, , 1993, p 53.
- (63) Tansley, T. L.; Foley, C. P. *Elec. Lett.* **1984**, *20*, 1066.
- (64) Jenkins, D. W.; Dow, J. D. *Phys. Rev. B* **1989**, *39*, 3317.

- (65) Ikuta, K.; Inoue, Y.; Takai, O. *Thin Solid Films* **1998**, *334*, 49.
- (66) Davydov, V. Y.; Klochikhin, A. A.; Seisyan, R. P.; Emtsev, V. V.; Ivanov, S. V.; Bechstedt, F.; Furthmüller, J.; Harima, H.; Mudryi, A. V.; Aderhold, J.; Semchinova, O.; Graul, J. *Phys. Stat. Sol. B* **2001**, *229*, R1.
- (67) Wu, J.; Walukiewicz, W.; Yu, K. M.; Ager III, J. W.; Haller, E. E.; Lu, H.; Schaff, W. J. *Appl. Phys. Lett.* **2002**, *80*, 3967.
- (68) Butcher, K. S. A.; Tansley, T. L. *Superlattices Microstruct.* **2005**, *38*, 1.
- (69) Shubina, T. V.; Ivanov, S. V.; Mjeric, V. N.; Solnyshkov, D. D.; Vekshin, V. A.; Kopev, P. S.; Vasson, A.; Leymarie, J.; Kavokin, A.; Amano, H.; Shimono, K.; Kasic, A.; Monemar, B. *Phys Rev Lett.* **2004**, *92*, 1174071.
- (70) Specht, P.; Ho, J. C.; Xu, X.; Armitage, R.; Weber, E. R.; Erni, R.; Kisielowski, C. *Sol. State Comm.* **2005**, *135*, 340.
- (71) Scott, K.; Butcher, A.; Wintrebert-Fouquet, M.; Chen, P. P. T.; Prince, K. E.; Timmers, H.; Shrestha, S. K.; Shubina, T. V.; Ivanov, S. V.; Wuhler, R.; Phillips, M. R.; Monemar, B. *Phys. Stat. Sol. C* **2005**, *2*, 2263.
- (72) Wu, J.; Walukiewicz, W.; Shan, W.; Yu, K. M.; Ager III, J. W.; Haller, E. E.; Lu, H.; Schaff, W. J. *Phys. Rev. B* **2002**, *66*, 2014031.
- (73) Davydov, V. Y.; Klochikhin, A. A.; Emtsev, V. V.; Kurdyukov, D. A.; Ivanov, S. V.; Vekshin, V. A.; Bechstedt, F.; Furthmüller, J.; Aderhold, J.; Graul, J.; Mudryi, A. V.; Harima, H.; Hashimoto, A.; Yamamoto, A.; Haller, E. E. *Phys. Stat. Sol. B* **2002**, *234*, 787.
- (74) Hamberg, I.; Granqvist, C. G. *J. Appl. Phys.* **1986**, *60*, R123.
- (75) Yoshimoto, M.; Yamamoto, H.; Huang, W.; Harima, H.; Saraie, J.; Chayahara, A.; Horino, Y. *Appl. Phys. Lett.* **2003**, *83*, 3480.
- (76) Bhuiyan, A. G.; Sugita, K.; Kasashima, K.; Hashimoto, A.; Yamamoto, A.; Davydov, V. Y. *Appl. Phys. Lett.* **2003**, *83*, 4788.
- (77) Mello Donegá, C. d.; Liljeroth, P.; Vanmaekelbergh, D. A. M. *Small* **2005**, *1*, 1152.
- (78) Green, M. *Current Opinion in Solid State and Materials Science* **2002**, *6*, 355.
- (79) Cumberland, R. W.; Blair, R. G.; Wallace, C. H.; Reynolds, T. K.; Kaner, R. B. *J. Phys. Chem. B* **2001**, *105*, 11922.
- (80) Bai, Y. J.; Liu, Z. G.; Xu, X. G.; Cui, D. L.; Hao, X. P.; Feng, X.; Wang, Q. L. *J. Cryst. Growth* **2002**, *241*, 189.
- (81) Wells, R. L.; Janik, J. F. *Eur. J. Solid State Inorg. Chem.* **1996**, *33*, 1079.

- (82) Wu, C. Z.; Li, T. W.; Lei, L. Y.; Hu, L. Y.; Liu, Y.; Xie, Y. *New J. Chem.* **2005**, *29*, 1610.
- (83) Xiao, J. P.; Xie, Y.; Tang, R.; Luo, W. *Inorg. Chem.* **2003**, *42*, 107.
- (84) Xu, Y. N.; Ching, W. Y. *Phys. Rev. B: Condens. Matter. Mater. Phys.* **1993**, *48*, 4335.
- (85) Ishida, M.; Morioka, T.; Hanaoka, D.; Taneya, M.; Fujita, S.; Kawakami, Y.; Harada, M.; Sasaki, T.; Mori, Y.; Google Patents: 2012.
- (86) Aymerich, X.; Dirote, E. V., Ed.; Nova Science: New York, 2004.
- (87) Scherrer, P. *Bestimmung der Grösse und der inneren Struktur von Kolloidteilchen mittels Röntgenstrahlen*; Nachr. Ges. Wiss. : Göttingen 1918; Vol. 26.
- (88) Langford, J. I.; Wilson, A. J. C. *J. Appl. Cryst.* **1978**, *11*, 102.
- (89) Lauth, J.; Strupeit, T.; Kornowski, A.; Weller, H. *Chem. Mater.* **2013**, *25*, 1377–1383.
- (90) Cingarapu, S.; Klabunde, S. J. *Inorg. Chem.* **2011**, *50*, 5000.
- (91) Chou, N. H.; Ke, X.; Schiffer, P. E.; Schaak, R. E. *J. Am. Chem. Soc.* **2008**, *130*, 8140.
- (92) Ibáñez, J.; Oliva, R.; Manjón, F. J.; Segura, A.; Yamaguchi, T.; Nanishi, Y.; Cuscó, R.; Artús, L. *Phys. Rev. B* **2013**, *88*, 115202(1).
- (93) Demangeot, F.; Frandon, J.; Piquier, C.; Caumont, M. *Phys. Rev. B* **2003**, *68*, 2453081.
- (94) Brus, L. E. *J. Chem. Phys.* **1984**, *80*, 4403.
- (95) Yin, Y.; Alivisatos, A. P. *Nature* **2005**, *437*, 664.
- (96) Kwon, S. G.; Hyeon, T. *Acc. Chem. Res.* **2008**, *41*, 1696.
- (97) Wang, X.; Peng, Q.; Li, Y. *Acc. Chem. Res.* **2007**, *40*, 635.
- (98) Dinh, C. T.; Nguyen, T. D.; Kleitz, F.; Do, T. O. *ACS Nano* **2009**, *3*, 3737.
- (99) Jun, Y.; Casula, M. F.; Sim, J.; Kim, S. Y.; Cheon, J.; Alivisatos, A. P. *J. Am. Chem. Soc.* **2003**, *125*, 15981.
- (100) Chang, Y. H.; Lu, Y. S.; Hong, Y. L.; Kuo, C. T.; Gwo, S.; Yeh, J. A. *J. Appl. Phys.* **2010**, *107*, 43710.
- (101) Crimmin, M. R.; Rosebrugh, L. E.; Tomson, N. C.; Weyhermüller, T.; Bergman, R. G.; Toste, F. D.; Wieghardt, K. *J. Org. Chem.* **2011**, *696*, 3974.

- (102) Comeau, A. N.; Khadka, C. B.; Konermann, L. *Anal. Chem.* **2013**, *85*, 1200.
- (103) Khadka, C. B.; Eichhöfer, A.; Weigend, F.; Corrigan, J. F. *Inorg. Chem.* **2012**, *51*, 2747.
- (104) Khadka; MacDonald, D. G.; Lan, Y. F., ; ; Powell, A. K.; Corrigan, J. F. *Inorg. Chem.* **2010**, *49*, 7289.
- (105) Warner, J. H.; Thomsen, E.; Watt, A. R.; Heckenberg, N. R.; Rubinsztein-Dunlop, H. *Nanotechnology* **2005**, *16*, 175.
- (106) Hu, J.; Li, L.; Yang, W.; Manna, L.; Wang, L.; Alivisatos, A. P. *Science* **2001**, *292*, 2060.
- (107) Kuno, M.; Lee, J. K.; Dabbousi, B. O.; Mikulec, F. V.; Bawendi, M. G. *J. Chem. Phys.* **1997**, *106*, 9869.
- (108) Moreels, I.; Lambert, K.; Smeets, D.; De Muynck, D.; Nollet, T.; Martins, J. C.; Vanhaecke, F.; Vantomme, A.; Delerue, C.; Allan, G.; Hens, Z. *ACS Nano* **2009**, *3*, 3023.
- (109) Wehrenberg, B. L.; Wang, C.; Guyot-Sionnest, P. *J. Phys. Chem. B* **2002**, *106*, 10634.
- (110) Semonin, O. E.; Johnson, J. C.; Luther, J. M.; Midgett, A. G.; Nozik, A. J.; Beard, M. C. *J. Phys. Chem. Lett.* **2010**, *1*.
- (111) Nighswander-Rempel, S. P. *J. Fluoresc* **2006**, *16*, 483.
- (112) Brus, L. E. *J. Phys. Chem.* **1986**, *90*, 2555.
- (113) Davydov, V. Y.; Klochikhin, A. A.; Seisyan, R. P.; Emtsev, V. V.; Ivanov, S. V.; Bechstedt, F.; Furthmüller, J.; Harima, H.; Mudryi, A. V.; Aderhold, J.; Semchinova, O.; Graul, J. *Phys. Stat. Sol. (b)* **2002**, *229*, R1.
- (114) Zubrilov, A. *Properties of Advanced Semiconductor Materials GaN, AlN, InN, BN, SiC, SiGe* John Wiley & Sons: New York, 2001.
- (115) Lambrecht, W. R.; Segall, B. *Phys. Rev. B.* **1993**, *47*, 9289.
- (116) Pugh, S. K.; Dugdale, D. J.; Brand, S.; Abram, R. A. *Semicond. Sci. Techn.* **1999**, *14*, 23.
- (117) Hou, X.; Jones, B. T. *Inductively Coupled Plasma/Optical Emission Spectrometry*; John Wiley & Sons Ltd: Chichester, 2000.
- (118) Fadeeva, V. P.; Tikhova, V. D.; Nikulicheva, O. N. *Zhurnal Analiticheskoi Khimii*, **2008**, *63*, 1197.